DEVELOPMENT OF NEW ZWITTERIONIC COATINGS FOR ULTRA LOW FOULING IN REVERSE OSMOSIS MEMBRANES

BY

HAFIZ ZAHID SHAFI

A Dissertation Presented to the

DEANSHIP OF GRADUATE STUDIES

KING FAHD UNIVERSITY OF PETROLEUM & MINERALS

DHAHRAN, SAUDI ARABIA

In Partial Fulfillment of the
Requirements for the Degree of

DOCTOR OF PHILOSOPHY

In

MECHANICAL ENGINEERING

MAY, 2015

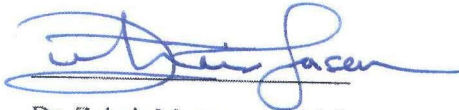KING FAHD UNIVERSITY OF PETROLEUM & MINERALS

DHAHRAN- 31261, SAUDI ARABIA

DEANSHIP OF GRADUATE STUDIES

This thesis, written by **Hafiz Zahid Shafi** under the direction of his thesis advisor and approved by his thesis committee, has been presented and accepted by the Dean of Graduate Studies, in partial fulfillment of the requirements for the degree of **DOCTOR OF PHILOSOPHY IN MECHANICAL ENGINEERING.**
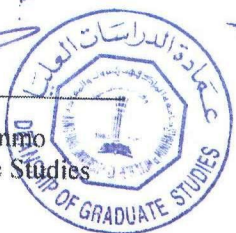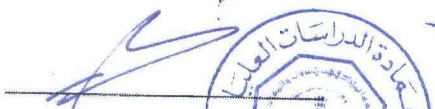
Dr. Zafarullah Khan
(Advisor)

Dr. Zuhair Mattoug Asa'd Gasem

Department Chairman

Dr. Karen K Gleason
(Co-Advisor)

Dr. Salam A. Zummo
Dean of Graduate Studies
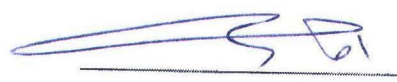
Dr. Tahar Laoui
(Member)

Dr. Mazan M. Khaled
(Member)

$2|6|15$

Date

Dr. Amjad Bajes Khalil
(Member)

Dedication

To my beloved father (late) and mother.

ACKNOWLEDGMENTS

TABLE OF CONTENTS

LIST OF TABLES

LIST OF FIGURES

LIST OF ABBREVIATIONS

AFM   :   Atomic Force Microscopy

CA   :   Contact Angle goniometry

EGDA   :   Ethylene glycol diacrylate

FTIR   :   Fourier transform infrared

iCVD   :   Initiated chemical vapor deposition

MFP   :   Molecular Force Mapping

TBPO   :   *Tert*-butyl peroxide

TFC   :   Thin film composite

4-VP   :   4-Vinyl pyridine

XPS   :   X-rays photo electron microscopy

3-BPA   :   3-bromopropionci acid

List of Nomenclature

C_F = Salt concentration in feed

C_P = Salt concentration in permeate

ΔF = Frequency shift

Δm = Mass adsorbed

J_w = Permeate flux

J_{SA} = Permeate flux after salt and sodium alginate addition

%R = Percentage salt rejection

Δp = Trans-membrane pressure

$\Delta \pi$ = Osmotic pressure

ABSTRACT (ENGLISH)

Full Name   : [Hafiz Zahid Shafi]

Thesis Title   : [Development of New Zwitterionic Coatings for Ultralow Fouling in Reverse Osmosis Membranes]

Major Field   : [Mechanical Engineering]

Date of Degree : [May 1, 2015]

Copolymer films of poly(4-vinylpyridine-co-ethylene glycol diacrylate) (p(4-VP-co-EGDA)) were synthesized and applied to commercial reverse osmosis (RO) membranes via initiated chemical vapor deposition (iCVD). As-deposited copolymer films were converted to surface zwitterionic structures containing poly(carboxybetaine acrylic acetate) (pCBAA) units by a quaternization reaction with vapors of the 3-bromopropionic acid (3-BPA). Conversion to a zwitterionic structure was confirmed by FTIR and high-resolution XPS N1s scans. Angle resolved XPS (ARXPS) analysis revealed that zwitterionic moieties are highly enriched in the top ~5-7nm surface of the deposited copolymer films. Biopolymer adsorption of the deposited copolymer coatings was investigated by quartz crystal microbalance with dissipation (QCM-D) using three model foulants−bovin serum albumin (BSA), humic acid (HA) and sodium alginate (SA). Inertness to bacterial adhesion of the optimized zwitterionic coating was investigated by counting the number of *E. coli*, *Bacillus licheniformis* and *Pseudomonas aeruginosa* cells attached on the membrane surface under static conditions. Bacterial adhesion studies revealed an almost 98% reduction in micro-organism attachment onto the surface of modified membranes compared to bare membranes, which clearly demonstrates

the effectiveness and superior performance of the zwitterionic coatings against bacterial adhesion. Permeate flux and salt rejection performance of the modified membranes resulted in a slight increase in salt rejection (98%); however, permeate flux was compromised by 18% compared to virgin RO membranes. Propensity of the modified and bare membranes to organic fouling was investigated by running cross-flow permeation tests using the sodium alginate as a model foulant. The modified membranes showed a modest permeate flux decline as compared to bare (unmodified) membranes where a larger permeate flux decline was observed. AFM analysis demonstrated that modified membranes showed lower RMS roughness compared to virgin membranes. Molecular force mapping (MFP) revealed that modified Koch membranes show at least an order of magnitude lesser adhesive force to BSA (a model foulant) as compared to the bare Koch membranes.

This is the first time that the library of iCVD functional groups has been extended to zwitterionic polycarboxybetaine moieties and a new antifouling zwitterionic coating has been successfully applied onto the surface of commercial RO membranes.

ABSTRACT (ARABIC)

الاسم الكامل: حافظ زاهد ش ف يع

عنوان الرسالة: تطوير طلاء زيتروايونيك جديد قليل الإتساخ يستخدم في إنتاج أغشية عملية التناضح العكسي

تاريخ الدرجة العلمية: 5-01-2015

لقد تم تصنيع و تطبيق غلاف الكوبلمر المشترك (poly(4-vinylpyridine-co-ethylene glycol diacrylate) على غشاء عملية التناطح العكسي (Reverse Osmosis) التجاري بإستخدام تقنية ترسيب الأبخرة الكيميائية بالابتداء. لقد تحول غلاف الكوبلمر إلى سطح زيتروايونيك يحتوي على وحدات (poly(carboxybetaine acrylic acetate) (pCBAA) عن طريق التفاعل الرباعي مع ثلاثي أسيد البورموبروبايونيك (3-bromopropionic acid (3-BPA)).

تم التحقق من التحول إلى تركيبة الزيتروايونيك بإستخدام إختبار كل من الانعكاس الطيفي بالأشعة تحت الحمراء (FTIR) و إختبار الأشعة السينية الضوئية الطيفي عالي الدقة (XPS). أظهر إختبار حيود زاوية الاشعه السينية الضوئية الطيفي (ARXPS) أن مركبات الزيتروايونيك غنية جداً في الطبقة العليا للغشاء (5-7 نانوميتر). تم إختبار إمتصاص المبلمرات الحيوية على غلاف الكوبلمر بطريقة التوازن الدقيق و التبديد لكرستال الكوارتز (QCM-D) و ذلك بإستخدام ثلاث أنماط من الملوثات و هي : ألبومين المصل البقري (BSA) و أسيد الهيوميك (HA) و ألجينات الصوديوم (SA).

لقد تم دراسة مقاومة غلاف الزيتروايونيك لإلتصاق البكتيريا بحساب عدد خلايا و مستعمرات كل من بكتيريا الايكولاي (E. coli) و بكتيريا عصية اللايكنوفوماس (Bacillus licheniformis) و بكتيريا الزائفة الزنجارية (Pseudomonas aeruginosa) الملتصقة بالغشاء خلال الحالة السكونية. أظهرت الدراسات أنه تم التخفيف بمقدار 98% من إلتصاق البكتيريا على الغشاء بالمقارنة بالغشاء التجاري (الغير معدل) و الذي يعكس بوضوح كفاءة الغلاف الزيتروايونيك.

لقد وجد زيادة طفيفة (98%) في عملية رفض الملح مع أن التدفق عبر الغشاء تراجع بنسبة 18% مقارنة مع الغشاء غير المعدل (التجاري). تم دراسة قابلية كل من الغشاء المعدل و غير المعدل للتلوث العضوي عن طريق دراسة التخلل عبر التدفق لألجينات الصوديوم (Sodium Alginate) حيث أظهر الغشاء المعدل إنخفاض طفيف للتدفق بالتخلل بالمقارنة مع الغشاء غير المعدل و الذي أظهر انخفاض ملحوظ بمعدل التدفق بالتخلل. أظهرت نتائج مجهر القوة الذرية (AFM) أن سطح الغشاء المعدل له جذر متوسط مربع (RMS) أقل من الغشاء غير المعدل.

يثبت هذا البحث و للمرة الأولى في مكتبة المجموعات الوظيفية الخاصة بتقنية ترسيب الأبخرة الكيميائية بالابتداء (iCVD) و التي تتحول إلى غلاف زيتروايونيك و الذي بدوره تم تطبيقه بنجاح على أغشية التناضح العكسي التجارية و أظهرت نتائج ممتازة بمقاومة التلوث.

إختبار تخطيط القوة الجزيئية (MFP) وجد أن غشاء الكوج (Koch) المعدل أظهر قوة إلتصاق بكتيريا ألبومين المصل البقري (BSA) اقل بالضعف مقارنة بغشاء الكوج غير المعدل.

CHAPTER 1

INTRODUCTION

1.1   Global Water Scarcity

Because of increasing population, urbanization, global warming and rapid industrialization, global water supply is under severe stress and this has a direct consequence on the scarcity of clean water resources globally [1]. In the past few decades, clean water supply has become very critical due to excessive water demand and contamination of the existing clean water sources. Furthermore, global water consumption is increasing (figure 1.1) and quality regulations on drinking water have become more severe [2].

The health and economic impacts of today's global water crisis are staggering as stated below.

o   Water-borne diseases result in the death of more than 3.5 million people per annually.

o   1.1 billion people survive with no clean drinking water

o   2.6 billion people are deficient in adequate sanitation [2002, UNICEF/WHO JMP 2004].

o   Diarrheal diseases cause death of 1.8 million people die every year.

- Water borne diseases are the source of death of 3900 children die every day [WHO 2004].

- The world's biggest cause of infection is lack of sanitation.

- 443 million school days are lost each year due to water-related illness.
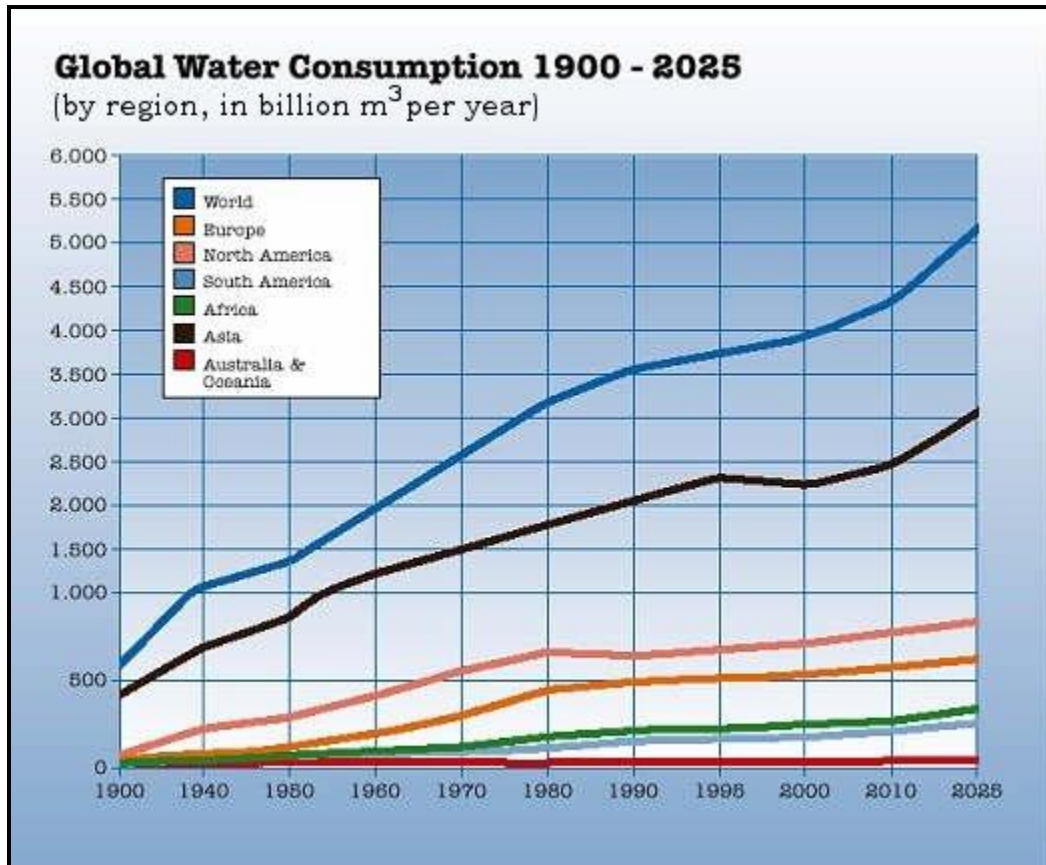
Figure 1.1 Global water consumption by region, in billion m³ per year.
[http:// oceanmotionintl.com/water]

The above facts demonstrate that there is a severe water crisis today. But the crisis is not about having insufficient water to suit our needs. The disaster is about managing the water so scantily that it affects billion of people and the environment suffers badly. As a result, to meet up the increasing demand for clean water, water separation technologies must be enhanced, and new resources must be investigated.

1.2   Seawater Desalination

Desalination is the process by which excess salts and minerals are removed from water to make it potable and fit for human use. A desalting device primarily divides saline water into two streams: one the fresh water stream (containing low concentration of dissolved salts) and the other concentrate or brine stream (that contains the remaining dissolved salts) as shown in figure 1.2. The device necessitates energy to operate and can employ a number of different technologies for the separation.

A range of desalting technologies have been developed over the years and based on their commercial success they can be classified into thermal (or distillation) and membranes-based processes. Thermal processes include: multistage flash distillation (MSF), multiple effect distillation (MED) and vapor compression whereas, membranes based processes are further sub-classified into reverse osmosis (RO) and electrodialysis (ED) process. The classification of major desalination processes is shown in figure 1.3 whereas, figure 1.4 indicates the contribution of each process to the global desalination capacity. Desalination is the alternative source that offers water to meet up the water demand for irrigational, industrial and municipal use.
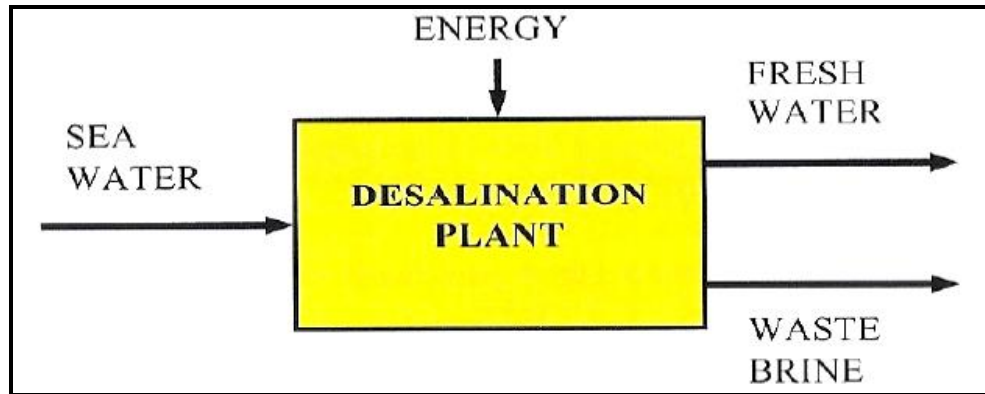
Figure 1.2 Schematic of a desalination device.
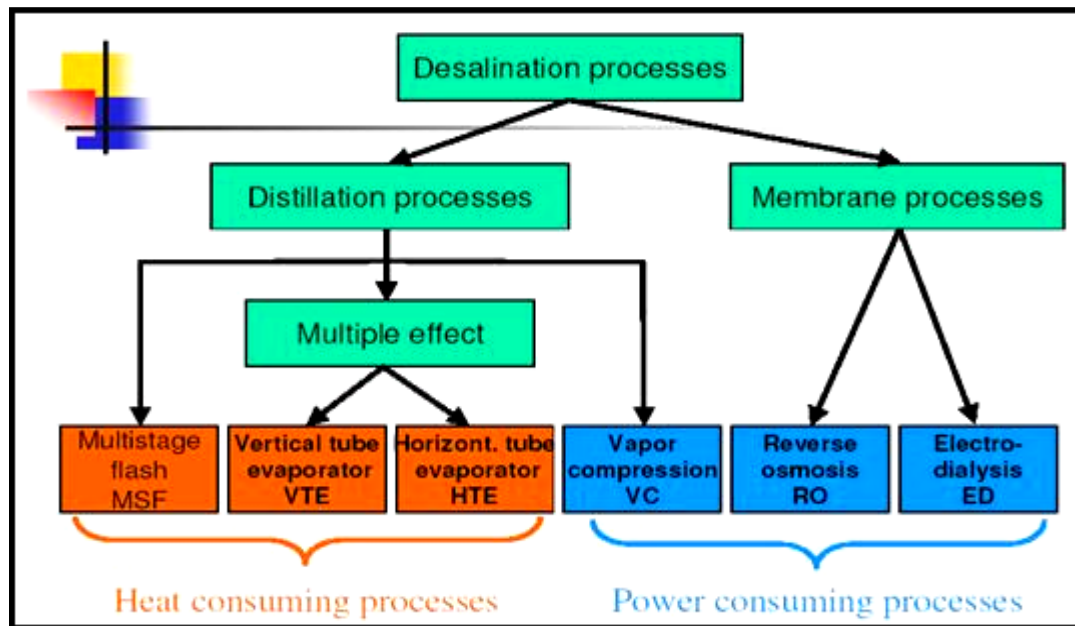
Figure 1.3 Classification of desalination technologies. (http://www.wioa.org.au/)

1.2.1 Membranes Based Separation Processes

The membranes-based processes can be further categorized in to: microfiltration (MF), ultrafiltration (UF), reverse osmosis (RO) and electrodialysis. The range of application of the three pressure-driven membrane water separation processes, namely, RO, UF and MF, is illustrated in figure 1.5. It is important to mention that RO membranes share the largest membrane market share as shown in figure 1.6.

UF and MF processes resemble each other with regard to their mode of separation that is molecular sieving through increasingly fine pores. MF membranes can filter colloidal particles and bacteria from 0.1 to 10 μm in diameter. UF membranes can be used to filter dissolved micro-molecules, such as proteins from solutions. However, the method of separation by RO membranes is rather different [3]. Section 1.3 describes various types of RO membranes and their application in seawater desalination.

5
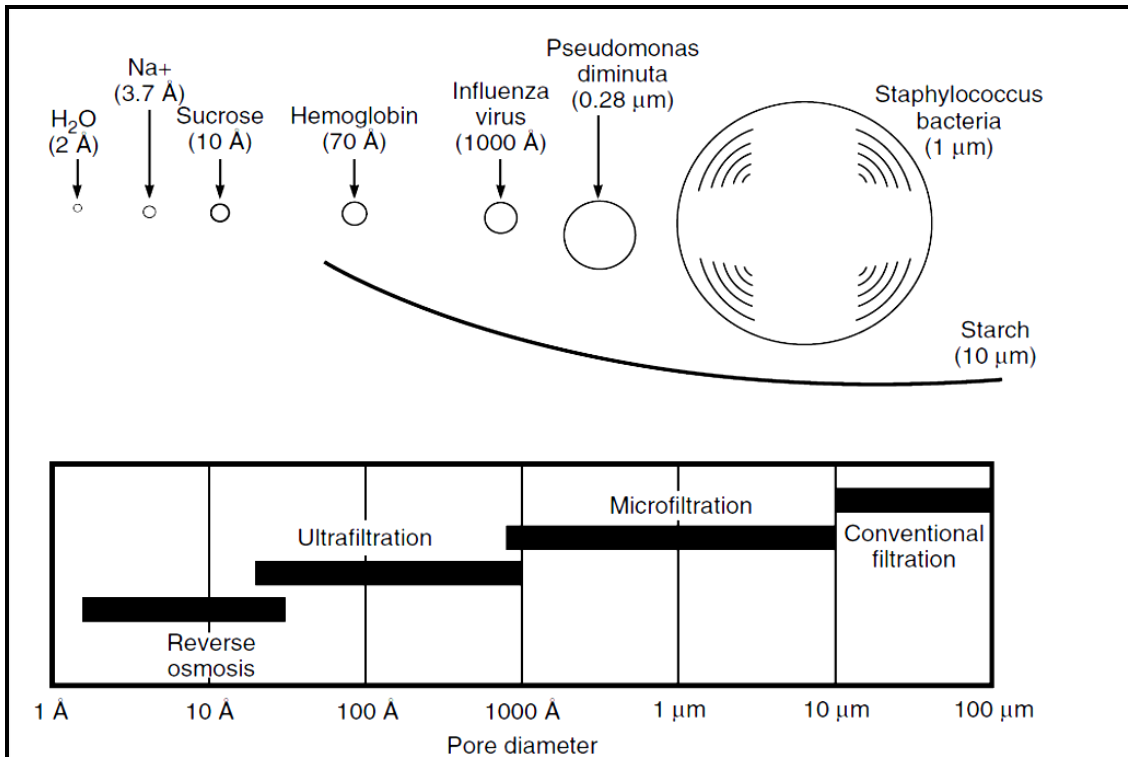
Figure 1.5 Membranes used for the four separation processes: RO, UF, MF and Conventional filtration. Relative size of different solutes separable by each membrane is also shown in this schematic [3].
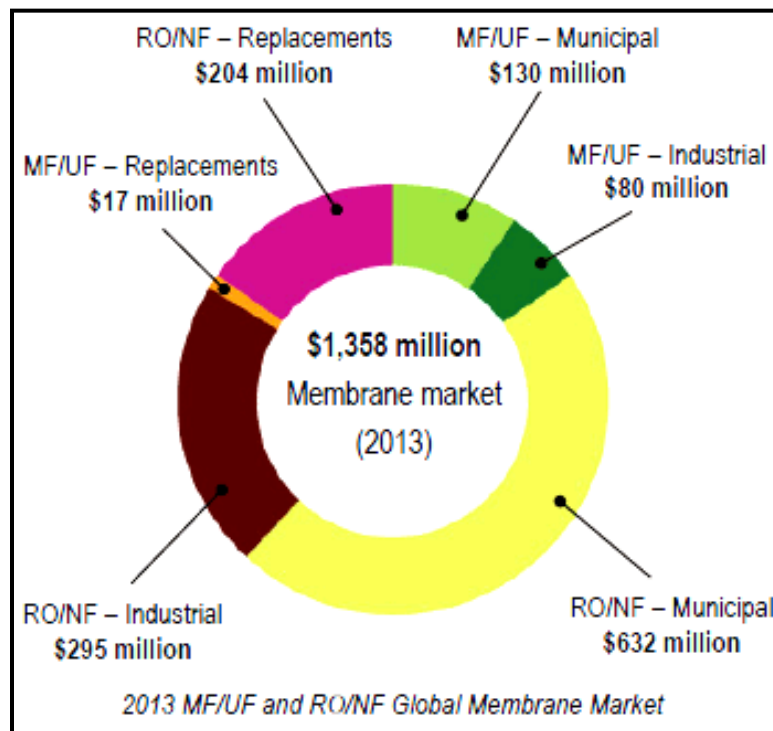
Figure 1.6 Global membrane market. (http://www.desalination.com)

6

1.3   Reverse Osmosis (RO) Technology

In an RO process, pressure higher than the osmotic pressure is applied to the salt side of the membrane, and water passes from the salt solution to the fresh water side of the membrane as depicted in figure 1.7.

In the past few decades RO has emerged as a promising desalination technology to overcome the clean water supply worldwide. Currently, RO technology is being utilized for seawater desalination, industrial wastewater reclamation and to obtain clean water from other nontraditional water sources such as brackish water [4-6]. Owing to its simpler design as compared to other energy intensive desalination processes such as ion exchange, distillation and vapor compression; it is considered as the simplest, lesser energy intensive (as compared to thermal processes) and most efficient desalination process [7]. However, the full utilization of the RO technology is severely challenged by membrane fouling and it presents the major bottle neck for the full viability of RO plants worldwide.

RO membranes are considered as the heart of an RO plant and account for more than 70% of cost of the plant. Among several innovative techniques to combat biofouling of RO membranes, the development of anti-biofouling coatings is a very promising methodology that is being actively pursued by many researchers. These antifouling coatings have been successfully applied to RO membranes and in several other applications as described in section 2.2 in detail.
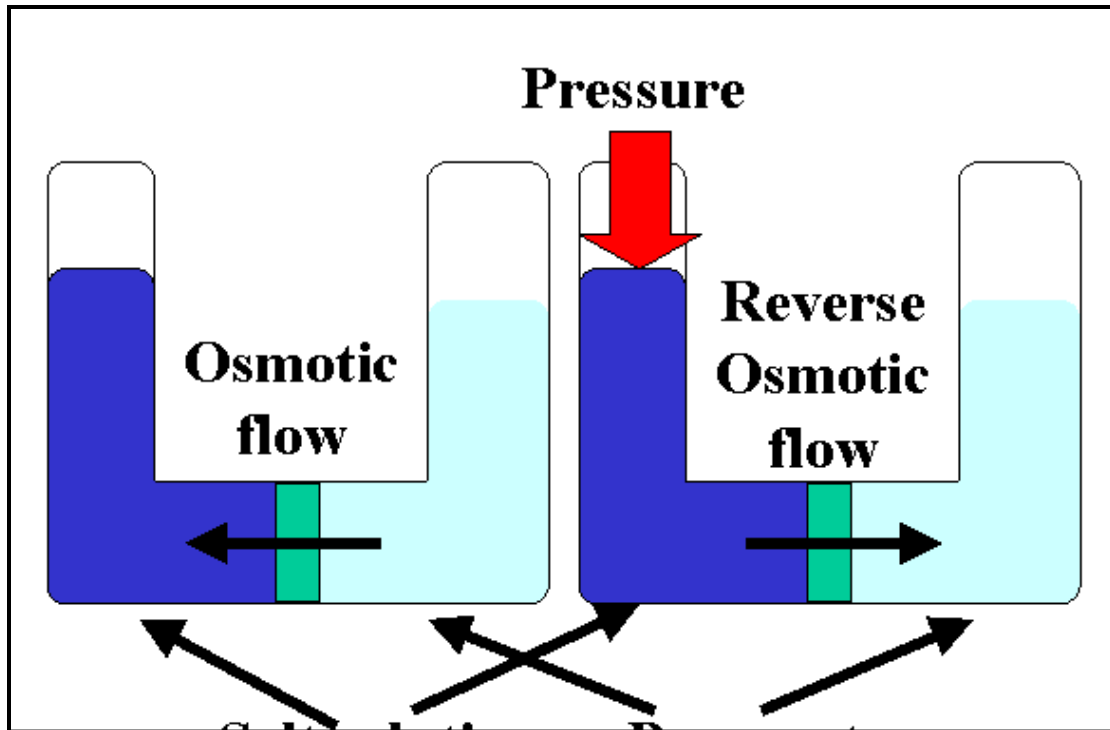
1.4 Goals and Organization of the Dissertation

This thesis is comprised of seven chapters. 1st Chapter is devoted to the introduction, wherein, global scarcity of clean water, major desalination methods, their classifications and contribution to global desalted water and increasing trend for the global membranes market are described. Chapter 2 describes the literature review of the various types of RO membranes fouling, adverse effects of fouling and the potential ways to combating the biofouling of RO membranes. Chapter 3 illustrates the theoretical background of RO membranes including their structure, composition(s), working principle and their applications in sweater desalination. Chapter 4 portrays the uniqueness and salient features of iCVD as being the sophisticated surface modification technique for commercial RO membranes. Chapter 5 explains the experimental work performed

including the materials and methods adopted to synthesize and optimize iCVD antifouling coatings. Various surface and compositional characterization techniques and performance evaluation methods used in this study have also been narrated under experimental section. Provided in chapter 6, are the detailed results and discussions of the experimental work performed in this study. The thesis brings to a close with the conclusions and recommendations for future work provided in chapter 7.

CHAPTER 2

LITERATURE REVIEW

2.1   Fouling of Reverse Osmosis Membranes

Fouling is defined as the unwanted/detrimental irreversible adhesion and accumulation of foulant. Based on the type of foulant, fouling in RO membranes can be classified in to the following four types [8]:

1   Crystalline: deposition and precipitation of inorganic matter on a surface.

2   Organic: adhesion of organic materials (e.g. oil, proteins, humic substances)

3   Particulate and colloidal: adhesion of clay, particulate, silt, humic substances, debris and silica.

4   Microbiological: biofouling, irreversible adhesion and attachment of microorganisms, forming biofilms [9].

Membrane fouling is by far the most serious problem found in separation processes such as water desalination, industrial water treatment, juice concentration, and hemodialysis [4-6]. Among the various types of RO fouling, the most challenging and severe in nature is the biofouling and is described in section 2.1.1.

2.1.1   Biofouling

Biofouling is referred to as the unwanted adhesion and accumulation of biopolymers or microorganisms (plants, algae, microorganisms, or animals) which can grow as biofilm on surface of membrane. A biofilm is referred to the gathering of surface-associated

microbial cells. Biofilm is permanently associated (not removed by gentle rinsing) with a surface and held tightly via matrix of extracellular polymeric substances. Almost all water systems are contaminated with micro-organisms which are capable of colonizing almost any surface [10].

Biofilms are primarily made up of microbial cells and extra cellular polymeric substances (EPS) as shown in figure. 2.1. EPS is considered as the primary matrix material of the biofilm and may compose of 50–90% of the total organic carbon (TOC) of biofilms. Polysaccharides, proteins, glycoproteins, lipoproteins may be considered as the building blocks of EPS, however, it may vary in chemical and physical properties and other macromolecules of microbial origin.
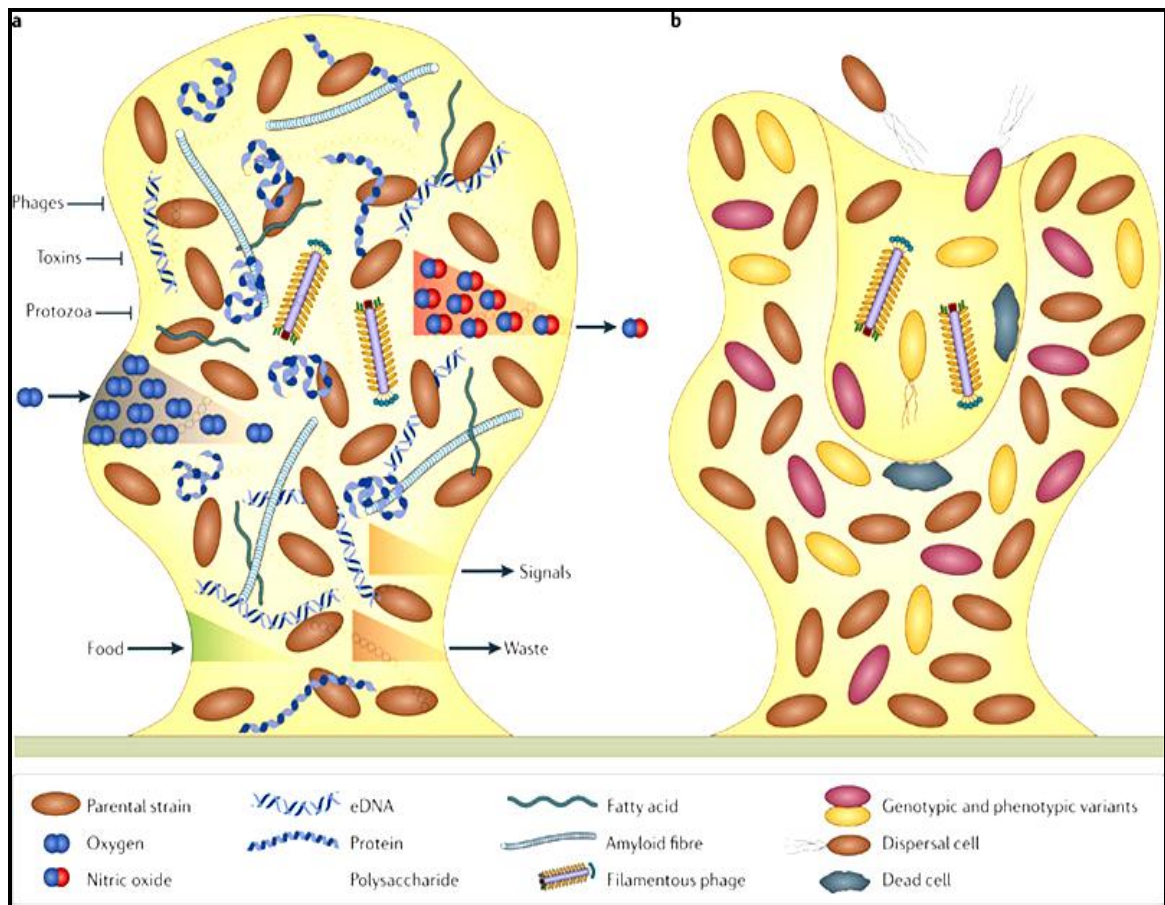
Figure 2.1 Components of EPS matrix. Adapted from [11].

Biofouling passes through the following sequence, initial attachment, growth and dispersal of microorganisms including the transfer, adhesion and accumulation of cells followed by EPX production, cell enlargement and propagation — all contributing to biofilm formation. Figure 2.2 below explains the main events occurring through the membrane biofouling process.
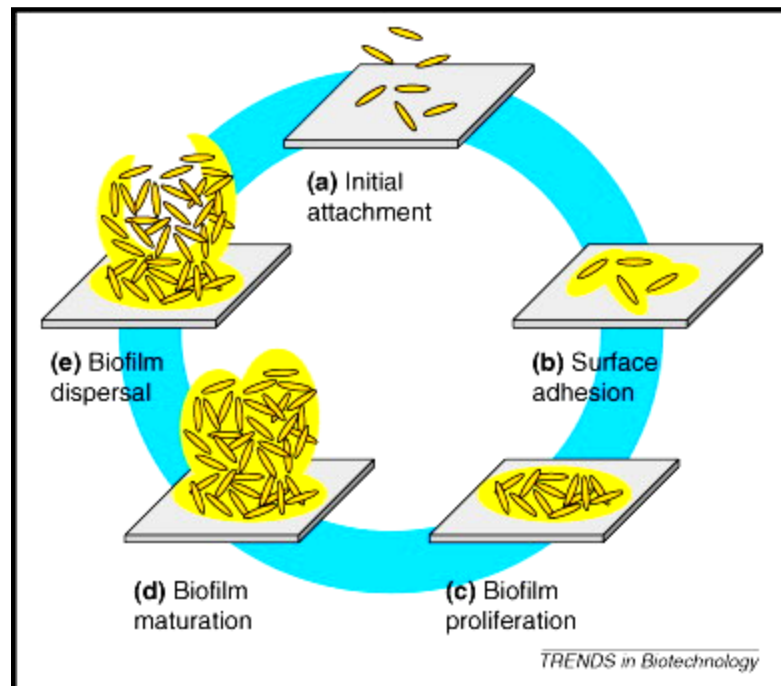
Figure 2.2 Sequences of major events leading to the biofilm formation [12].

A conditioning film is formed instantly on surfaces immersed in water that consists of both organic macromolecules (polysaccharides, humic substances and proteins), and inorganic compounds [13]. These conditioning films have been found to alter the surface properties (such as charge, surface free energy) which encourages the attachment of micro-organisms present in the surrounding medium. [14-16].

2.1.2 Adverse Effects of Biofouling

When a biofilm matrix coats a separation membrane, e.g., reverse osmosis (RO) membranes, the matrix acts as a secondary membrane, which adversely affects the separation process. Furthermore, the irregular and viscoelastic surface of the biofilm enhances fluid frictional resistance and leads to a feed–brine–pressure (FBP) drop as elucidated in figure 2.3. Given below are the major consequences of the biofouling on the RO membrane processes.

- Increased differential pressure, resulting in higher operating cost.

- Permeate flux decline (due to reduced convective pressure across the membrane surfaces)

- Decrease in salt rejection (which results in poor quality product water)

- Frequent cleaning (which reduces the membrane life)

- Biofouling in RO module elements
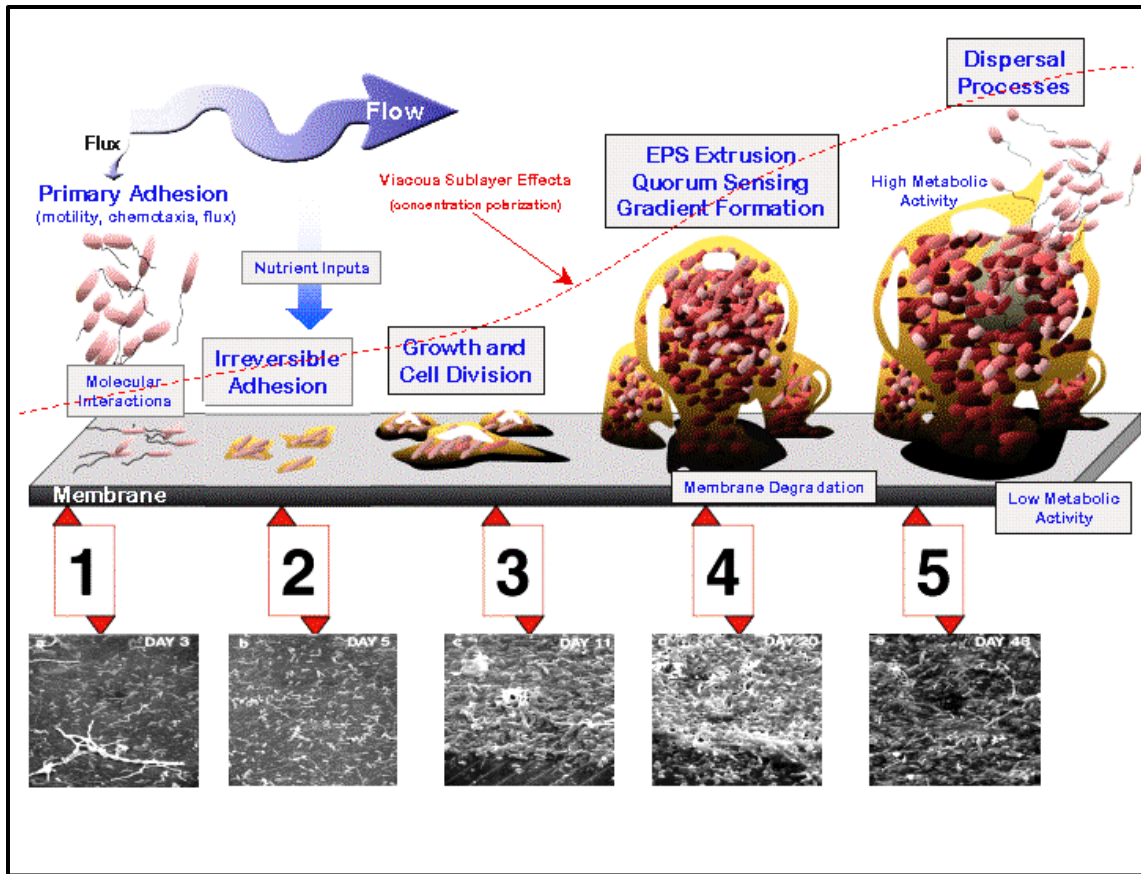
Figure 2.3 Schematics of increase in hydraulic resistance during the progression of biofilm on membranes. The bottom part of the figure shows respective SEM images of each biofilm stage.

Biofilm formed on RO desalination membranes acts as a secondary layer (figure 2.4) and causes a significant decrease in trans-membrane pressure [17], resulting in a decline in permeate flux over time. To maintain an optimum permeate flux, higher operating pressures are required. Furthermore, the physical damage to the membrane caused by biofilm activity results in an increase in salt passage, i.e., reduced salt rejection. To minimize the adverse effects of biofouling, frequent chemical cleaning is used, which shortens membrane life. The cumulative effect of these factors causes a significant increase in the operating cost of the desalination process [18].
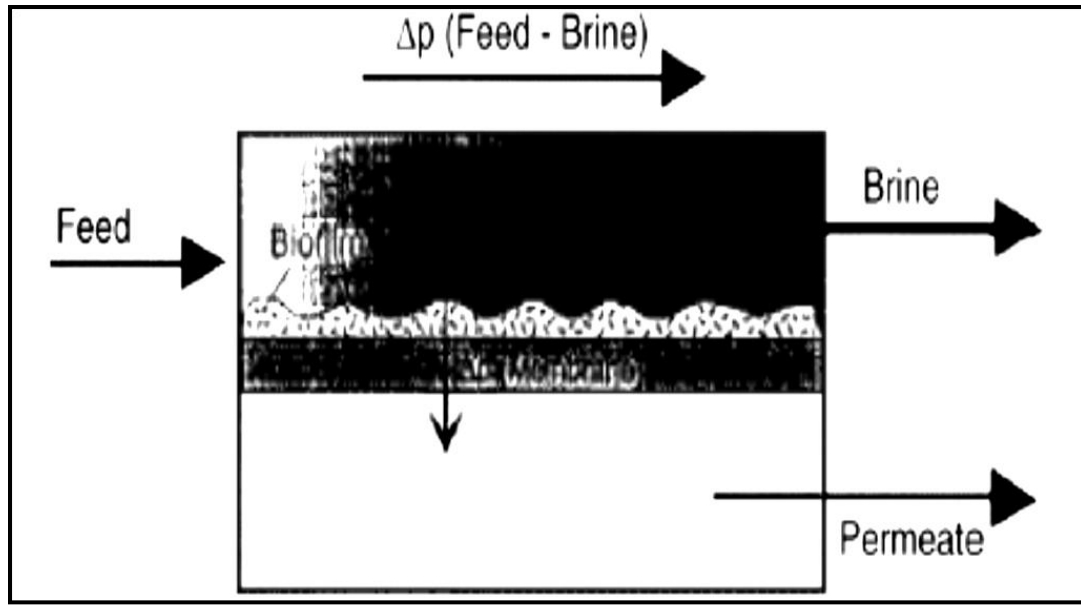
Figure 2.4 Schematic showing the biofilm acting as secondary layer [9].

2.2   Combating Fouling of Reverse Osmosis (RO) Membranes

The biofouling of RO membranes can be minimized or belated by techniques such as pre-treating the feed water [19], sporadic cleaning [20] or surface modification of these membranes [21-26]. However, the former two techniques are expensive and time-consuming, and intermittent clean-up will curtail the membrane lifetime.

Among several methods of surface modification used to combat biofouling, the development of anti-biofouling coatings is a very promising methodology that is being actively pursued by many researchers. These antifouling coatings seek to impart the three key parameters to the RO membrane surfaces, namely enhancing hydrophilicity, reducing surface roughness and producing neutral or near neutral surfaces. Antifouling mechanism of an antifouling coating applied to an RO surface is depicted in figure 2.5. These antifouling coatings have been successfully used in applications such as coatings for ship

15

hulls [27], marine equipment, biomedical implants [28], biomedical devices, biomedical biosensors [29], food packaging, and other industrial equipment. However, application of these coatings to separation membranes, such as RO membranes, has not been fully explored.
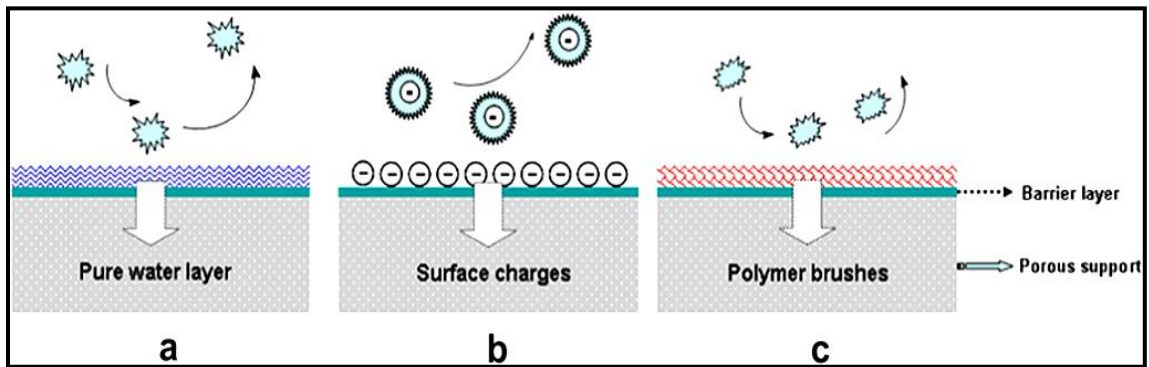
Figure 2.5. Schematic diagram of antifouling actions. (a) Formation of water film (conditioning layer), (b) electrostatic repulsion and (c) steric repultion [30].

2.2.1 Types of Surface Modification

As mentioned earlier, the major stages in biofilm development are bacterial attachment, micro-colony configuration, and biofilm maturation. The primary objective of any surface modification technique is to stop/hinder one or more of these stages, e.g., bacterial attachment has been found to reduce considerably by making the surface more smoother, hydrophilic and negatively charged. Figure 2.6 shows major approaches adopted for developing anti-biofouling surfaces. Surface modification of existing membranes is also regarded as a prospective and effective route to develop antifouling membranes. The surface modification method spans from physical to chemical treatments as explained in the next section.
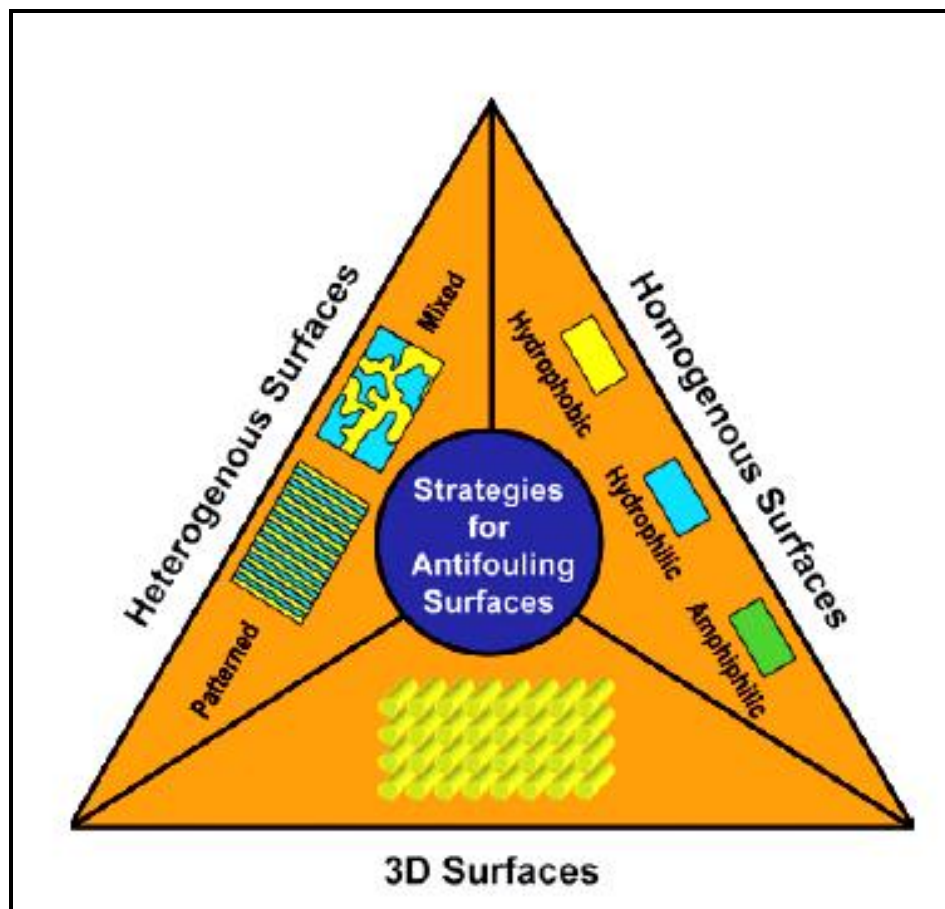
Figure 2.6. Three main approaches to produce anti-biofouling surfaces. Homogeneous surfaces of hydrophobic (yellow), hydrophilic (blue), or amphiphilic (green) character can be utilized. Heterogeneous surfaces (mixed or patterned hydrophobic and hydrophilic character) and 3D surfaces can be used to modify the surface of an anti-biofouling coating by control of surface topography [31].

2.2.2 Physical Treatment

A simple method of surface modification is by physical adsorption and structuring of polymer surfaces. The surface adsorption of industrial RO membrane are modified by using: i) polyethylene-oxide surfactants (T-X series and P series) that acts as a surfactants [32], ii) the charged polyelectrolytes by electrostatic self-assembly of polyethyleneimine (PEI) on the membrane surface [33] and iii) adsorbing a film of

17

negatively charged sulfonated poly (ether ether ketone) (SPEEK) onto the surface of a positively charged NF membrane [34].

Surface coating is another type of physical treatment that takes advantage of the application a protective layer to minimize or to get rid of the adsorption and adhesion of foulants onto membrane surface and it has been usually adopted to alter the surface properties of conventional RO membranes. For this purpose, hydrophilic polymers with hydroxyl, carboxyl or ethylene oxide groups are coated on membranes surface to improve membrane antifouling property. This is consistent with the research results by Tan et al [35]. It is import to note here that the penetration of coating material into the ridge-and-valley structure of polyamide RO membrane may lead to increased permeation resistance that result in declined water flux after modification. Therefore, for practical reasons, the coating layer should be adequately thin and have inherently high water permeability to retain high water flux.

2.2.3   Chemical Treatment

In this type of surface modification, membrane surface is altered by a chemical reaction that takes place between the membrane surface and the chemical specie(s) present in the coating precursor. Various types of chemical treatment include: (1) hydrophilization treatment [36] of TFC RO membranes, (2) radical grafting (both grafting to and grafting from the polyamide membrane surface is possible), (3) chemical coupling of relatively active groups (such as free carboxylic acid and primary amine groups) present on RO membranes [37, 38] as shown in figure 2.7, (4) Plasma polymerization and plasma induced polymerization and (5) initiated chemical vapor deposition (iCVD).
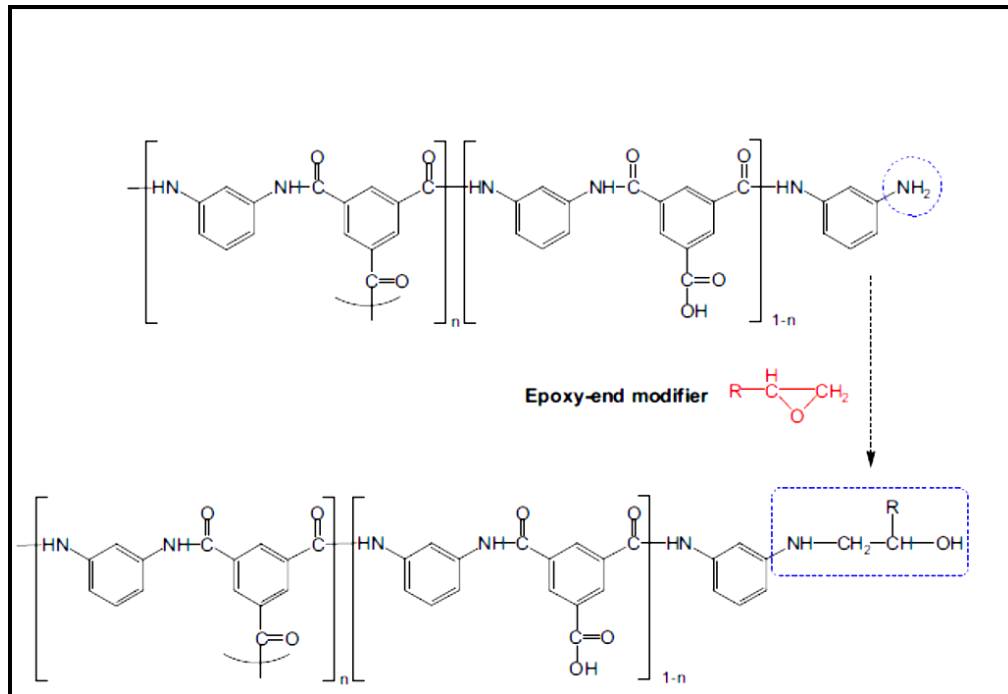
Figure 2.7. Surface modification of thin film composite type polyamide RO membrane based on the chemical reaction between amine groups and the epoxy-end modifiers.

2.2.3.1 Initiated Chemical Vapor Deposition (*i*CVD)

A variant of chemical vapor deposition, termed as *initiated* chemical vapor deposition (*i*CVD), is a solventless free radical polymerization technique that is carried out at ambient temperatures and low operating pressures. *i*CVD technique has demonstrated great potential as a surface modification technique [39]. These modest temperature and pressure ensure the retention of sensitive functional groups present in coating materials and avoid undesirable cross linking of polymer chains. Table 2.1 shows salient features of iCVD method of thin film deposition [68]. Detailed discussion of iCVD process is given in chapter 4.

Table 2.1. Salient features of iCVD technique.

Process Characteristic	Advantage
Solvent-free	Easy stacking of polymeric films Limited damage to the substrate Copolymerization with immiscible monomers Reduced waste generation
Vapor-phase	Conformal coverage One-step film formation Extremely low level of impurities Tunable film properties
Uniqueness of iCVD/oCVD	Retention of organic functionality Applicability of various monomers Scalable Mild, low power processes
Use of polymeric materials	Low cost Flexible Wide variety of functional groups Well-known structure-property relationships

2.2.4 Types of Antifouling Coatings for RO membranes

Among the various antifouling coatings developed are poly(ethylene glycol) (PEG)/Oligo
(ethylene glycol) (OEG) [40]. Being more hydrophilic PEG/OEG coatings can bind the
surface water molecule tightly and as a result are less susceptible to biofouling due to
hydration via hydrogen bonding [41]. However, due to oxidative degradation of
PEG/OEG, these materials are not suitable for long-term applications [31]. Even stronger
electrostatic force between surface water molecules and zwitterionic-based materials via

electrostatically induced hydration has been found [42, 43]. Owing to their stronger electrostatic bonding, zwitterionic materials have shown great potential for preparation of ultralow fouling surfaces [44, 45] and are discussed in detail in section 2.2.5. Polyhydrophilic and polyzwitterionic are the two main classes of antifouling materials, however, only zwitterionic polymers are summarized in table 2.2, detailed description of polyhydrophilic materials has been provided in reference [46].

Table 2.2. Overview of zwitterionic antifouling materials [46].

Polybetaine	Protein adsoprtion	Cell adhesion
Poly(CBAA) [43,62,85,102,122,123]	Yes	Yes
Poly(SBMA) [100,102,124,125]	Yes	Yes
Poly(CBMA) [83,126]	Yes	Yes
Poly(MPC) [119,127,128]	Yes	Yes
PC-SAM [87,102]	Yes	Yes
OPC-SAM [87,102,129]	Yes	Yes
Polyampholyte		
SA/TMA-SAM [19,87,102]	Yes	Yes
CA/TMA-SAM [19,87,102]	Yes	Yes
PM/TMA-SAM [19,87,102]	Yes	No
Peptide surfaces derived from natural amino acids [90]	Yes	No
Poly(TM-SA) [12]	Yes	No
Poly(METMA-MES) [14]	Yes	No
PDDA/PSS [130]	Yes	No

2.2.5 Zwitterionic Antifouling Coatings for RO membranes

A zwitterion may be defined as a neutral molecule that contains both positive and negative charge (*but not dipoles*) at different locations within that molecule. In other words, zwitterions are ionic polymers with their total charges neutralized, or broadly speaking, amphoteric polymers are known as zwitterionic polymers [43]. Although, protein adsorption can be reduced by most water soluble polymers to some degree, the most excellent non-fouling ability of polymers can only be achieved when surface

21

hydration and steric repulsion work together. It is regarded that both chain flexibility and chain hydration are essential for antifouling characteristics, however, chain hydration has been found to have a dominant role if chain flexibility plays little role as depicted in figure 2.8.
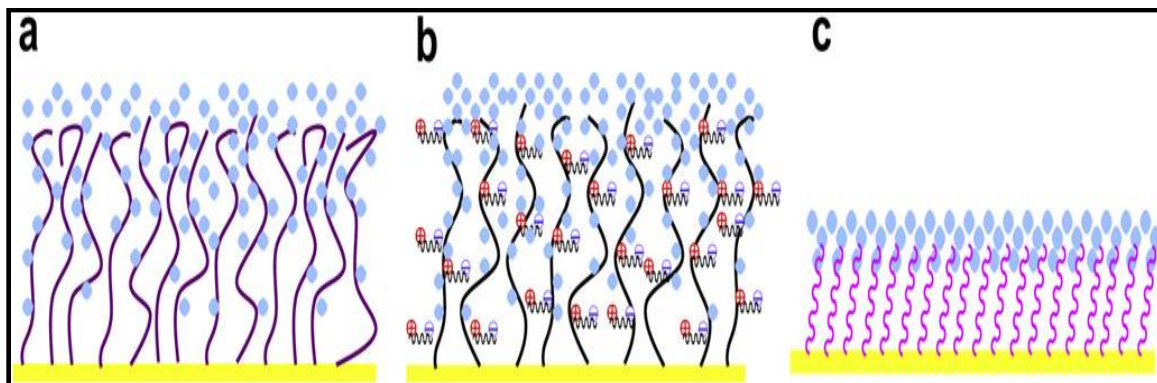
Figure 2.8 Demonstration of chain flexibility and chain hydration of (a) hydrophilic polymers, (b) zwitterionic polymers, and (c) Self assembled monolayers (SAMs), which attribute to surface resistance to nonspecific protein adsorption in different ways. [46].

Encouraged by the anti-biofouling characteristics of blood cell membranes, polymers containing zwitterions molecules have been employed as potential ultra-low fouling or anti-biofouling coatings (due to their ultra-low protein adsorption and outstanding antifouling properties) in areas such as biomedical applications [47]. Additionally, these materials have been extensively investigated as hydrophilic or fouling-resistant modifiers [48-51]. Some relevant examples include the synthesis of sulfobetaine methacrylate (SBMA), 2-methaeryloyloxy ethyl phosphorylcholine (MPC) and carboxybetaine methacrylate (CBMA). These zwitterionic coatings have been frequently used as hydrogels [52, 53], polymer brushes [50, 54], double-hydrophilic copolymers [55, 56], and polyelectrolytes [57]. Polyzwitterionic brushes grafted on flat surfaces have gained

particular attention as potential candidates for fabricating "zero" fouling or non-fouling surfaces [58, 59]. Recently, Zhuan Yi et al. produced polysulfobetaine methacrylate (pSBMA) and polycarboxybetaine methacrylate (pCBMA) by ATRP [60]. Bãrboiu et al. have prepared macromolecular carboxybetaines by reacting vinyl pyridine polymers with α,β-unsaturated carboxylic acids. They found that reacting 4-VP with alpha,beta unsaturated acids (i.e., the weak acid acrylic acid) resulted in major fractioning of betaine units; however, reacting 4-VP with maleic acid (a strong acid) resulted in betaine and corresponding salts [61].

A number of novel methods have been developed to synthesize zwitterionic coatings. The most common of these techniques include self-assembled monolayer (SAM) formation [45], solution polymerization with solvent evaporation [43, 62] and atom transfer radical polymerization (ATRP) [59, 63-65]. These methods have several limitations, e.g., SAMs require specific surface functionality, which limits this method to gold substrates. The use of harsh solvents in ATRP, such as pretreatment with 3,4-dihydroxyphenyl- L-alanine (DOPA) [45] prior to ATRP, are not suitable for delicate RO membranes. Furthermore, use of solvents in solution polymerization and ATRP not only damage delicate substrates such as RO membranes but may also lead to increased surface roughness, which deteriorates anti-biofouling properties. Therefore, solvent-free deposition of antifouling coatings on RO membranes is the best strategy.

Initiated chemical vapor deposition (*i*CVD) is a solventless and all-dry deposition technique. The iCVD method is capable of retaining functional groups on deposited polymeric surfaces as opposed to other deposition processes such as plasma-enhanced chemical vapor deposition (PECVD) and UV plasma and solution-phase polymerization.

For instance, labile functional groups are not well retained and may be easily cleaved from the surface during PECVD. During UV plasma coating, the high-energy excitation from the UV plasma results in a range of side reactions that influence monomer functionality and therefore compromise the antifouling character of the gel coating [66]. Zhuan Yi et al. [60] synthesized amphiphilic precursor poly(vinylidene fluoride)-graft-N,N-dimethyl aminoethyl methacrylate (PVDF-g-PDMAEMA) by ATRP followed by blending with PVDF to synthesis flat membranes. Synthesized membranes were then reacted with tetrahydrofuran (THF) solution and a quaternizing agent: either 1,3 propane sultone (PS) or 3-bromopropionic acid (3-BPA), which yielded SBMA or CBAA, respectively. XPS results showed that only 70% of PDMAEMA was quaternized in 48 hours with 1,3-propane sultone, while only 62% of PDMAEMA was quaternized in 96 hours with 3-bromopropionic acid. The lower conversion (quaternization) of PDMAEMA precursor and resulting reduced surface zwitterionic content may be the result of both the synthesis by ATRP, which may burry some of the PDMAEMA, and the liquid-phase reaction conditions, which has even lower diffusion kinetics compared to gas-phase reactions.

The first chlorine-resistant sulfobetaine zwitterionic chemistry has recently been synthesized by depositing 4-vinylpyridine and divinylbenzene copolymer via iCVD followed by reacting the copolymer with 1,3-PS in the vapor phase. The novel pyridine-based zwitterionic polymers enabled by iCVD have demonstrated good fouling resistance and exceptional chemical stability. These polymers compare favorably to methacrylate-based zwitterions, PEG and its derivatives, which suffer from various degradation pathways in real-world environments [67]. Recently, Kondo et al. synthesized a

zwitterionic poly(carboxymethylbetaine) (PCMB) brush on fused quartz substrate by surface initiated ATRP of CMB monomer. Their sum-frequency generation study revealed that electric neutralization diminished the effect of charges on side groups of the polymer chains in PCMBs that resulted in a small perturbation of the structure of vicinal water. An adjacent layer of water over the substrate (or RO membrane in this study) is highly desirable and is key to producing zwitterionic polymers (e.g., PCMBs) with very low-fouling properties [68].

CHAPTER 3

RO MEMBRANES: THEORY AND PRINCIPLES

3.1   Reverse Osmosis Membranes

A thin film composite (TFC) RO membrane is essentially composed of three layers as shown in figure 3.1. The bottom layer is highly porous and made of polyester, the intermediate layer with micron size pore is generally made of polysulfone and, the top layer, also known as active or barrier layer, is made up of either polyamide (fully aromatic) or polypiperazinamide (partially aromatic) as shown in figure 3.2(a) and 3.2(b) respectively. The active layer of TFC-RO membranes is virtually dense and nonporous (with pore size ranging from 3 to 5 A° in diameter), and this size range falls within the range of thermal motion of the polymer chains that form the membranes.
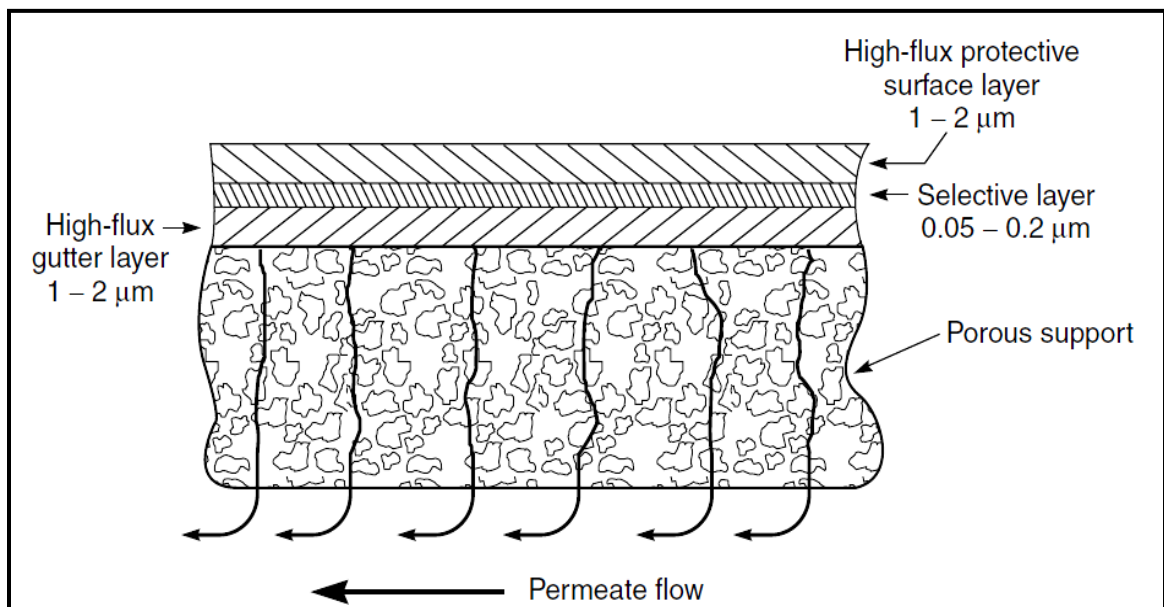
Figure 3.1. Structure of thin film composite (TFC) RO polyamide membranes [69].
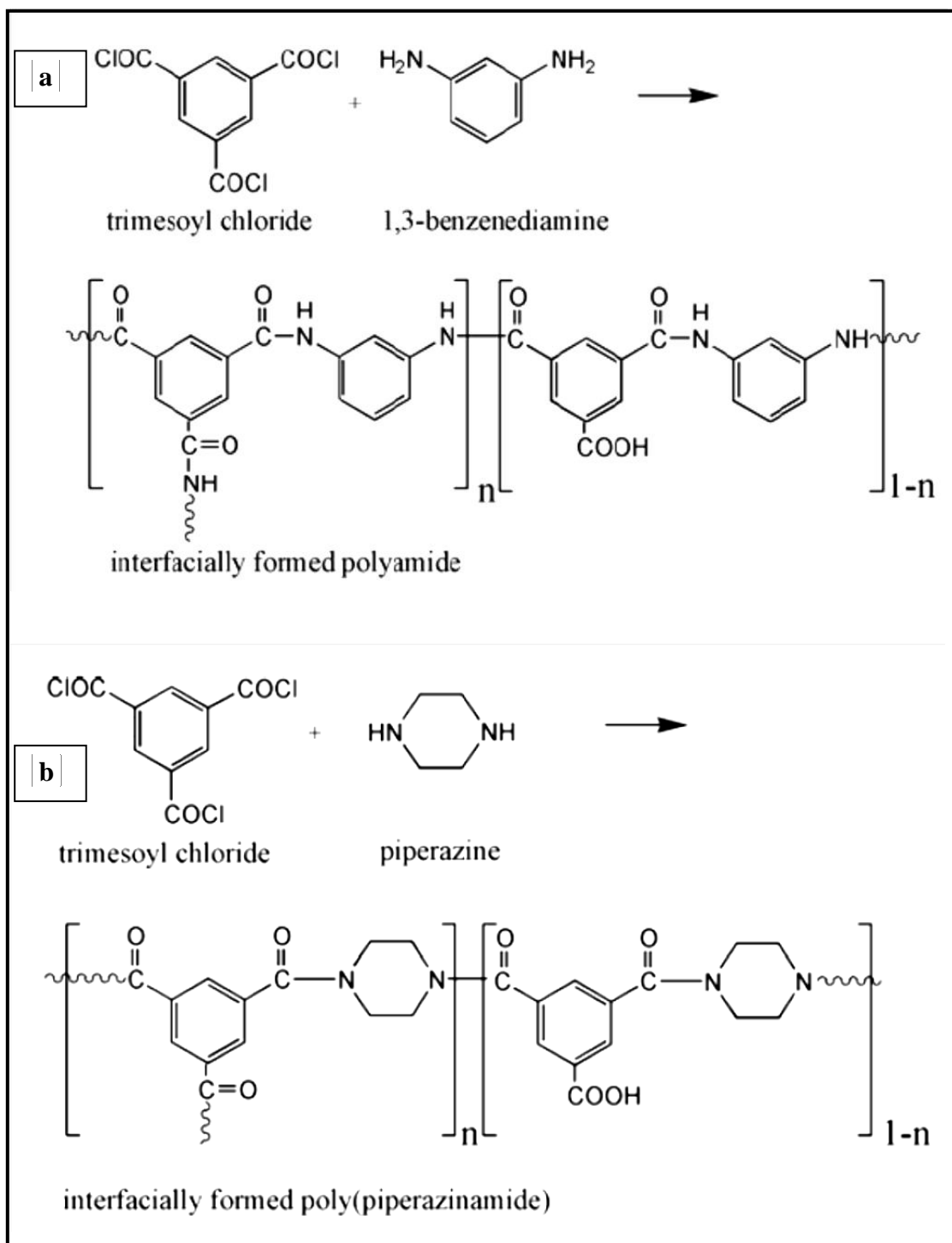
Figure 3.2 Typical chemistry of interfacially formed TFC-RO membranes. The symbol n represents the extent of crosslinking (value of n ranges from 0–1; where n = 1 means fully cross-linked polyamide and n = 0 implies fully linear one). (a) Fully aromatic polyamide and (b) semi-aromatic polyamide based on trimesoyl chloride and piperazine [70] .

Based on performance and pore size, RO membranes can be classified into three major groups:

1. Seawater membranes (SWM): these membranes are at higher salt concentration (3-5 wt. % salt solutions) and higher pressure (800 to 1000 psi).

2. Brackish water membrane (BWM): these are operated with intermediate salt concentration (2000 to 10,000 ppm salt solution) and pressure (200 to 400 psi).

3. Nanofiltration membranes (NF): these are normally operated with lower salt concentration (200- 500 ppm salt solutions) and pressure (100 -150 psi).

3.1.1 RO Membrane Transport Theory

For dense membranes (pore size 5 A° or lesser) like RO membranes, the well understood method of transport through RO membranes is known as the solution diffusion model (SDM) [3]. According to this model, solute dissolves itself in the membrane material followed by diffusion along the concentration gradient. Separation is achieved on the basis of varying solubilities and motilities of different solute in the membrane. The major application of RO membrane is in the desalination of seawater or brackish ground water.

3.1.2 Solution Diffusion Model (SDM)

In RO membranes, permeation is not a pressure-driven process but a diffusive process that is controlled by the motion of the polymer chains [69] and is dictated by Fick's law of diffusion, which states that the flux of a component i is proportional to the concentration gradient of that component (eq. 3.1).

$$J_i = -D_i \frac{\mathrm{d}c_i}{\mathrm{d}x}$$

Equation 3.1

Where J_i is flux of component i (g/cm^2.s), D_i is the diffusion coefficient (cm^2/s) and is an indicative of the mobility of individual molecules and dc_i/dx is the concentration gradient of component i. The term is called the diffusion coefficient and is a measure of the mobility of the individual molecules. The negative sign represents that the direction of diffusion is down the concentration gradient.

The SDM model is based on the two assumptions: first; *the pressure within a membrane is uniform* and second; *the chemical potential gradient across the membrane* is expressed only as a concentration gradient. The results of these two assumptions are explained in figure 3.3, which dipicts pressure-driven permeation of a one-component solution through a membrane by the SDM.

Integrating equation 3.1 over the thickness of the membrane then gives;

$$J_i = \frac{D_i(c_{i_{o(m)}} - c_{i_{\ell(m)}})}{\ell}$$

Equation 3.2

An important expression for osmotic equilibrium, relating the chemical potential gradient to osmotic pressure, pressure drop across the membrane and velocity of the component (i) is given below:

$$\Delta(\gamma_i n_i) = \gamma_{i_\ell} n_{i_\ell} - \gamma_{i_{\ell(m)}} n_{i_{\ell(m)}}$$

Equation 3.3

Where, n_i *and* γ_i are the mole fraction (mol/mol) of component i and activity coefficient (mol/mol) respectively. For small change in activities equation 3.3 reduces to;

$$\Delta(\gamma_i n_i) = \frac{-\upsilon_i(p_o - p_\ell)}{RT} = \frac{-\upsilon_i \Delta\pi}{RT}$$

Equation 3.4
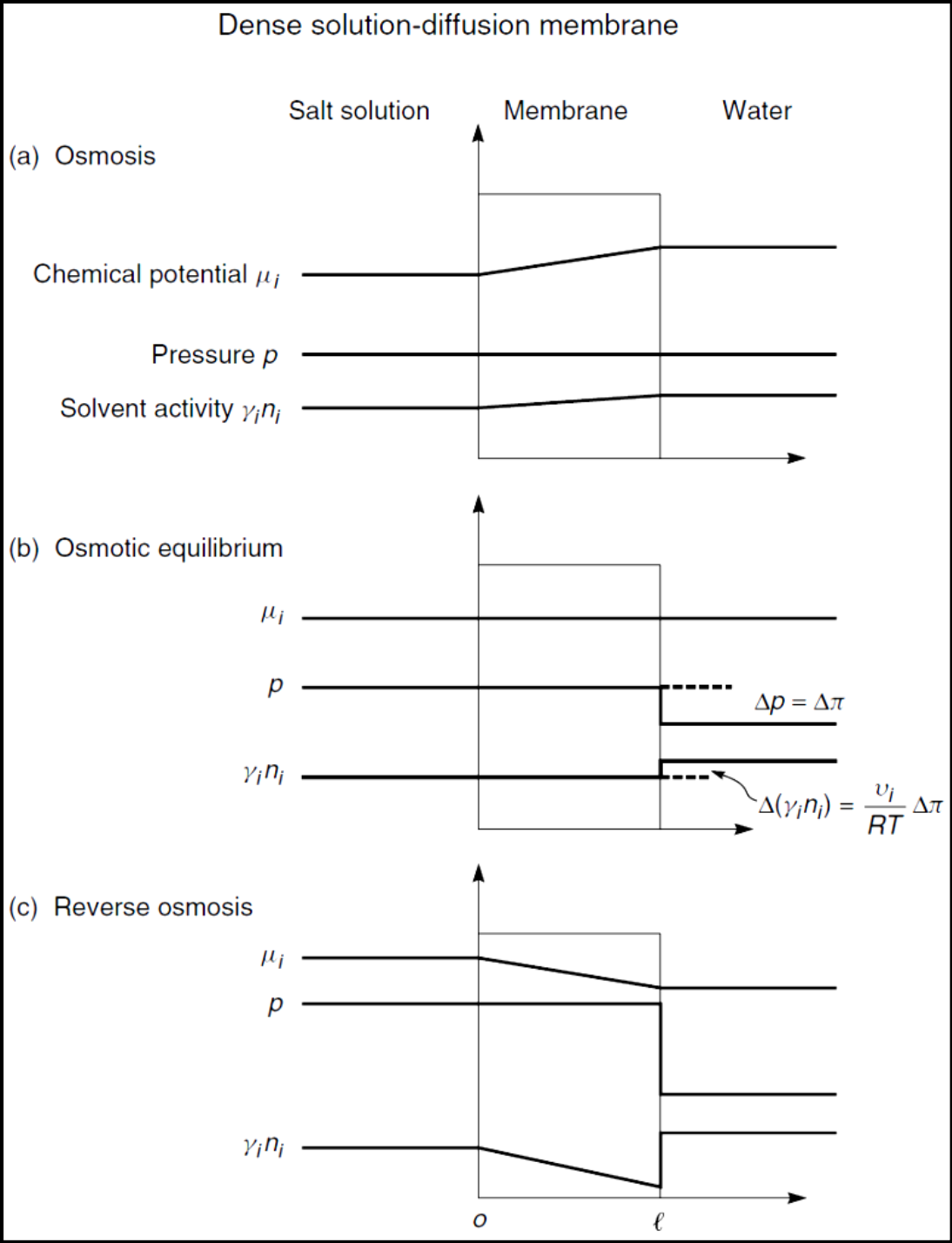
Figure 3.3. Illustration of pressure-driven permeation of a one-component solution through a membrane according to solution-diffusion model that explains chemical and pressure gradients in dense solutions membranes [69].

As a result, the solvent activity difference, $\Delta(\gamma_i n_i)$, across the membrane is balanced by the pressure difference $((p_o - p_l) = \Delta\pi)$ across the membrane, and the flow is zero. If a flow from left to right is desirable then pressure higher than the osmotic pressure needs to be applied on the feed side of the membrane, as depicted in figure 3.3(c), this is accompanied by further increase in solvent activity difference across the membrane. This is the process of reverse osmosis. The important point to be noted is that, even though the concentration and pressure of the fluid on either side of the membranes may be different, there is no pressure gradient (but only a concentration gradient) within a perfect solution-diffusion membrane, as elucidated in figure 3.3. Flow through this type of membrane is represented by Fick's law, Equation (3.2).

As mentioned earlier, in an RO process, pressure higher than the osmotic pressure is applied to the brine/salt side of the membrane, thereby reversing flow of water from salt solution to the pure water side of the membranes as illustrated in figure 3.4.
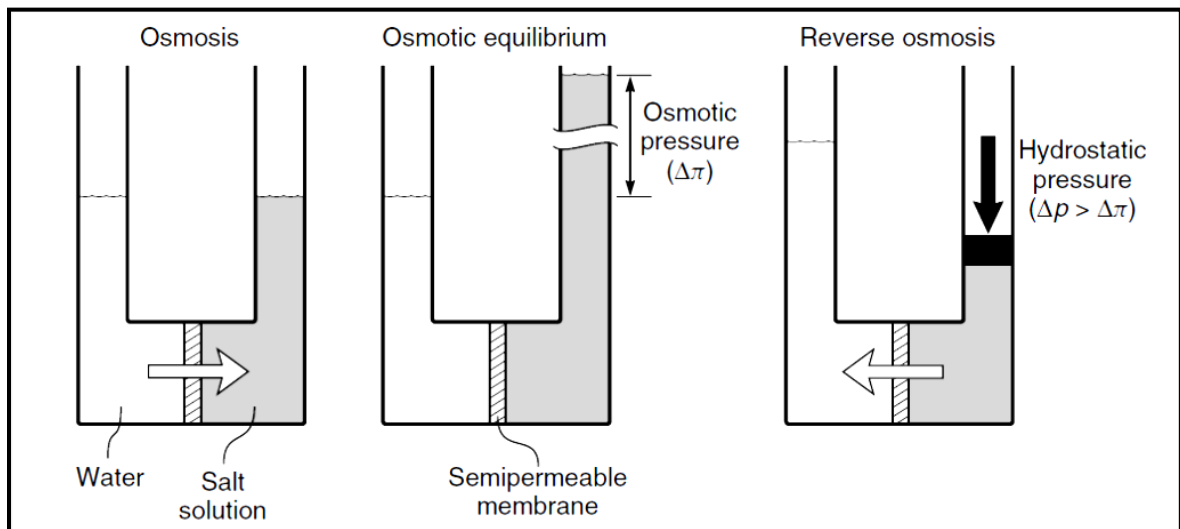
Figure 3.4. A schematic demonstration of the relationship between osmosis (dialysis), osmotic equilibrium and reverse osmosis.

At hydrostatic pressures higher than $\Delta\pi$, a simplified equation of Fick's law yielding the water flux (permeate), J_i, under normal RO process, can be approximated as:

$$J_i = A(\Delta p - \Delta\pi)$$

where Δp is the difference in hydrostatic pressure across the membrane $(p_o - p_l)$. The constant A is known as the *water permeability constant*. Likewise, a simple equation for the salt flux, J_j , through the membrane may be deduced as:

$$J_j = B(c_{j_o} - c_{j_\ell})$$

where B is known as the *salt permeability constant*. The SDM can be applied to RO process in order to predict the transport of salt and water. Equation (3.5) suggests that the water flux through an RO membrane increases with increasing applied pressure once a pressure greater that the osmotic pressure of the salt solution is applied, however, water flux remains small up to osmotic pressure. Whereas, Equation (3.6) implies that the salt flux is actually independent of pressure. Salt rejection can be quantified by a term known as the rejection coefficient, R, and is defined as:

$$\mathbb{R} = \left(1 - \frac{c_{j_\ell}}{c_{j_o}}\right) \times 100\,\%$$

where cj_o and cj_l are the concentrations of salt in feed and permeate respectively. Thus rejection coefficient is an index of salt rejection and quantifies the separation ability of the membrane to separate salt from the feed solution. It is important to note that by increasing applied pressure rejection coefficient increases, since the water flux increases with pressure, but the salt flux does not.

CHAPTER 4

*i*CVD: THEORATICAL BACKGROUND

4.1   Chemical Vapor Deposition (CVD)

Thin films synthesis methods, such as Ink-jet printing, tape casting, spin-coating or dip-coating are widely used since they are cheaper and ease to scaling up [71]. Nevertheless, use of solvents required in these processes have deleterious effects on the deposition process, e.g. the solvent used may spoil the delicate (or fragile) substrate, it may even cause the underlying layer to degrade and/or alter the mechanical properties of the fragile substrate. In addition, defective films could be the result because of the impurities introduced by the solvent such impurities are not desirable for high-purity applications. Solvent drying process also results in the inhomogeneous deposition of solutes [72].

On the other hand, CVD methods are a dominant technology for tailoring and engineering surfaces. CVD is another thin film synthesis technique that involves the evaporation of the target (materials to be coated) and simultaneous deposition on the substrate (the material/component on which the coating is desired), thus avoiding the deleterious effects of solvent on thin films. The use of CVD methods provides several attributes such as, better control over film thickness and conformal coatings that uniformly coats various geometric features, including microparticles, nanotubes and trenches [73, 74].

Nevertheless, CVD is most commonly used for the deposition of inorganic thin films where high substrate and process temperatures are involved. These process conditions, however, are not suitable for the synthesis of polymer thin films since they can destroy the functionality desired in polymer film. With the rapid advancement of polymeric thin

films, these are being utilized in a multitude of application fields ranging from biomedical, electronics, energy, selective permeation of gases and liquids. However, the use of polymeric thin films in these fields require the retention of functional group present in the monomers and thus necessitating the mild temperature conditions that are not possible in a traditional CVD processes.

4.1.1 *Initiated* Chemical Vapor Deposition (iCVD)

A variant of traditional CVD method, termed as the initiated CVD (*i*CVD), is unique in that it requires mild thin film synthesis conditions, i.e. low energy input, low surface temperatures, and yet produces higher deposition rates. *i*CVD is an all dry, solventless and vapor phase thin film deposition technique. Another salient feature of *i*CVD technique is conformal coating and the benign reaction conditions used during deposition makes sure that chemical functionality is retained [75, 76].

Being a one-step film-growth method, the *i*CVD proceeds with free-radical chain-growth polymerization. Mild deposition conditions (ambient temperature and low pressure) make it possible to modify the surface with functional polymers. Substrate modification can be achieved on nearly any substrate: organic, inorganic, stiff, plastic, planar, three-dimensional, dense, or porous. In *i*CVD polymerization, the monomer(s) are passed over the substrate (surface to be modified) in vapor phase wherein simultaneous polymerization and thin film formation takes place. An initiating species is also fed in the gas phase along with the monomers. Free radical polymerization proceeds via thermal decomposition of initiator as it passes through filament under mild temperature condition as shown in figure 4.1(a) [77]. *i*CVD method can ensure 100% functional group retention with high deposition rate through linear free-radical polymer chains.
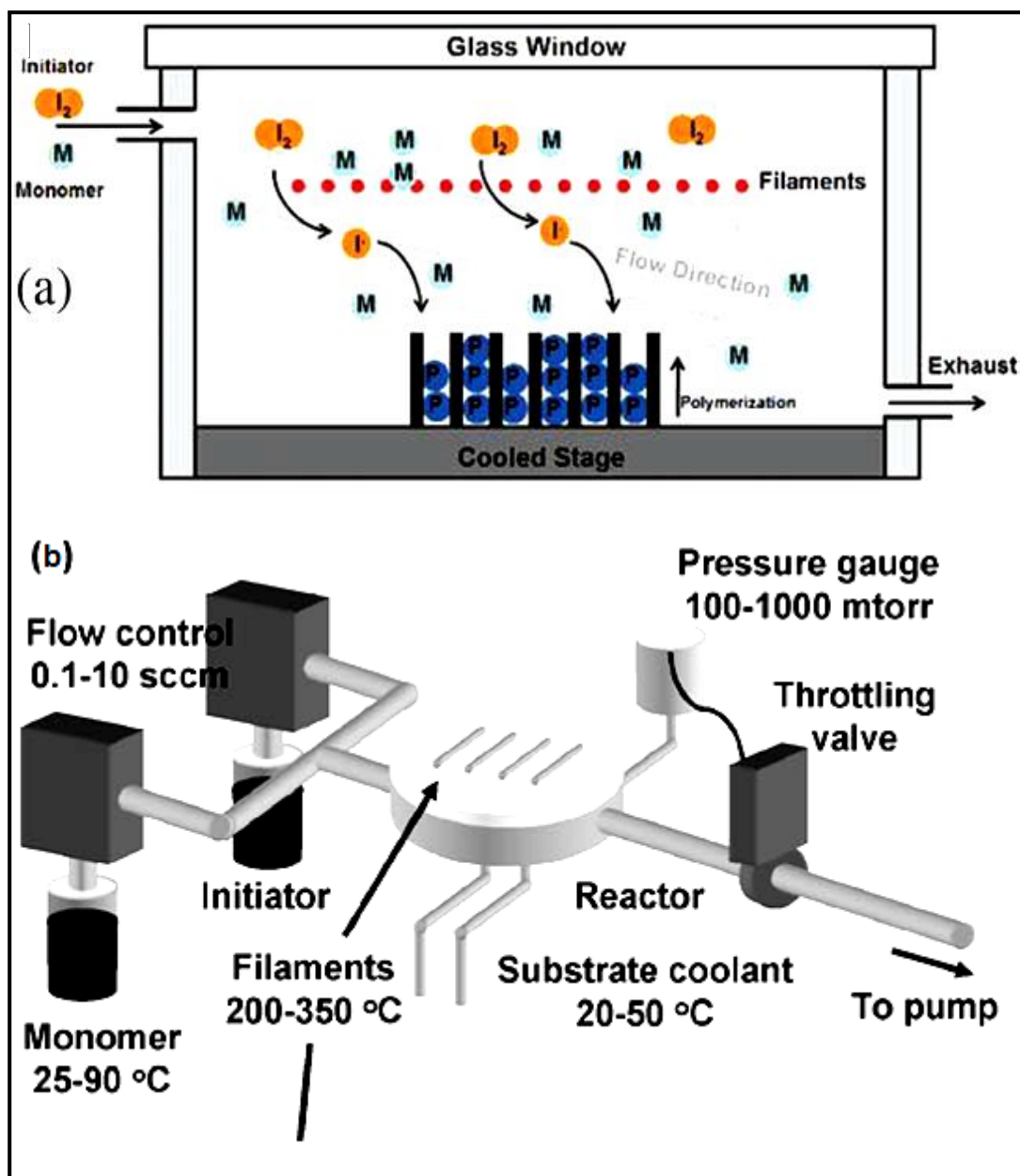
Figure 4.1. (a) Schematics of iCVD process and (b) essential components of an *i*CVD reactor.

*i*CVD coatings have been employed for microelectronics, sensing, wettability, reduced or antibacterial bacterial adhesion and protein adsorption control applications [78, 79]. Furthermore, *i*CVD coating have been successfully applied to applications requiring, tailored surfaces and interfaces, responsive surfaces (for biotechnology) and selective

permeation. In addition, *i*CVD is a unique method for modifying the surfaces of delicate, flexible, and nonplanar substrates where the wet chemistry methods are not possible. Figure 4.2 provides highlights of the *i*CVD thin films used as antifouling applications [76].

*i*CVD has several advantages over other thin films deposition techniques. To mention a few, by eliminating the need to dissolve macromolecules, *i*CVD makes sure insoluble polymers to be coated and avoids solvent damage to the substrate and it also ensures full retention of the functional groups. *i*CVD demonstrates successful results to control molecular interactions at material surfaces for the designed micro- and nano-engineered materials [66]. Table 4.1 shows comparison of iCVD with other surface modification techniques for the synthesis of zwitterionic chemistries.
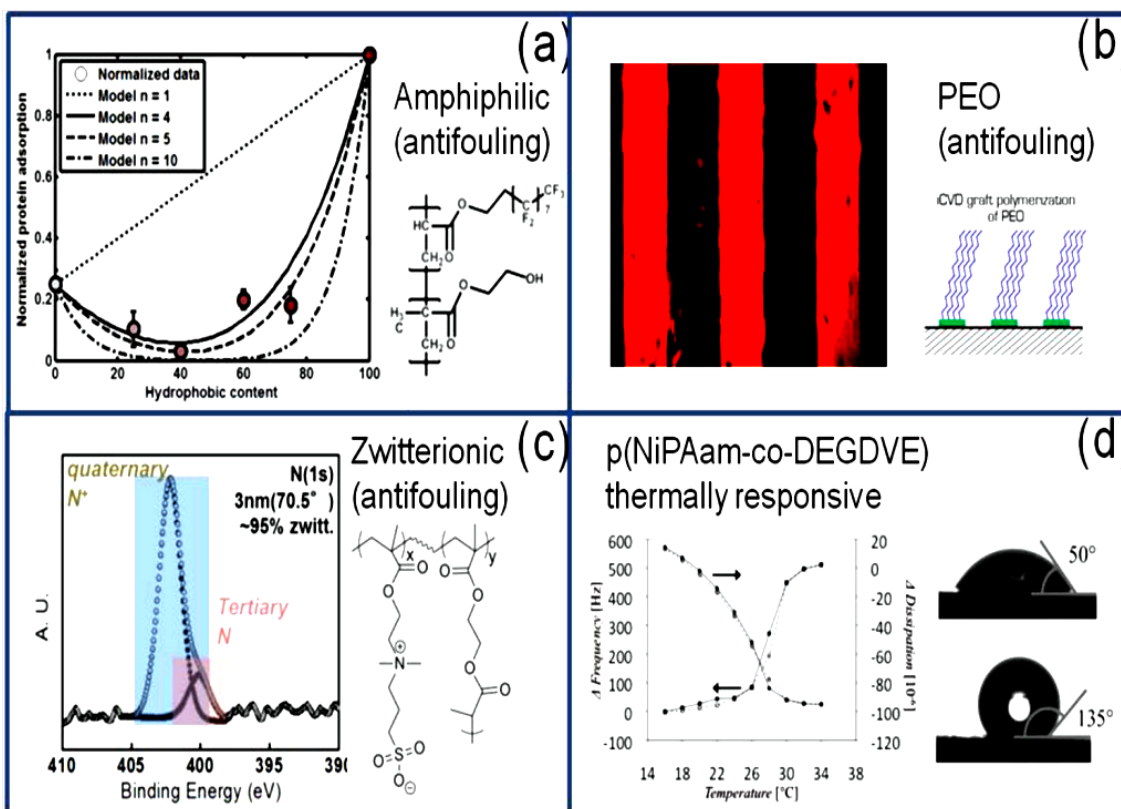
Figure 4.2. iCVD surfaces showing controlled interface with biomolecules and/or protein. a) Structure and antifouling action of iCVD p(HEMA- *co* -PFDA) with various compositions. b) iCVD polyethylene oxide (PEO) patterned coatings on silicon wafer and subject to protein adsorption tests; coated areas oppose protein attachment effectively. c) Structure and surface enrichment of zwitterionic coatings as illustrated by high resolution N1s XPS scans. d) Water contact angle of multi walled carbon nanotubes modified with iCVD PNIPAAm films below (top) and above (bottom) the LCST. The mass and viscoelasticity display a step change near the LCST as revealed by QCM-D [66].

Table 4.1. A comparison of the potential surface modification techniques for synthesizing zwitterionic antifouling chemistries. Adapted from [67].

Methods	[a]SAMs	[b]ATRP	[c]BSP	[d]LBL	[e]iCVD
All dry processing	No	No	No	No	Yes
Substrate Independence	No	No	Yes	No	Yes
Synthesis rate (mm min^{-1})	10^{-3}	10^{-3}	10^{-3}	-1	-10
Small post-treatment roughness	Yes	Yes	No	No	Yes
Conformal coating	Yes	Yes	No	Yes	Yes
Ultra-thin coating	Yes	Yes	No	Yes	Yes
Greater surface-enrichment of zwitterionic contents	Yes	Yes	No	Yes	Yes

a= self assembled monolayers; b= atom transfer radical polymerization; c= bulk solution polymerization; d=layer by layer deposition and e= initiated CVD.

CHAPTER 5

Experimental

5.1 Materials

4-Vinylpyridine (4-VP) (95% 4-VP, from Sigma Aldrich, USA) and ethylene glycol diacrylate (EGDA) (90% EGDA, from Sigma Aldrich, USA) were the two monomers used in this study. 4-VP was used as the precursor for quaternization reaction as it contains a tertiary nitrogen in the aromatic ring of pyridine whereas, the EGDA was utilized as the cross linker to make the copolymer water insoluble. *Tert*-butyl peroxide (TBPO) (97% tert-butyl peroxide, Sigma Aldrich, USA), was employed as the imitator. 3-bromoproionic acid (3-BPA) (97%, Sigma Aldrich, USA) was utilized as the quaternizing agent during the post-deposition reaction. All the three chemicals were used without additional treatment/purification and are shown in figure 5.1.
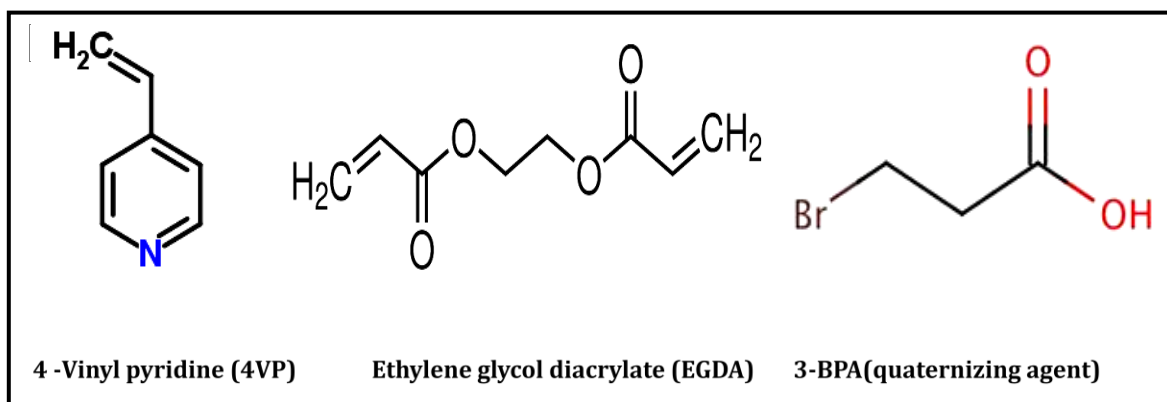
Figure 5.1. Structure of two monomers (4-VP, EGDA) and the quaternizing agent (3-BPA).

Two commercial RO membranes, TFC-HR and SW-30HR were surface modified by the synthesized zwitterionic antifouling coating. Table 5.1 summarizes the specifications of these two membranes.

Table 5.1. Commercial RO membrane specifications.

Commercial RO membranes	Manufacturer	Performance parameters		
		Salt Rejection	Flux at 800 psi $(L/m^2 \cdot hr)$	pH Range
TFC-HR	Koch	99.5	140	4-11
SW-30 HR	Dow FILMTECH	99.7	27.4	2-11

5.2   Methods

5.2.1   Synthesis of Copolymer Films and Zwitterionicalization

Different compositions of copolymer p(4-VP-co-EGDA) coatings were deposited on silicon wafers and commercial RO membranes using an iCVD reactor (Sharon Vacuum) previously described in detail [80, 81]. In separate glass jars attached to the reactor, the EGDA monomer (vapor pressure = 0.0939 Torr at 25 °C) and the 4-VP monomer (vapor pressure = 1.68 Torr at 25 °C) were heated and the TBPO initiator was maintained at room temperature, and their vapors were fed into the chamber over heated filament arrays (80% Ni-20% Cr, Good fellow, USA). Copolymer compositions within the deposited films were varied by systematically changing the vapor flow rate of each monomer while keeping the initiator flow rate fixed.

Copolymer p(4-VP-co-EGDA) coatings were deposited on test grade silicon (Si) wafers (Wafer World, USA) without any pretreatment. Before deposition, commercial RO membranes TFC-HR (Koch Membrane System, USA) with area approximately 11x7 cm^2 were cleaned with high purity argon and then treated with oxygen plasma for five minutes. According to the manufacturer specifications, the Koch membranes are of polyamide type and do not contain any antifouling coating on their surfaces. During iCVD depositions, 97% *tert*-butyl peroxide TBPO, (Aldrich), 90% EGDA (Sigma Aldrich), 95% 4-VP (Sigma Aldrich) and argon were fed into the iCVD reactor at room temperature through mass flow controllers (1479 MFC, MKS Instruments, USA). EGDA and 4-VP monomers were heated to 85°C and 55°C, respectively, and the flow rates of both monomers were systematically varied to yield varying zwitterionic content on the deposited copolymer films. During thin film synthesis, the filament temperature was maintained at 200 °C while the substrate was fixed at 20 °C. Total pressure in the vacuum chamber was maintained at 0.450 Torr for all depositions. Table 5.2 describes all parameters adopted during iCVD depositions and provides subsequent compositions obtained for all deposited copolymer films.

Deposited film thicknesses were examined *in situ* by interferometry with a 633 nm He-Ne laser source (JDS Uniphase). Thicknesses of deposited Si wafers were more accurately measured by a Woollam M-2000 Spectroscopic Ellipsometer (J. A. Woollam Co., Inc., USA). Ellipsometery was performed using 190 wavelengths from 315 to 718 nm at three different incident angles (65°, 70°, 75°). The data was fit using the Cauchy-Urbach model.

Table 5.2. iCVD parameters adopted for the synthesis of homo and copolymer films (p(4-VP-co-EGDA)).

Material	4-VP Flow Rate (SCCM)	TBPO Flow Rate (SCCM)	EGDA Flow Rate (SCCM)	Ar Flow Rate (SCCM)	4-VP contents in the film[a] (%)
pEGDA	0	2.0	5.0	2.0	0
Copolymer 1	6.4	2.0	0.24	2.6	85
Copolymer 2	6.0	2.0	0.58	2.5	45.5
Copolymer 3	6.2	2.0	0.72	2.2	25
p(4-VP)	6.4	2.0	0	2.0	100

[a] Composition was calculated by measuring carbonyl peak area of respective FTIR spectra and was normalized to the carbonyl peak area of homopolymer (pEGDA).

Zwitterionicalization of the deposited copolymer was obtained by exposing the film to vapors of the quaternizing agent (3-BPA). Coated substrates were securely fixed in a crystallization dish (from VWR, International, LLC.) with the coating facing downwards with 1gm of 3-BPA (Sigma Aldrich, 97%) placed at the bottom of the dish. The dish was then kept in a water bath heated to a temperature of 60 °C for a specified period of time to let the 3-BPA vapors react with the coating present on the substrate. Treated specimens were carefully rinsed with deionized water (DI) to get rid of loosely adhered quaternizing agent.

5.2.2 Compositional Characterization of Deposited Copolymer Films

A Nicolet Nexus 870 ESP Spectrometer (Thermo Nicolet, WI, USA) in normal transmission mode was used to obtain Fourier transform infrared (FTIR) spectra. A deuterated triglycine sulfate (DTGS) KBr detector over the range of 400 to 4000 cm^{-1}

was utilized with 4-cm^{-1} resolution. FTIR spectra were taken on freshly deposited Si wafers and after post-treatment. Signal-to-noise ratio was improved by averaging at least 100 measured spectra.

X-ray photoelectron spectroscopy (XPS) survey spectrum and higher resolution spectra of N1s were obtained using SSX-100 Kratos Axis Ultra Spectrometer (Surface Science Instrument, USA) with a monochromatic Al Kα source. Samples were kept under vacuum overnight prior to analysis. Casa XPS processing software (CasaXPS Manual 2.3.15, rev 1.3, 2009, Casa Software Ltd., USA) was used to fit the high-resolution spectra with Shirley-type background. The obtained high-resolution spectra (C1s, O1s and N1s) were calibrated with respect to C1s = 284.5 eV to remove any charging effects.

5.2.3 Surface Characterization of Synthesized films: XPS and ARXPS Analysis

X-ray photoelectron spectroscopy (XPS) and angle resolved XPS (ARXPS) was performed using a SSX-100 Kratos Axis Ultra Spectrometer (Surface Science Instrument, USA) with a monochromatic Al Kα source (1486.66 eV). Survey scan was obtained at 150 W with pass energy and step size of 160W and 1eV, respectively. For high resolution scans, the pass energy and step size were 20W and 100 eV, respectively. Pressure during the analysis was maintained at 2×10^{-8} Torr. XPS measurements were taken from an elliptical area of ~1x3 mm^2 at two emission angles of 0° and 71° for the angle-resolved XPS (ARXPS). Escape depth corresponding to each emission angle was calculated utilizing the inelastic mean free path (IMFP) of the element under consideration. Prior to analysis, all the samples were stored under vacuum overnight. To remove any charging effect, all core level spectra were calibrated to C1s neutral carbon peak at 284.5 eV that

was obtained at emission angle of 55°. Each spectrum was curve fitted by using CasaXPS software (CasaXPS Manual 2.3.15, rev 1.3, 2009, Casa Software Ltd., USA) and keeping Shirley as background.

Depth profiling was performed on thicker (~250 nm) copolymer films deposited on Si substrates and were conducted by removing the coating material (ArP$^+$P ions bombardment) at an approximate etch rate of 3-4 nm/sec. At least 10 etch cycles were performed removing material (~ 8-10 nm/etch step) to go deep down to ~ 90 nm from the surface. XPS measurements were taken after every etch step. For reproducibility, analysis were performed on duplicate samples and average reported as the amount of quaternary and protonated nitrogen present in the thickness direction (along the cross section of deposited film) as a function of film depth.

5.2.4   Contact Angle (CA) Goniometry

Sessile drop contact angles were measured under ambient conditions (25 °C and 1 atm) utilizing a goniometer equipped with an automatic dispenser (Model 500, Ramé-Hart). A 2-µL droplet of deionized water was placed on the specimen, and the contact angle was measured immediately after contact. At least five measurements were performed on each specimen sufficiently apart from each other, and the average was reported as the contact angle of the surface under study.

5.2.5   Fouling Resistance Testing: QCM-D Analysis

Fouling propensity of bare, as-deposited and zwitterionic coatings in three model foulants bovine serum albumin (BSA), sodium alginate (SA) and humic acid (HA) was investigated using QCM-D (Model E4, Q-sense, Sweden). This was done by depositing the coatings on sensors (QSX-303, from Q-Sense). BSA, SA and HA represent protein,

polysaccharide and natural organic matter, respectively. SA and HA were dissolved in DI water, whereas, BSA was dissolved in phosphate-buffered saline (PBS) and solution concentration of 1mg/mL was used for all the three foulants in all test runs. $SiOR_2R$ sensors with a fundamental frequency of 5 MHz were used as iCVD coating substrates. Zwitterionic, as-deposited and bare (reference) sensors were placed in flow cells and allowed to equilibrate for at least 20 minutes at 25°C by flowing DI water (for HA and SA) and PBS for BSA at flow rate of 100 μL/min. After achieving the stabilized flow, the solution was promptly changed to SA or HA in DI water, or to BSA in PBS, and the frequency shift was monitored. Adsorbed mass of each foulant was calculated by using Sauerbrey relation, for the frequency shift at the third and fifth harmonics. The average of Δm_3 and Δm_5 (masses calculated from 3rd and 5th harmonics, respectively) was reported as the foulant mass adsorbed.

5.2.6 Static Bacterial Adhesion Tests

Resistance to bacterial adhesion under a static environment was tested in nutrient broth (supplied by Scharlau, Barcelona, Spain) utilizing three different bacterial strains; a non-pathogenic strain of Escherichia coli (E. coli, K12 wild-type MG 1655), pseudomonas aeruginosa strain and bacillus licheniformis. An appropriate amount of nutrient broth was dissolved in DI water at room temperature according to the supplier's instructions. Broth solution was autoclaved at 121 °C and 1.12 bar for 3 hours. The three bacterial strains were then inoculated in cooled broth solutions separately and cultured overnight at 37 °C in Trypton media until reaching mid exponential phase. Aliquots of pre-culture were inoculated in fresh medium and incubated under the same conditions stated above until reaching an absorbance of 0.41 at 600 nm, which corresponds to approximately 4.1×10^8

CFU/ml. Approximately 30 ml of each bacteria solution was then transferred to test tubes.

Duplicate bare and modified membrane samples, approximately 1x1 cm^2, were immersed in the test tubes making sure that each membrane coupon was completely exposed to bacterial suspension and remained isolated from air during exposure to the bacterial strain for 2 hrs. Exposed samples were gently rinsed with fresh nutrient broth (without bacteria) to remove any loosely adhered bacteria. The membrane coupons were then dried by mildly blowing N_2 gas over each specimen. The membrane coupons were fixed onto specimen stages with double sided copper tape, sputter coated for 5 minutes, and then observed under SEM (JEOL, JSM, 6460LV, Japan). For quantification of attached bacteria, a 0.0133 mm^2 area of each sample was observed at relatively smaller magnification (3000X), and at least 25 images were taken at locations sufficiently apart on duplicate samples. The number of attached bacteria on the images was counted manually.

5.2.7 Performance Evaluation (permeation, separation and alginate fouling tests)

Performance (permeate flux, salt rejection and alginate fouling) evaluation tests were performed on a permeation test rig equipped with a cross flow permeation cell CF 042 (STRELITECH, Corp. USA). Koch membranes were compacted for 18-20 hours at 300 psi in DI water before taking any measurements. DI water was pumped from the feed tank by a Hydra Cell pump (Model no. M03SASGSSCA, MN, USA) and was recirculated into the feed tank to maintain a constant concentration. The temperature of the feed water was maintained at 21 °C ± 1 °C via a constant temperature circulation bath

(Polystat, Cole Parmer, USA) connected to the permeation test setup. Permeate volume was collected for five minutes in a measuring flask (100 ml) and was converted to flux in L/m^2 hr. At least three readings were taken every hour and the average was reported as permeate flux. After compaction, an appropriate amount of sodium chloride (NaCl) was thoroughly mixed in 1 liter of DI water and then added to the feed tank to make a feed water concentration of 2000 mg/L salt. After further stabilization for 45 minutes, permeate volume was once again collected for 5 minutes and measured to determine the permeate flux of the feed salt water. Such measurements were repeated three times every hour and averaged for the reported average flux. Percentage salt rejection was measured using the following equation:

$$\%R = (CF - CP)/CF, \qquad\qquad \text{Equation 5.1}$$

Where CF and CP are the concentration of salt in the feed and permeate solutions, respectively, which were measured with a conductivity meter (YSI-3200, Conductivity instruments, Yellow Spring, OH, USA) equipped with a type 3252 conductivity cell.

Alginate fouling tests were performed using alginic acid (sodium alginate, SA) as a model foulant (representing the polysaccharides) under identical conditions of temperature and pressure. Required amount of SA (Sigma Aldrich, USA) was first dissolved in 1 liter of DI water and magnetically stirred at room temperature until dissolved completely and was then transferred to the feed tank to make feed water concentration of 100mg/L. After stabilization of one hour, permeate water flux, J_{SA} in the presence of SA and salt was recorded as described above. The flux J_{SA} was compared to the permeate flux J_w before alginate and salt addition to calculate the flux decline. At least 3 readings were taken every hour until 6 hours. For consistency, duplicate samples

of bare and modified Koch membranes were tested under identical conditions. Post-alginate fouling analyses were performed by characterizing the surface morphology of deposited foulant (SA) on the bare and modified Koch membranes. This was accomplished by taking the SEM images of duplicate fouled membranes samples.

5.2.8 Atomic Force Microscopy (AFM)

Surface roughness was measured using an MFP-3D AFM (ASYLUM Research, USA) in tapping mode. Taping mode was selected to avoid damaging membrane samples with the AFM tip. Dry membrane samples, with dimensions 1 cm $\times$ 1 cm, were mounted perfectly flat on a glass slide using double-sided tape. For better accuracy and precision, measurements were performed at different locations and with variable scan areas. At least three images of each sample were taken by scanning 10x10 μm^2 and 20x20 μm^2 areas sufficiently apart from each other utilizing tips with spring constants between 0.5-4.5 N/m and fundamental frequencies between 315-366 kHz (OTESPA, Bruker). The average surface roughness was reported in terms of root mean square (RMS) measurements.

5.2.9 Molecular Force Mapping (MFP)

MFP was performed by using bovin serum albumin (BSA) functionalized AFM tip (600 nm SiO2 tip from Nova scan with spring constant 0.06 N/m) to investigate the interaction forces between the foulant (BSA) and the bare and modified (coated and functionalized with 3-BPA) Koch membranes surfaces. During these tests the cantilever deflection is measured as a function of the vertical displacement of piezoelectric scanner. This results in a cantilever deflection (d) vs. scanner displacement (z) curves which were transformed into respective force- separation distance (F-d) curves. This was accomplished by

converting the cantilever deflection into a force (F) using Hooke's law (F = - k x d, where k is the cantilever spring constant) and subtracting the deflection from the scanner displacement to get the distance (z-d). The zero separation distance (or point of contact) is determined as the position of the vertical (or near vertical) parts of the curve in the contact region.

Force spectroscopy measurements were carried out using MFP-3D (model: 805-696-6466 by ASYLUM Research) in Phosphate buffer saline (PBS) environment, where a BSA-functionalized AFM tip approached the membrane surface at a constant AFM piezo displacement rate of 1 μm s^{-1} in PBS. The maximum adhesion force gauged from the retraction portion of the force-distance curves was defined as attractive force between the cantilever and the surface under study. Experiments were performed on duplicate samples (approximately 1 cm^2) of both bare and modified Koch membranes. The measurements were repeated at least 36 times at different locations for each tip-surface pair.

To gain further insight into the foulant and the membrane surface interaction, adhesive force as a function of tip dwell time (ranging from zero second to 10 seconds) was measured on the bare and zwitterionicalized Koch membranes. An area of 20x20 μm^2 of each membrane was scanned and 36 measurements were taken on each specimen for dwell time of 0, 2, 4, 6, 8 and 10 seconds. Average adhesive force (F_{ad}) as a function of tip dwell time was thus obtained in this way.

CHAPTER 6

RESULTS AND DISCUSSION

6.1 Synthesis of Copolymer Film and Zwitterionicalization

iCVD is a facile vapor-phase method used for conformal deposition of a variety of homo/copolymers on virtually any substrate. The solventless/all dry nature of iCVD makes it particularly attractive when substrates to be coated are delicate such as commercial RO membranes. Thicker films (up to 250 nm) of homo-polymers p(4-VP) and pEGDA and copolymer p(4-VP-co-EGDA) were first deposited on Si wafers. The ratio of the partial pressure (P_m) and saturated partial pressure (P_{sat}) of the monomer at the temperature of the substrate during deposition, P_m/P_{sat}, was adjusted to control the deposition rate and growth of the films. This ratio was varied from 0.3 to 0.5 to optimize deposition conditions and to control different compositions of the copolymer p(4-VP-co-EGDA) films. Higher values of P_m/P_{sat} lead to higher deposition rates and poor conformality [82]. P_{4-VP}/P_{sat} of ~0.30 and P_{EGDA}/P_{sat} of ~ 0.24 were employed during copolymer deposition after optimization. The chemical composition of copolymer was tuned by adjusting flow rates of precursors, as described in Table 5.2. To keep the total flow rate constant and maintain the same residence time for each deposition, continuous flow of argon gas was used.

Prior to deposition, Koch membranes were cleaned by high purity argon gas and were then treated with O_2 plasma for 5 minutes to render some oxide dangling bonds on the membrane surface (Figure 6.1(a)). These dangling bonds most likely form between amine
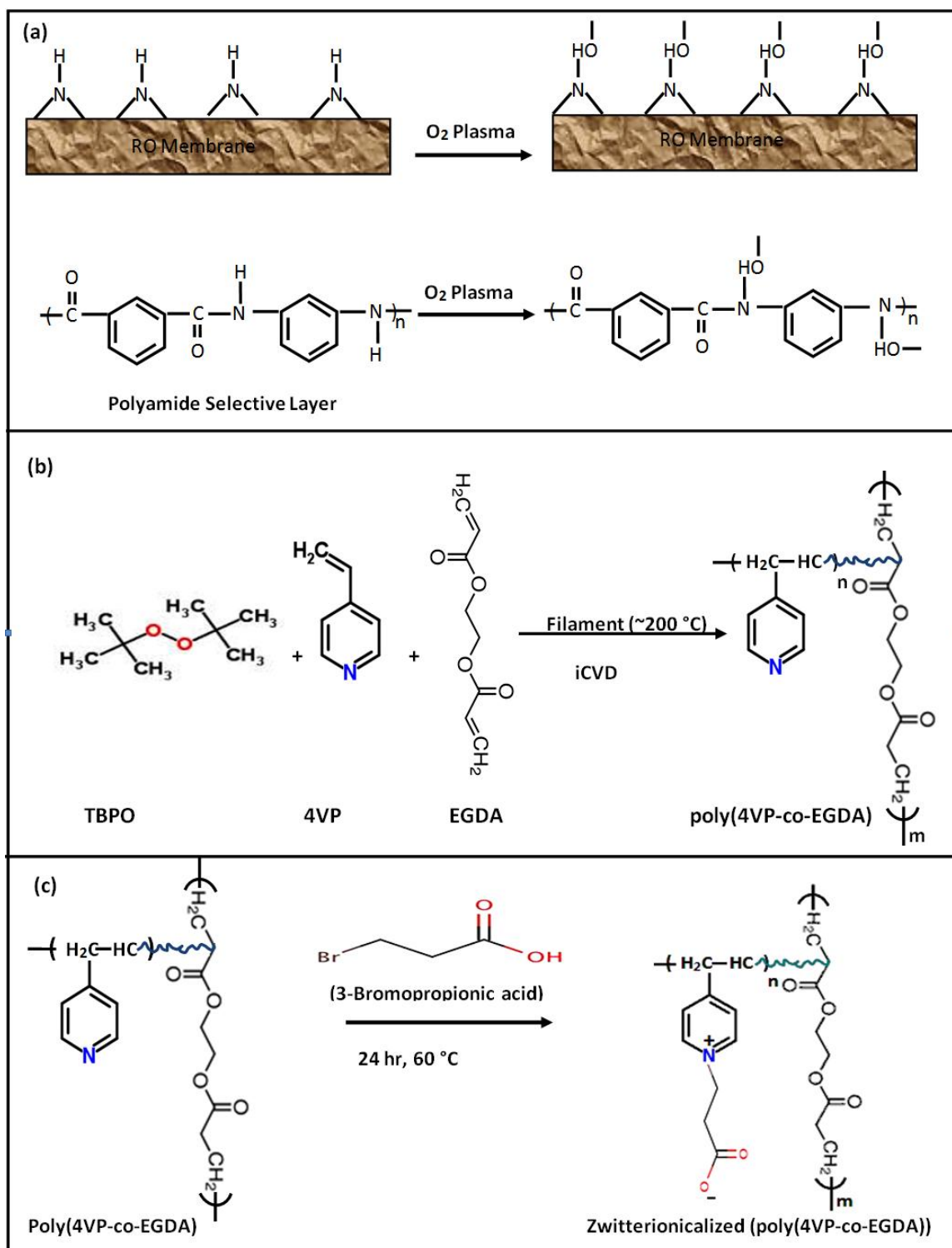
Figure 6.1. Structure and synthesis route for the formation of copolymer films: (a) surface modification of active polyamide layer by O_2 plasma treatment, (b) synthesis of copolymer films by iCVD and (c) post-deposition functionalization with quaternizing agent 3-BPA.

groups present in the active layer of polyamide RO membranes and help to establish a strong interface via covalent bonding between the membrane surface and the copolymer film. This strong bonding eliminates delamination of deposited copolymer film when placed in water. Recently, R. Yang et al. [39] used maleic anhydride (MA) to provide grafting between copolymer and substrate (RO membranes). However, the use of MA may be a serious concern because it can condense in mass flow controllers (MFCs) and clog their surfaces; the iCVD reactor would need to be pumped for a few hours to remove any physisorbed MA. Therefore, oxygen plasma treatment provides a two-fold advantage by eliminating chances of film delamination and avoiding cumbersome MA treatment.

The reaction between 4-VP and α/β unsaturated salts of carboxylic acid acetates (CAAs) has been reported earlier [4]. More recently, Zuhan Yi et al. used tetrahydrofuran (THF) solution with 3-BPA to convert DMAEMA precursor to poly-carboxybetaines; however, possibly due to use of liquid-phase reaction conditions, low surface zwitterionic content (~62% after 96 hrs.) was obtained at the surface of RO membranes. However, in the present work, gas-phase diffusion limited reaction between quaternizing agent (3-BPA) and copolymer film, yielding higher conversion (~88% as calculated from high resolution N1s scan by XPS) of precursor tertiary nitrogen (the nitrogen in aromatic ring of the reactant 4-VP) to quaternary nitrogen (the nitrogen in the reaction product pyridinium ion). It is interesting to note that this higher content of zwitterions was achieved only in 24 hours, which is only one third of the time used in the study of Li-Ping Zhu's group [60]. It is also important to note that a higher surface concentration of zwitterions (at the very top ~10 nm) is crucial to provide low fouling properties.

6.2 Thin Film Characterization (FTIR and XPS studies)

Figure 6.2 shows FTIR spectra of as-deposited iCVD coatings: homopolymers (p4-VP and pEGDA) and different compositions of copolymer films with varying amounts of EGDA (cross-linker). FTIR spectra of the copolymers are resolved into spectra of the characteristic functional groups present in both constituent monomers. The peak at 1734 cm^{-1} is characteristic of carbonyl stretching present in EGDA whereas peaks present at 1597, 1558 and 1415 cm^{-1} are characteristic of the aromatic pyridine ring. Relatively broader peaks at 2960 cm^{-1} are representative of various methyl and methylene groups attached to 4-VP and EGDA units in the copolymer film. To have different cross-linking densities and zwitterionic content in the copolymer films, the amount of EGDA was varied and calculated by the area under carbonyl peaks of respective FTIR spectrum, which were normalized with respect to the homo-polymer (pEGDA) spectra.

Post-deposition functionalization was performed by reacting a copolymer film with 3-BPA at 60 °C for 24 hours. During functionalization, precursor tertiary nitrogen (reactant) in the pyridine was converted to quaternary nitrogen producing pyridinium ion. The high wave number shift in the pyridine peak from 1597 cm^{-1} to 1641 cm^{-1} confirmed conversion of tertiary nitrogen in pyridine into quaternary nitrogen in pyridinium ion. The higher frequency peak at 1632 cm^{-1} was ascribed to ring stretching of pyridinium ions in zwitterionic copolymer films [83, 84]. Our observed increase of 9 cm^{-1} is explained below. Appearance of a new peak (present only in the reacted copolymer) at 1380 cm^{-1} is due to COO^{-} symmetric stretching [85]. The formation of zwitterionic structure was witnessed by emergence of peaks at 1641 cm^{-1} and 1380 cm^{-1} in the reacted copolymer films after reaction with 3-BPA as shown in Figure 6.3(a). The quaternizing

53
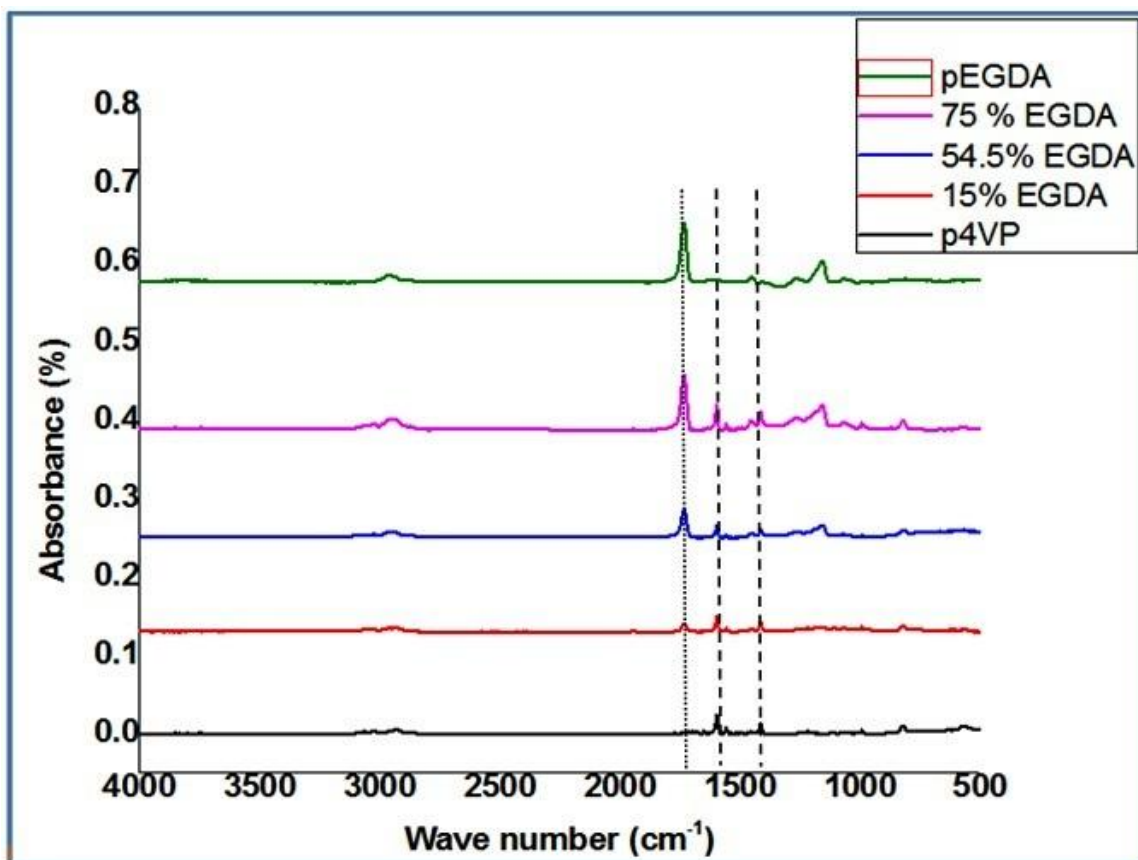
Figure 6.2. FTIR spectra of the as-deposited homopolymers and copolymer (p(4-VP-EGDA)) films. Dotted line indicates the carbonyl peak at 1734 cm^{-1} and dashed lines represent major pyridine peaks at 1597 cm^{-1} and 1415 cm^{-1}.

reaction (pyridine to pyridinium ion formation) was confirmed by high resolution N1s XPS scans of reacted and unreacted p(4-VP-EGDA) films as depicted in Figure 6.3 (b, c). The binding energy of ~398.8 eV corresponds to the tertiary nitrogen (unreacted nitrogen) in the pyridine. In our case this energy was shifted to higher values of ~400.1 eV and ~402.1 corresponding to hydrogen bonded nitrogen and quaternary nitrogen (fully protonated nitrogen: pyridinium ion), respectively, resulting from the reaction between the copolymer film and the vapors of quaternizing agent (3-BPA) as shown in figure 6.3 (c). The latter species has been reported to undergo a positive binding energy shift of 2.1
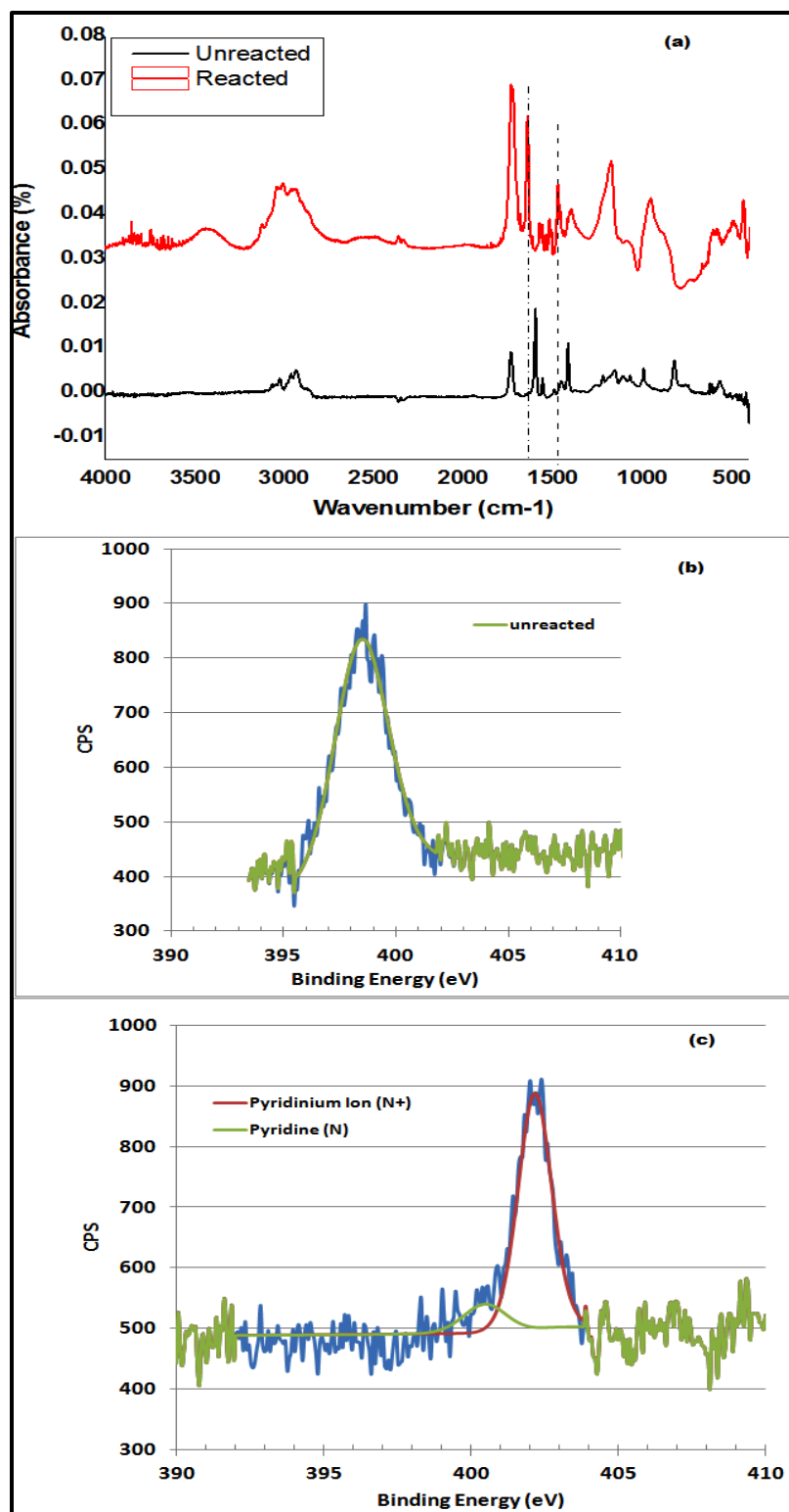
Figure 6.3. (a) FTIR spectra of unreacted (as-deposited) and reacted (functionalized with 3-BPA) copolymer films, (b) high resolution N1s scan of unreacted copolymer film and (c) high resolution N1s scan of copolymer film functionalized with 3-BPA.

to 2.5 eV from neutral nitrogen in pyridine [86]; however, in our study, the higher binding energy shift was ~3.3 eV, which explains the 9 cm^{-1} higher frequency shift observed earlier in the FTIR spectra. Thus, we demonstrated that iCVD produced the zwitterionic copolymer (p(4-VP-co-EGDA)), which contains carboxybetaine units, as confirmed by both FTIR and XPS data. As the diffusion limited gas-phase reaction with quaternizing agent never reaches 100%, the zwitterionic conversion as result of quaternizing reaction was found to be almost 90% as calculated from the respective peak areas under tertiary and quaternary nitrogen from N1s high resolution spectra. This set of data was obtained at an emission angle of 55° and corresponds to an analysis depth of ~5-7 nm.

6.2.1 Surface Characterization of Synthesized films: XPS and ARXPS Analysis

XPS being the surface sensitive elemental technique was employed to investigate the surface concentration of zwitterionic moieties. The quaternary nitrogen, product of the reaction, introduces a new bonding environment that can be evidenced by higher binding energy (BE) peak shift observed in high resolution N1s spectra. As mentioned in the last section, a positive shift of ~ 2-2.5eV is associated to the bonding environment change between tertiary nitrogen (the reactant) and quaternary nitrogen (the product of the reaction). This higher BE shift confirms the hypothesis that zwitterionic structure has been obtained. As the diffusion limited gas-phase reaction with quaternizing agent never reaches 100%, the zwitterionic conversion as a result of quaternizing reaction was found to be almost 90% as calculated from the respective peak areas under tertiary and quaternary nitrogen N1s high resolution spectra.

This set of data was obtained at an emission angle of 55° and corresponds to an analysis depth of ~5-7 nm. After confirming the formation of zwitterionic moieties, the next step was to test the second hypothesis that zwitterionic groups are surface enriched. For this purpose depth profiling analysis were performed on thicker films (~250 nm) in order to obtain an analysis of variation of zwitterionic contents as a function of coating depth.

Almost ~10 nm-thick portion of the film was removed utilizing Ar^+ ion bombardment with each time step, and XPS measurement taken at each corresponding depth. Figure 6.4(a) represents the total percentage of quaternary ammonium and protonated nitrogen along the cross section as a function of film depth. It is obvious from the plot that up to an escape depth (depth sampled in high resolution XPS scan) of ~ 5 nm, the amount of quaternary ammonium and the protonated nitrogen is almost 90%, which significantly reduces to ~ 20% at an escape depth of ~10 nm and eventually vanishes beyond a depth of ~36 nm. It is important to mention here that surface concentration of zwitterionic groups observed currently is much higher than the zwitterionic groups obtained via solution based quaternizing reactions by Huang et al [87]. Their XPS results revealed that only 67% of tertiary nitrogen was converted to surface zwitterionic moieties after a liquid phase quaternizing reaction. These authors report that the surface concentration of zwitterionic moieties further reduces to 25% (for the case of solution-phase deposition). Angle-resolved XPS (ARXPS) is a well-known analytical technique to obtain more detailed compositional information in the z-direction (along the thickness of deposited film) deep down to ~10 nm. ARXPS measurements were also performed in order to investigate the fine composition profile of the top-surface (down to ~10nm). These measurements were performed at two emission angles of 0° and 71° to extract

compositional information from the two corresponding escape depths (depths examined in ARXPS scan) of ~9nm and ~3nm respectively. It is important to note that amount of tertiary nitrogen (pyridine) is almost 10 % (upto top ~3nm) which significantly increases to almost 30% (corresponding to analysis depth of ~10 nm) as estimated from the respective area of peaks (Figure 6.4 (b,c)). These results reveal that zwitterionic moities are highly surface enriched (within top ~3nm of the copolymer films).

Several other researchers [88-91] have also performed ARXPS studies to investigate the surface concentration of zwitterions (resulted from solution-phase methods). The surface concentration of zwitterions obtained in their films was significantly lower as compared to that obtained in our study. The higher surface concentration promotes greatly enhanced antifouling performance. It is worth mentioning that higher surface enrichment of the zwitterionic moieties achieved in our study is attributed to the diffusion limited gas phase reaction with quaternizing agent, 3-BPA. This higher surface enrichment of zwitterionic moieties at the membrane surface is highly desirable for attaining effective antifouling/ultralow fouling properties.
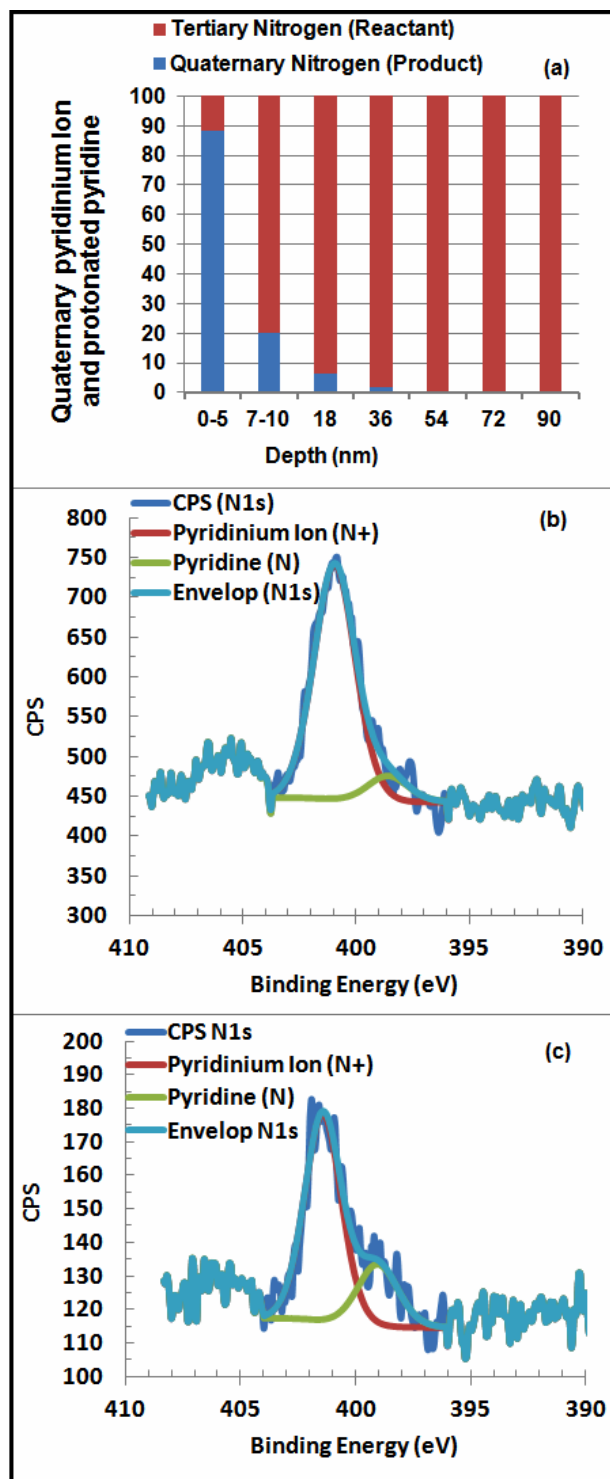
Figure 6.4. (a) Depth distribution of quaternary pyridinium and protonated pyridine in copolymer films (p(85% 4-VP-co-EGDA) functionalized with 3-BPA for 24 hrs at 60 C°. Angle resolved X-rays photoelectron spectroscopy (ARXPS) spectra of copolymer films deposited on Si wafers. High resolution N1s ARXPS scans taken at emission angles of (a) 71° and (b) °0, corresponding respectively to an escape depth of ~ 3 nm and ~ 9nm.

6.3   Contact Angle Goniometry

Contact angle measurement is a well-established method for measuring the hydrophilicity of a surface. Hydrophilicity is characterized by lower values of water contact angles. Lower values of contact angles are also indicative of higher wettability, which helps in the formation of a surface water layer. It is hypothesized that the non-fouling ability of both polyhydrophilic and polyzwitterionic materials are tightly correlated with a hydration layer near the surface [92, 93]. This surface water layer has also been reported to inhibit and/or discourage attachment of bacteria on surfaces immersed in water. Stability of deposited copolymer films was tested in DI water. For this purpose, modified Koch membranes, with different chemistries of as-deposited copolymer films, and bare Koch membranes were immersed in DI water for 24 hours, and static contact angles were measured before and after soaking as represented in Table 6.1. The copolymer film with the highest 4-VP content (85%) exhibited very similar water contact angles before and after soaking in DI water, indicating the excellent stability of this deposited copolymer film in DI water. However, copolymer films with higher EGDA content and bare Koch membranes showed increased values in contact angles after soaking. This increase in contact angle was attributed to an increase in surface roughness after soaking; had there been any delamination of the coating, there would have been a sudden drop in the contact angle. Therefore, all copolymer films were stable in DI water.

Figure 6.5 represents water contact angles of modified and bare Koch membranes. It is worth mentioning that the copolymer film with 85% 4-VP consistently showed the lowest contact angle (highest hydrophilicity), indicating a much lower increase in surface roughness after soaking compared to other copolymer chemistries. Water contact angles

were also measured before and after functionalization (zwitterionicalization) with 3-BPA on the same copolymer chemistry (85 % 4-VP) deposited on Si substrates. It was found that the water contact angle was greatly reduced (from 55.8° to 39.7°) after functionalizing as-deposited copolymer film with 3-BPA.

Table 6.1. Effect on contact angle from soaking coated and bare Koch membranes in deionized water for 24 hours

Specimen	Contact Angle before soaking in DI		Contact Angle after soaking in DI	
	Range	**Average**	**Range**	**Average**
Copolymer 1	25-32	29	26-34	29.9
Copolymer 2	36.6-47.3	41.6	33-57	39.8
Copolymer 3	37-46.5	42.9	39-58.5	47.8
Bare Koch Membrane	55-63	60.4	57-68	66.5

This sharp reduction in contact angle after functionalization is attributed to higher surface zwitterionic content in this copolymer film; this sample has the highest amount of precursor moieties (4-VP), which resulted in formation of zwitterions after reacting with quaternizing agent. As mentioned earlier, higher surface zwitterionic content helps maintain a strong surface hydration layer and is highly desirable for producing RO membranes with ultra-low fouling properties.
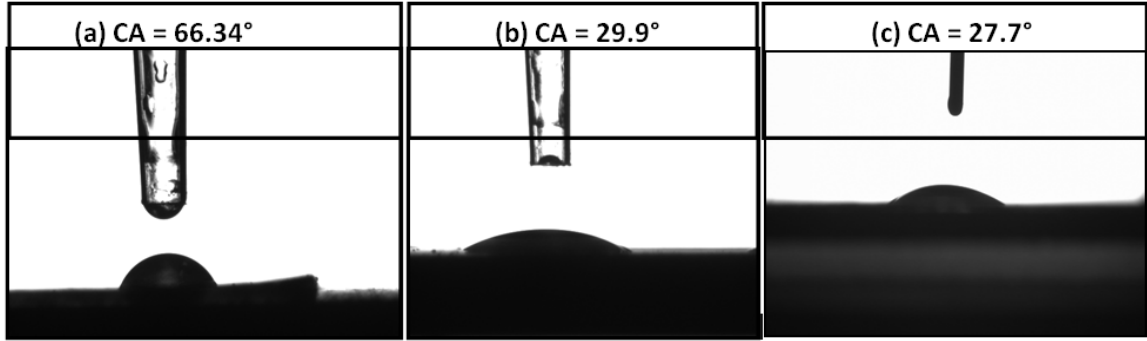
Figure 6.5. Average contact angles of (a) uncoated Koch membrane, (b) Koch membrane coated with copolymer p(85% 4-VP-co-EGDA) film and (c) Koch membrane coated with copolymer p(85% 4-VP-co-EGDA) after a six month shelf life.

6.4   Fouling Resistance Testing of Zwitterionic Coating

The fouling propensities of the three different compositions of copolymer coatings were first investigated with a model foulant (BSA) using quartz crystal microbalance with dissipation (QCM-D) monitoring. For this purpose, three different chemistries of copolymer-coated and functionalized quartz sensors (QSX-303) were monitored for adsorption of BSA by measuring the frequency shift (ΔF in Hz) when BSA solution was charged into QCM-D flow cells. To determine the optimal chemistry, the adsorption behavior of all copolymer coatings (copolymer 1, copolymer 2 and copolymer 3 in table 5.2) was tested in BSA solution under similar conditions. Figure 6.6 represents the QCM-D data obtained when 1 mg/mL BSA solution was flown over three zwitterionic copolymer coatings with different chemistries at constant temperature (25 °C). The mass adsorption of BSA was quantified using the Sauerbrey relationship, which gives a liner relationship between mass change and frequency shift:

$$\Delta m = -C\left(\frac{\Delta F}{n}\right),$$
<div align="right">Equation 6.1</div>

Where, Δm is the mass changed (ng./cm^2), C is the crystal-specific constant (17.7 ng. sec. cm$^{-2)}$, n is the overtone and ΔF is the frequency shift resulting from mass absorbed/adsorbed. For this relation to be valid, the adsorbed mass must be evenly distributed, not slip over the surface, be sufficiently rigid (so that it forms a very thin film) and offer negligible internal resistance [94]. Dissipation changes correlate with the viscoelasticity of the film formed by the adsorbed mass. Very small dissipation changes, particularly in the zwitterionic coating (copolymer 1), $\sim 1x \ 10^{-6}$ Hz), implies that BSA was surface adsorbed as opposed to absorbed. For the same zwitterionic coating (copolymer 1), the mass change was calculated to be ~ 9.51 ng.cm^{-2}, which corresponds to a frequency change of ~2.1 Hz. Much lower adsorption of BSA onto copolymer 1 (9.5 ng.cm^{-2} compared to 74.41 ng.cm^{-2}, 80.70 ng.cm^{-2} and 106.25 ng.cm^{-2} for the sensors coated with copolymer 2, copolymer 3 and bare sensor, respectively) indicated excellent antifouling properties of this zwitterionic chemistry (p(85% 4-VP-co-EGDA). Much lower adsorption of BSA onto zwitterionic coating (9.51 ng.cm^{-2} as compared to 80.70 ng.cm^{-2}and 98.25 ng.cm^{-2} for the as-deposited (coated) and uncoated respectively) indicate the excellent antifouling properties of zwitterionic coating. It has been both theoretically and experimentally accepted that higher surface zwitterionic contents help in forming a hydration layer (due to higher electrostatic interaction with ambient water), which helps in reducing the fouling of the surfaces [42, 43]. It has been both theoretically and experimentally accepted that higher zwitterionic content helps formation of a hydration layer (due to higher electrostatic interaction with ambient water), which helps reduce fouling of surfaces [42, 62].

Significantly reduced adsorption of BSA on the zwitterionic copolymer coating p(85% 4-VP-co-EGDA) compared to other zwitterionic coatings with lower 4-VP content (45.5% and 25%, table 5.2) was attributed to the higher 4-VP amount in this chemistry. As mentioned earlier, nitrogen in 4-VP is the precursor for the quaternizing reaction and yields higher surface zwitterionic content when treated with 3-BPA. Therefore, surface zwitterionic groups, which are produced by a diffusion-limited gas phase reaction at the very top surface, are responsible for the enhanced fouling resistance. It is important to mention that 15% EGDA in the copolymer film was enough to render the copolymer film water insoluble and to yield higher surface zwitterionic content, which was sufficient to provide enhanced fouling resistance. Conversely, copolymer chemistries with 54.5% and 75% EGDA contain lower amounts of precursor 4-VP moieties, which resulted in reduced surface zwitterionic moieties and hence enhanced mass adsorption (BSA adsorption). Consequently, we demonstrated that 85% 4-VP in the copolymer is optimal for improving fouling resistance.

The above findings, in conjunction with the earlier findings on SA adsorption [95], provide very promising insight for the zwitterionic copolymer films (p(85% 4-VP-co-EGDA)) as potential antifouling coatings for RO membranes. Even though, actual feed water of a particular RO plant is very complex, these findings are however quite significant with practical implications.
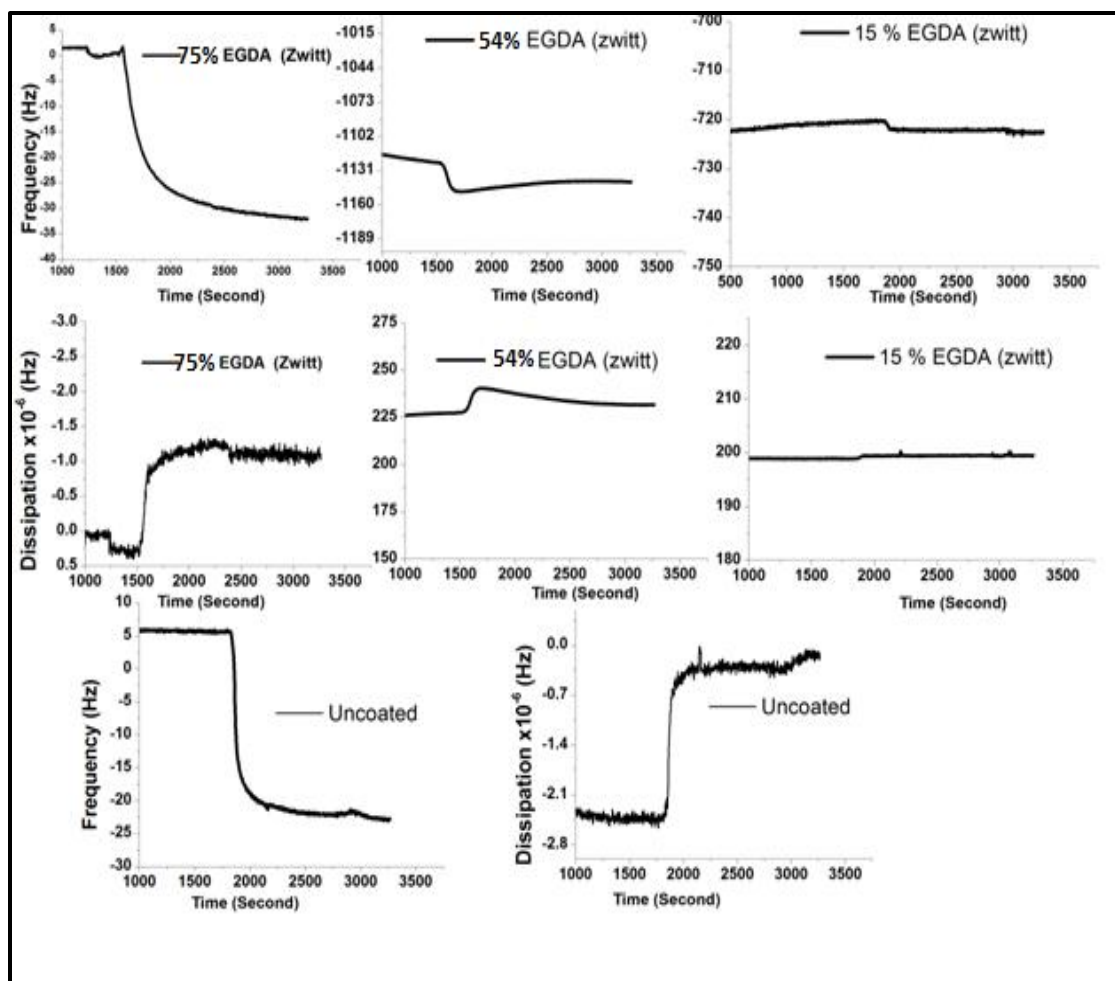
Figure 6.6. QCM-D data revealing the effect of different zwitterionic copolymer compositions on protein (BSA) adsorption on SiO$_2$ sensors. The uncoated sensor is presented for reference at the bottom of the figure. Dotted lines indicate the times when BSA solution was charged (~ 1500-1900 seconds).

Similar fouling tests were performed by flowing the same concentration (1 mg/mL) of SA or HA in DI water over the optimized zwitterionic chemistry (p(85% 4VP-co-EGDA), as-deposited and bare SiO$_2$ sensors placed in QCM-D flow cells. Fouling behaviors (masses adsorbed) of the three model foulants were calculated and were drawn as bar charts as shown in Figure 6.7. HA is a model foulant representing the humic substances and is commonly adopted in marine fouling tests. Higher dissipation and frequency shifts were observed when HA solution was passed over the sensors. Mass

changes calculated were ~33.34 ng.cm^{-2}, ~59.44 ng.cm^{-2} and ~74.71 ng.cm^{-2} respectively

for the sensors coated with zwitterionic copolymer (p(85% 4VP-co-EGDA) coatings, as-

deposited and bare. Rong Yang et al., have recently measured the adsorbed mass of HA

on the pSBs zwitterionic coatings to be 80 ng.cm^{-2} (the value is estimated from the
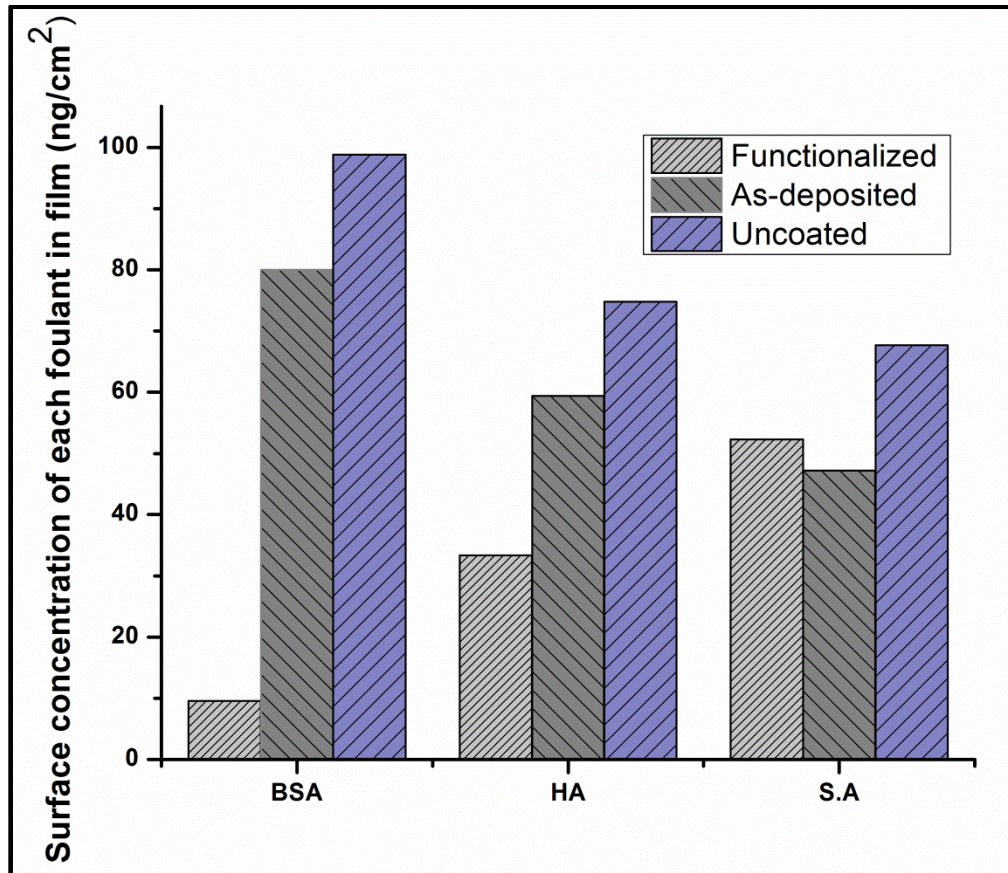
Figure 6.7. QCM-D data: Adsorbed mass on SiO$_2$ sensors as a function of the three foulants (BSA, HA and S.A) used.

figure 4(b) in their work) [96]. Whereas mass adsorbed found in the present work is only

~33.34 ng.cm^{-2} (which is approximately one third of the adsorbed mass of HA in their

study). This much lower adsorbed mass of HA on the zwitterionic coating p(85% 4VP-

co-EGDA) clearly indicates the superior performance (ultra-low fouling in HA solutions as well) of the zwitterionic coatings (with pCAAs units) in humic acid environment.

Finally, fouling due to SA was investigated. SA is another model polysaccharide that is widely used as a representative foulant in desalination and marine fouling studies [97]. However, when SA solution of the same concentration (1mg/L) was flown over the sensors even higher values of dissipation and frequency shifts were observed suggesting the multilayer deposition of SA on the sensors. Possible reason for the higher mass adsorbed in this case may be due to the ionic interaction between carboxylate and tertiary nitrogen. This ionic interaction may be caused by the protonation of the unreacted nitrogen (as quaternary reaction with 3-BPA never reaches 100% conversion) in the SA solution rendering the surface positively charged. However, further studies are warranted to prove this hypothesis.

6.5   Static Bacterial Adhesion Tests

Commercial reverse osmosis (RO) membranes are prone to fouling (specifically biofouling when the fouling source is of organic, inorganic or microbial origin), which results in a reduction in efficiency and an increase in chemical cleaning. Both of these factors result in loss of production and lower quality of final product, which is clean water. However, the most serious concern of RO plants is biofouling, and the reported economical loss ranges in the millions of dollars for larger plants [9].

After determination of the optimum film chemistry with regard to biopolymer adsorption (using BSA, HA and SA), the next step was to compare and contrast bacterial adhesion between the commercial membranes and the membranes modified with the optimized composition. For this purpose, the resistance to bacterial adhesion of the modified and

bare Koch membranes under static environment was investigated by exposing membrane coupons to E. coli, Pseudomonas aeruginosa and Bacillus bacterial strains. Attached bacteria were analyzed (both qualitatively and quantitatively) by SEM imaging. Figures 6.8-6.10 show attached bacteria on Koch membranes.

Figure 6.8 (a-e) shows attached E. coli cells on virgin Koch whereas Figure 6.8 (b-f) shows attachment of E. coli cells on membranes modified with optimized copolymer coating (p(85% 4-VP-co-EGDA)) and functionalized with 3-BPA in 24 hrs. Several colonies of E. coli bacterial cells were observed on the bare membranes with almost complete surface coverage of the exposed bare membranes, but no such colony was observed on the modified membranes, which clearly demonstrates the superior performance of the modified membranes against bacterial adhesion.

Quantification of attached bacteria was performed on SEM images taken at relatively smaller magnification (3000X or 3500X) to observe as much area as possible in the SEM images, while enabling easy identification of attached cells. Each SEM image was 0.0133 mm^2, and 25 SEM images were taken on two replicate membrane coupons for both bare and modified Koch membranes at locations sufficiently separated from each other to cover a larger area with greater distribution of attached bacterial cells.

Similar analyses were made for the modified and bare Koch membranes exposed to two other bacteria, namely Pseudomonas and Bacillus strains, which are abundantly present is sea water. Again the modified Koch membranes show significantly lower attachment of both bacteria compared to their counterpart bare Koch membranes as shown in figures 6.9 and 6.10.

Quantification was performed on 5,10,15, 20 and 25 SEM images following the method used by A. Matin et al. [95] with minor modification. The average number of attached bacteria was normalized to the area observed in each SEM image (0.0133 mm^2) and drawn as a bar chart (fig. 6.11). It is obvious from fig. 6.11 that bare membranes are very prone to biofouling with much higher bacterial attachment, 9145.8 ±234.5, 1270 ±45 and 787±36 of E. coli, pseudomonas aeruginosa and bacillus licheniformis cell/mm^2 respectively, compared to modified membranes, which show much lower number of attached bacteria, 192.2 ±42.5, 45± 4 and 31± 4 of E. coli, pseudomonas aeruginosa and bacillus licheniformis cells per unit area respectively. This difference corresponds to a ~98%, 96.5 and ~96.1% reduction in the attached E. coli, pseudomonas aeruginosa and bacillus licheniformis cells respectively. The results of static bacterial adhesion tests are summarized in table 6.2.
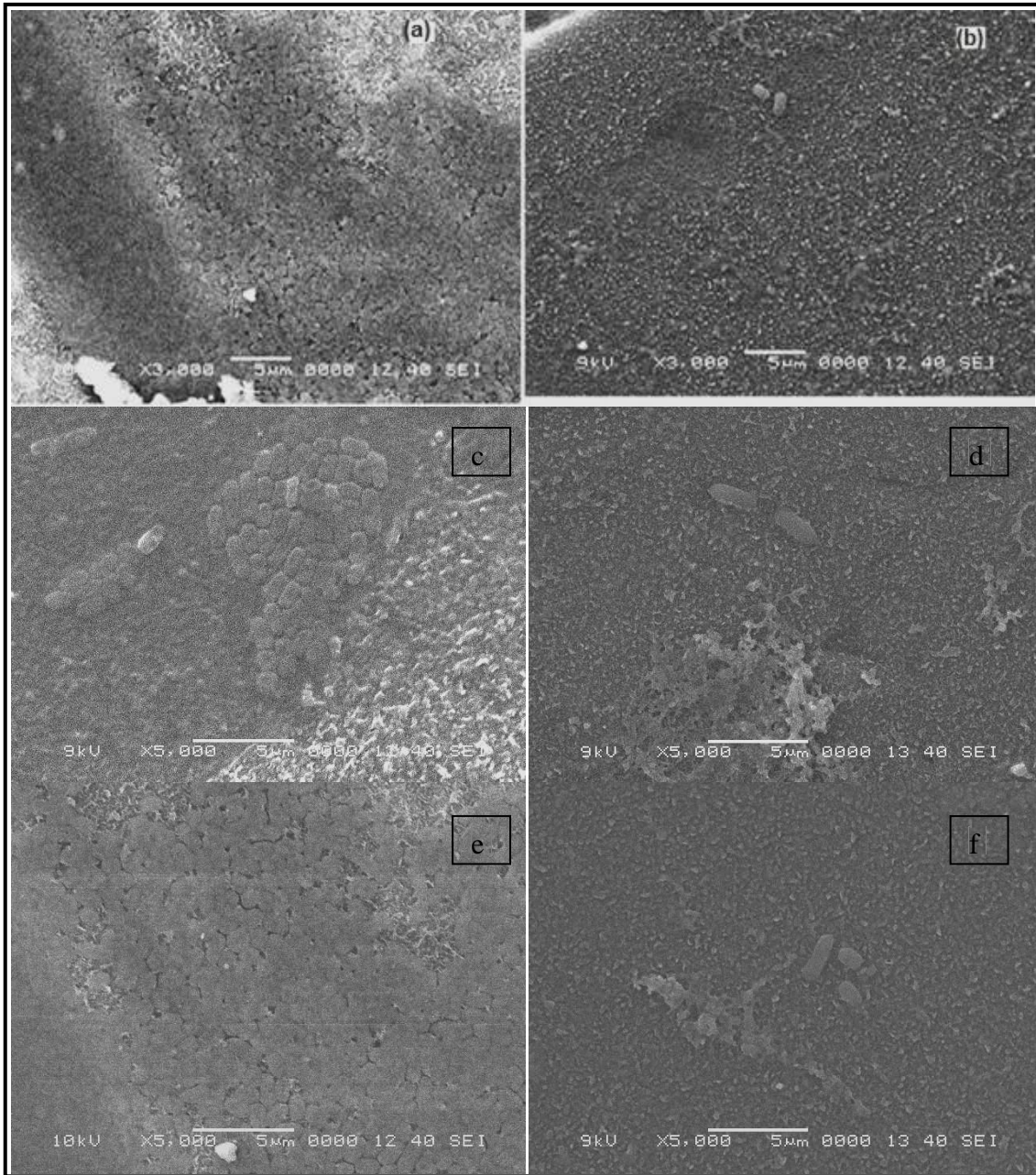
Figure 6.8. SEM images (a, c and e) of bare Koch membrane showing nearly full coverage of the surface with bacterial colonies of E. coli, and (b, d and f) iCVD coated and functionalized Koch membranes exposed to E. coli cells.
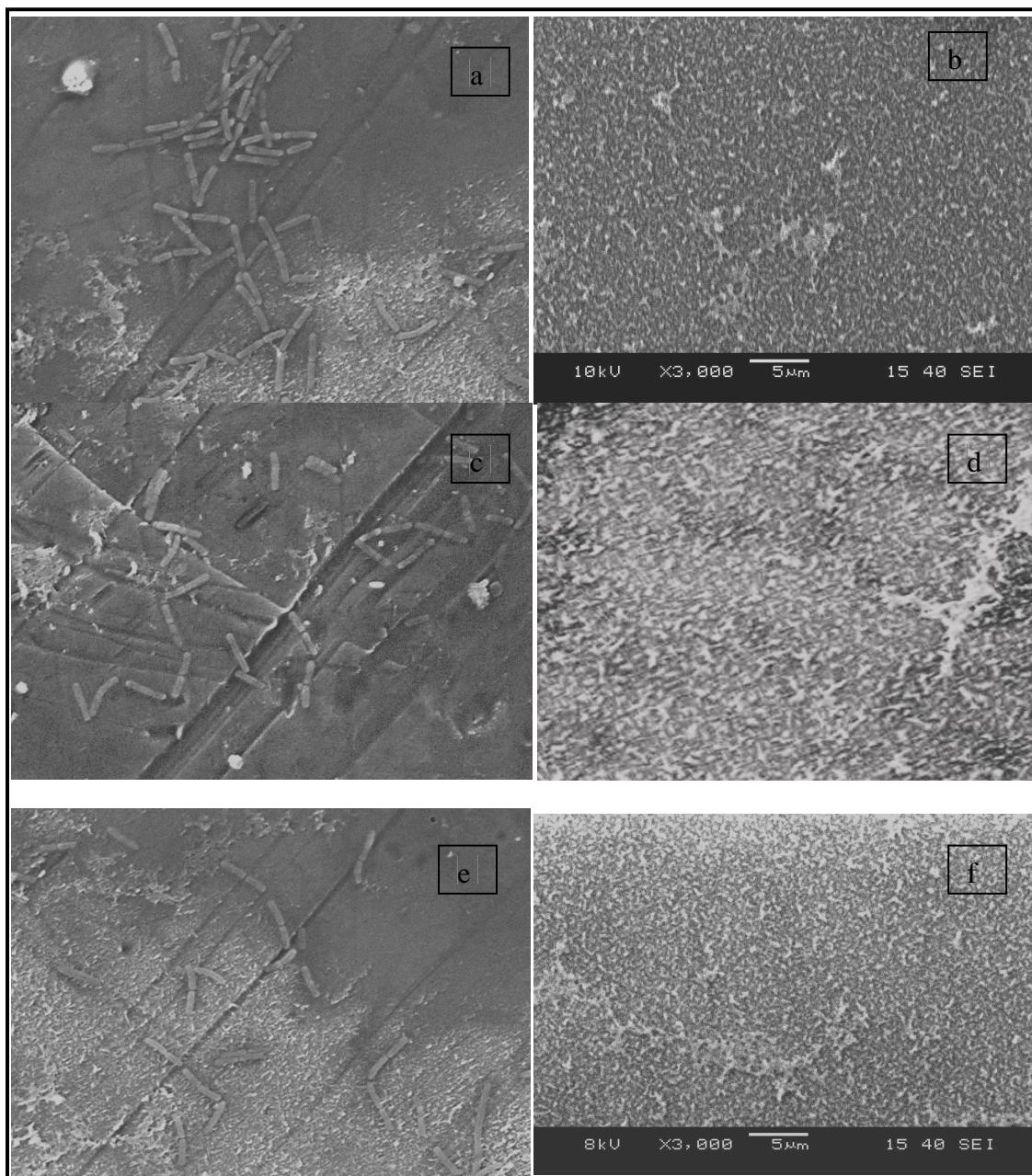
Figure 6.9. SEM images (a, c and e) of bare Koch membrane showing several colonies of Pseudomonas formed on the surface of membranes, and (b, d and f) iCVD coated and functionalized Koch membranes exposed to Pseudomonas cells.
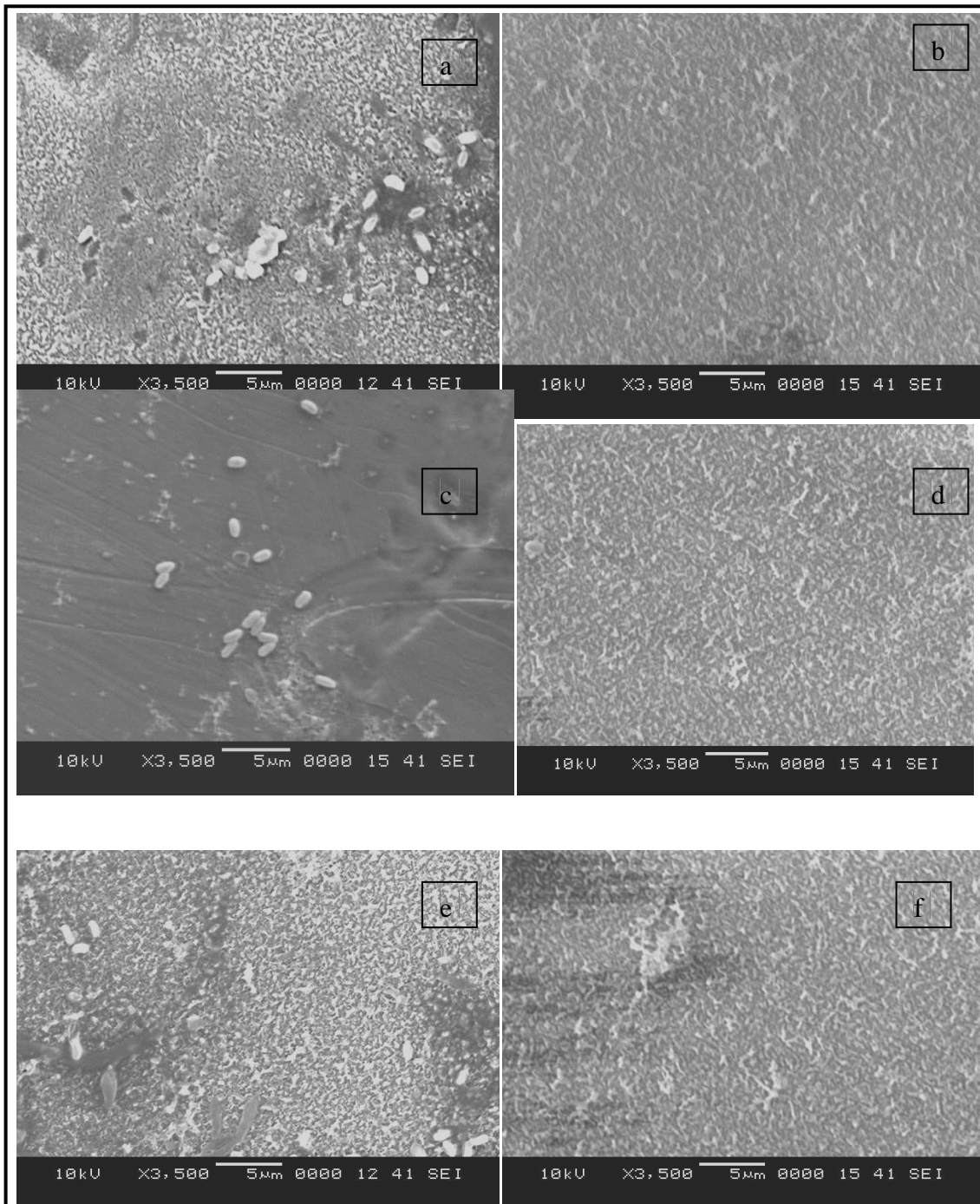
Figure 6.10. SEM images (a, c and e) of bare Koch membrane showing several colonies of Bacillus formed on the surface of membranes, and (b, d and f) iCVD coated and functionalized Koch membranes exposed to Bacilluscells.

The SEM images also revealed a marked variance in the number of attached cells: enormous colonies of both types of bacteria can be identified on bare Koch membranes (figures 6.8 (a, c and e), 6.9 (a, c and e) and 6.10 (a, c and e)), whereas only a few individual cells (if any) can be observed on modified Koch membranes (figures 6.8 (b, d and f), 6.9 (b, d and f) and 6.10 (b, d and f). These results demonstrate the effectiveness of the zwitterionic copolymer films (p(85% 4-VP-co-EGDA)) in interfering with bacterial adhesion in a manner similar to their interference with biopolymer adsorption (BSA).
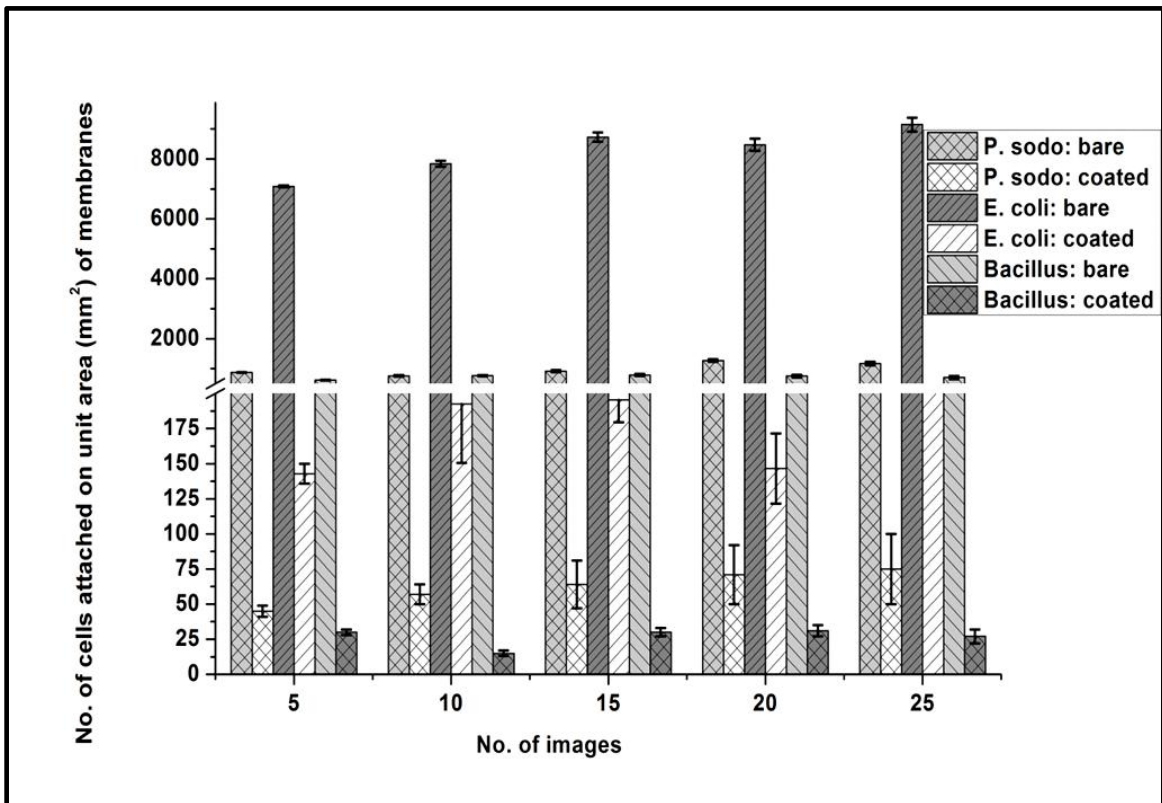
Figure 6.11. Number of E. coli, pseudomonas and bacillus cells attached to the unit membrane surface (per mm^2). Membrane samples were immersed in nutrient broth for 2 hr. at room temperature in air-isolated TTs containing ~ 4.1x10^8 Cell/ml. Break shown on the vertical axis is from 200-500.

Table 6.2. Number of attached E. coli, pseudomonas and bacillus cells on unit area (per mm^2) of membranes.

No. of images observed	Attached E. coli cells on bare Koch membrane	Attached E. coli cells on modified Koch membranes	Attached pseudomonas cells on bare Koch membranes	Attached pseudomonas cells on modified Koch membranes	Attached bacillus cells on bare Koch membranes	Attached bacillus cells on modified Koch membranes
5	7082 ± 26	315 ± 4	872 ± 12	45±4	616± 10	30±2
10	7842 ± 95	142 ± 7	759 ± 23	57±7	767± 22	15±2
15	8731±155	195 ± 16	917 ± 33	64 ± 17	787± 36	30±3
20	8473±201	146 ± 25	1270 ± 45	71 ± 21	752± 47	31±4
25	9145±234	192 ± 42	1167 ± 62	75 ± 25	704± 53	27±5

6.6 Permeation Tests

Figure 6.12 shows the permeate fluxes and percentage salt rejection of bare Koch membranes and Koch membranes modified with optimized chemistry before and after salt addition. Bare Koch showed an average permeate flux of 45.6±2.7 L/m^2 hr, whereas modified membranes showed a permeate water flux of 37.5±3.1 L/m^2 hr. This is approximately an 18% reduction in permeate flux, comparable to the flux decline observed by R. Yang et al. [39] under similar test conditions. The two bar columns on the right in Figure 6.12 represent salt rejection of bare and modified membranes after a test run of 4 hr at 300 psi. Higher salt rejection (~98% ± 0.38%) was observed for modified Koch compared to bare Koch membranes (96% ± 0.45%).
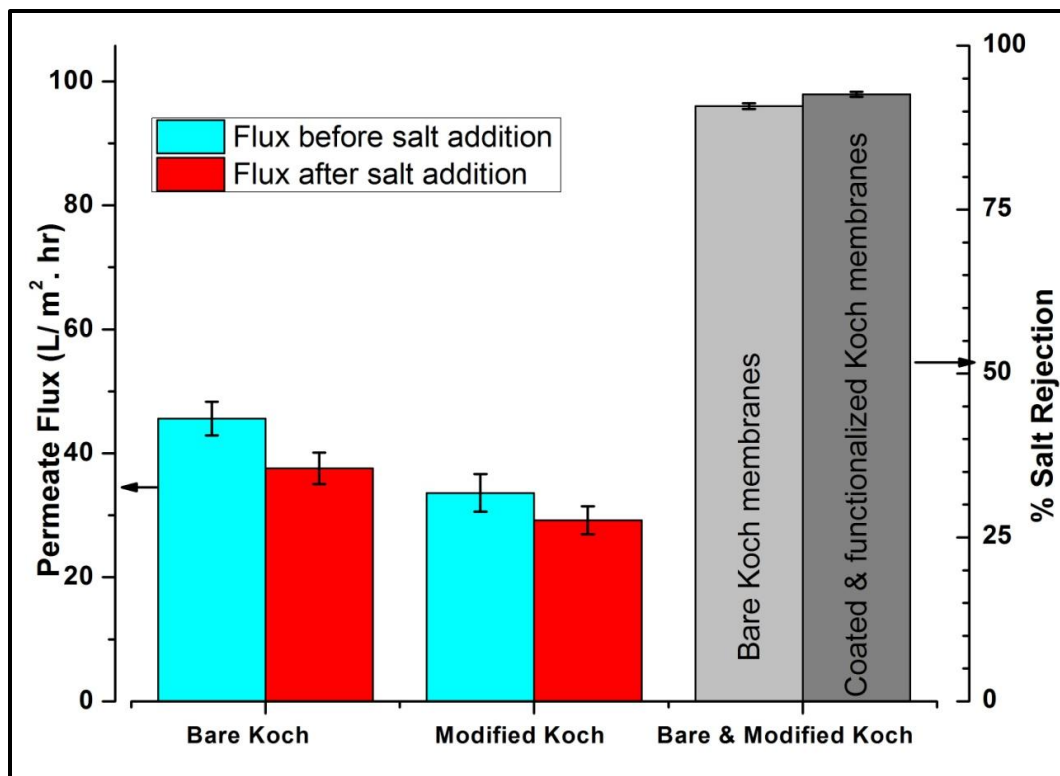
Figure 6.12. Permeate water flux and percentage salt rejection of bare and modified (38 ± 3 nm-thick coating of p(85% 4-VP-co-EGDA)) Koch membranes. Flux was calculated at 300 psi and 21 °C using active membrane areas of ~ 42 cm^2.

It is important to note that permeate flux reduction of modified membranes appears slightly higher; however, their better salt rejection compared to unmodified membranes compensates for this decline in flux. Table 6.3 summarizes the performance evaluation (permeate flux and salt rejection) of modified and bare Koch membranes.

Table 6.3. Permeation test results: permeate water flux and percentage salt rejection. Error reported is standard deviation.

Sample	Permeate Flux [L/m^2.hr]	Permeate Flux after salt addition [L/m^2.hr]	Salt Rejection (%)
Bare Koch Membrane	45.6 ± 2.7	37.5 ± 2.5	96.0 ± 0.45
Coated and Functionalized Koch membrane	33.7 ± 3.0	29.4 ± 2.2	97.9 ± 0.38

6.6.1 Permeation Tests with Sodium Alginate

Propensity to organic fouling of the bare and modified Koch membranes under cross-flow conditions was tested with sodium alginate, a representative of the natural organic matter (NOM) found in seawater. Figure 6.13 (a,b) shows digital camera photograph of the bare and modified Koch membranes after a test run of 6 hours under alginate flow in the presence of salt. Much higher alginate deposition (fouling) is clearly visible on bare Koch membrane as compared to negligible fouling on modified Koch membranes.
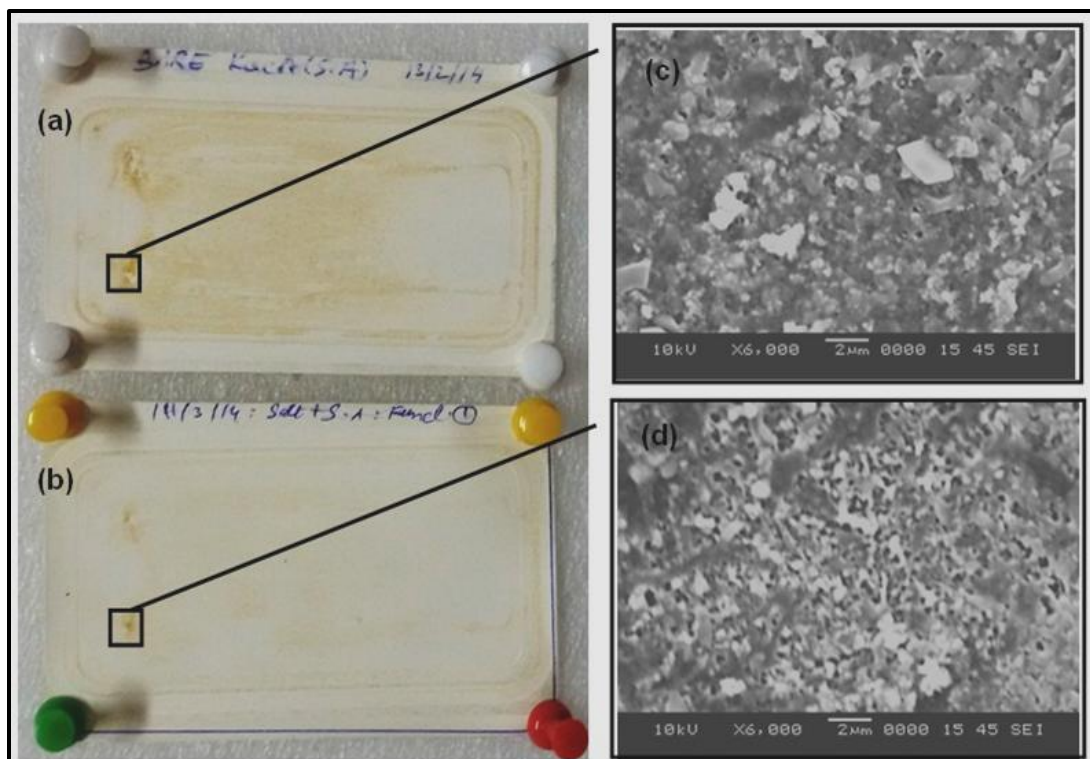
Figure 6.13. Membrane coupons after a filtration run of 6 hours with a model foulant (sodium alginate). (a) Bare Koch membrane, (b) modified Koch membrane. Panel on the left indicates SEM images of the deposited alginate layer on (c) bare and (d) modified Koch membrane.

Post-alginate fouling analyses were performed by SEM to reveal the surface morphology of deposited foulant (SA) layer on both bare and modified Koch membranes (figure 6.13 (c,d), supplementary information). The results showed marked difference in foulant adhesion between the commercial and modified Koch membranes; the unmodified membranes had an almost dense and continuous layer of alginate, while the foulant deposition on the modified Koch membranes was more sporadic and the layer was discontinuous. The highly porous surface morphology (of foulant layer) on the modified membranes is attributed to the very conformal nature of zwitterionic copolymer coating and has two important implications: firstly it discourages and/or hinders the membranes-
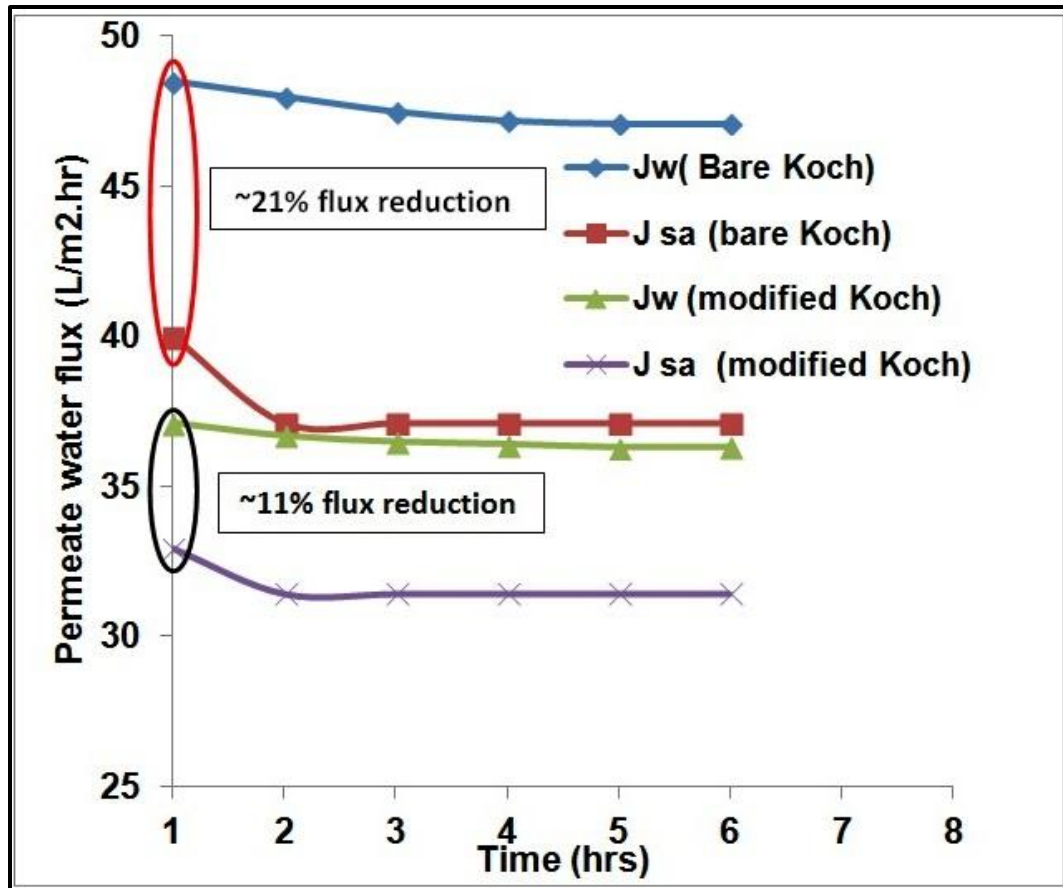
Figure 6.14. Permeate water flux as a function of time under sodium alginate (100 mg/L) exposure. J_w and J_{SA} represent permeate flux before and after sodium alginate and salt addition respectively.

alginate interactions; and secondly, it results in much lower flux decline (even in the presence of alginate and salt) which is evidenced by much lower permeate flux decline (~11% reduction: the flux decline during the first hour of alginate run) of modified Koch membranes as opposed to much higher flux decline (~21% reduction: flux decline for the same duration) for the case of bare Koch membranes as shown in figure 6.14. It is worth mentioning that the permeate flux decline, especially in the initial stage of alginate fouling has been reported to have a direct relation between membrane-foulant interactions [98]. It is important to note that both bare and modified Koch membranes

showed no statistical difference of salt rejection before and after SA addition. Another important point to mention here is that the reduced alginate deposition may also hinder/discourage the bacterial growth on the membranes; as the alginate has been found to be the major component of EPS−the biofilm matrix that provides strength and integrity to biofilm [17, 97]. However, further studies are warranted to prove this hypothesis.

6.7   AFM: Surface Roughness Studies

Neutral surface charge, higher surface hydrophilicity and lower surface roughness are the three major parameters responsible for enhancing fouling resistance of RO membranes in virtually all environments. Several researchers have investigated surface properties of different commercial membranes from the same manufacturer and from different manufacturers [98, 99] and found that differing morphological properties between RO membranes is mainly the result of differences in synthesis conditions: 1) using different monomer types and 2) subjecting the membrane to post-fabrication treatments, such as coating the membrane with an alcohol rich aliphatic polymer [35]. Furthermore, G. Ozaydin-Ince et al. [100] stated that higher surface roughness will lead to the following: (i) uneven boundary layers or flow distribution over the coated surface, (ii) increased probability of pinhole type defect formation and (iii) more binding sites for foulant attachment and shielding of attached cells from the hydraulic shear forces that lead to fouling.

The other important observation was reduction in surface roughness (RMS) after deposition of 85% 4-VP-co-EGDA copolymer film (figure 6.15). RMS roughnesses of 12.18 nm and 7.10 nm were found for virgin Koch and Koch membrane modified with 4-VP-co-EGDA copolymer, respectively. This finding agrees with similar reduction in

RMS roughness observed in our earlier studies [95, 101] and literature conclusions [100, 102]. This reduction in RMS roughness is attributed to the unique nature of iCVD that ensures deposition of a very conformal and uniform thickness antifouling layer coating.
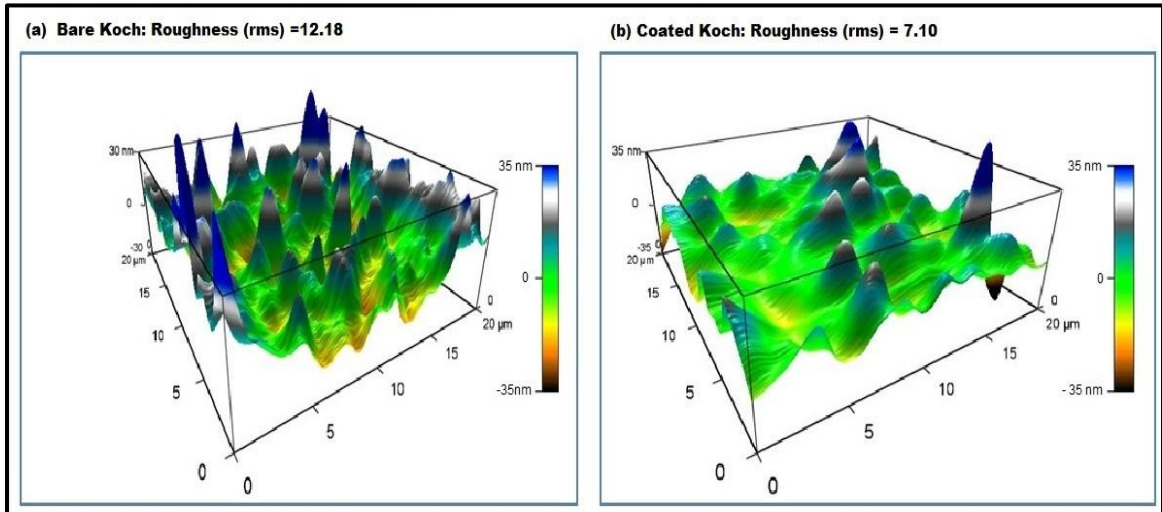
Figure 6.15. AFM images of (a) bare Koch membrane and (b) Koch membrane modified with 38 ± 3 nm copolymer p(4-VP-EGDA) film.

6.7.1 Molecular Force Mapping (MFP)

Several studies have shown that AFM with functionalized probes is a powerful method for probing foulant-membrane interaction [103, 104]. This technique represents a quantitative and reproducible method to evaluate fouling resistance of various foulants and to screen a collection of antifouling surface chemistries rapidly [104]. BSA-functionalized AFM tips are usually used in these investigations. BSA has a rich assortment of functional moieties that are capable of interacting with a surface, including amine ($-NH_2$), carboxylic ($-COOH$), and alkyl ($-CH_3$) groups among others.

MFP was utilized to assess the molecular interaction between the foulant (BSA) and RO membrane surfaces (both virgin and modified (coated and functionalized) Koch membranes). Figure 6.16, represents the force-separation distance (F-d) curves for the bare and modified Koch membranes. At least 36 such curves were taken for each tip-surface pair. The maximum adhesive force between the BSA-functionalized tip and the surface was calculated from the retraction portion of the F-d curve and the average adhesive force was found to be 3.45 ($\pm$0.41) nN, and 0.362 ($\pm$0.052) nN respectively for the bare and modified Koch membranes. It is important to note that the iCVD zwitterionic surface (modified Koch membrane) has approximately an order of magnitude lesser molecular interaction as compared to bare Koch membrane, which clearly shows that the zwitterionic surface has the lesser interaction (adhesive force) and thus has the stronger fouling resistance.

Further insight to molecular interaction forces between the model foulant (BSA) and the Koch membrane surfaces (both bare and modified) was gained by measuring the weight average adhesive force (F_{ad}) between the BSA-functionalized tip as a function of tip

dwell time for the membrane surface under study. Presented in Figure 6.17, the top part (Figure 6.17(a) and Figure 6.17(b)) are the force maps of modified and bare Koch membranes respectively, whereas the bottom part (Figure 6.17(c)), portrays weight average adhesive force (F_{ad}) as a function of tip dwell time. Figure 6.17 elucidates that functionalized Koch membrane surfaces show at least an order of magnitude lower adhesive force as compared to the bare Koch membrane surface. These results corroborate well with molecular forces (maximum adhesive forces) calculated for bare and modified RO membranes by F-d curves. The lesser adhesive forces observed for the case of modified Koch membranes is also reflected in discouraging and/or hindering the adhesion of foulant (BSA), and is attributed to the very conformal nature of the *i*CVD deposition. Another possible and perhaps the most relevant reason for the reduced adhesive force between the modified Koch membranes and foulant (BSA) may be the surface enrichment of zwitterionic moieties that helps in forming a thin surface water layer via strong electrostatic forces between water molecules and surface zwitterionic groups. It has already been reported that hydrophobic surfaces adsorb more proteins and the surface that resist protein adsorption may also inhibit bacterial adhesion. [105]

It is worth mentioning that the higher hydrophilic nature of the surface due to hydration provided by the zwitterionic moieties is considered the molecular origin of the excellent fouling resistance of zwitterionic chemistry [44, 106, 107]. As pointed earlier, hydrophilic surfaces have also been reported to attract a strongly-bound water layer. This surface-water layer acts as a buffer and minimizes direct foulant–surface interaction and discourages hydrophobic–hydrophobic interactions [100]. The later phenomenon is believed to have a direct relation to the bacterial adhesion as explained in section 6.5.
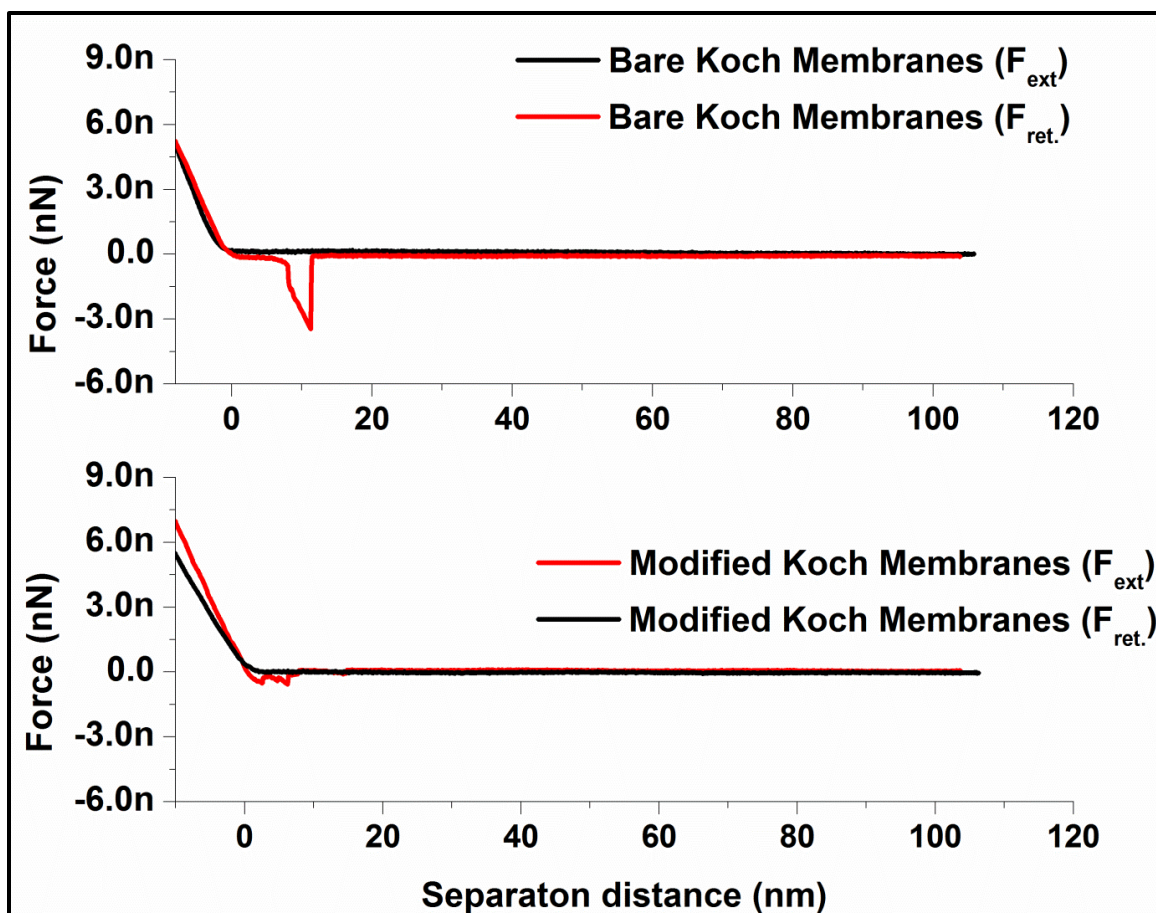
Figure 6.16. Force-distance curves of bare and modified (with zwitterionic copolymer coating) Koch membranes obtained via molecular force mapping. Black curves indicate the case where the BSA-functionalized tip is approaching the surface, whereas red curves represent the force-displacement measured during tip retraction.
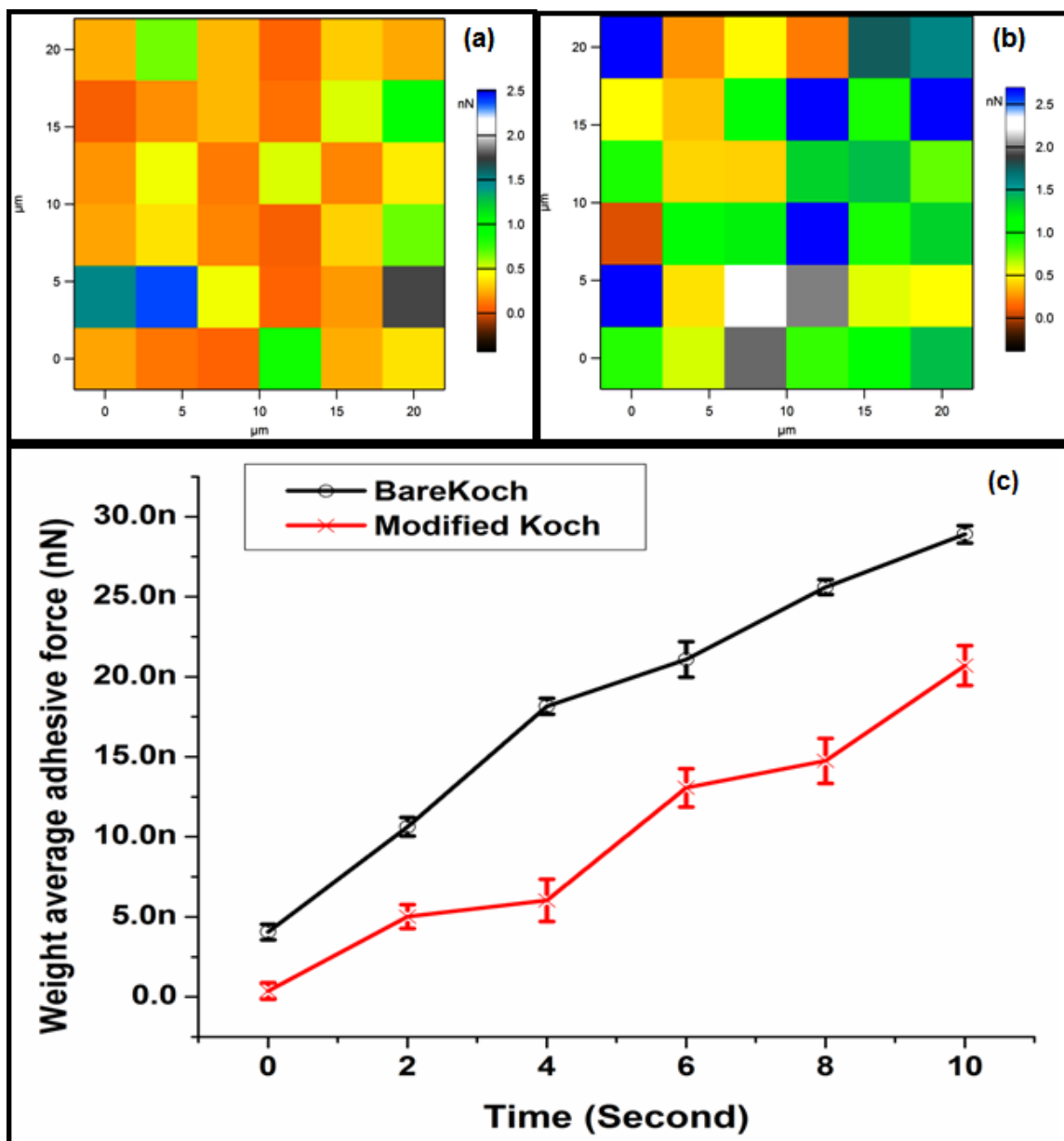
Figure 6.17. Molecular force maps of (a) modified and (b) bare Koch membrane surface recorded from 20x20 μm² area of each membrane sample. (c) Weight average adhesive force as a function of BSA-functionalized tip dwell time on each membrane surface. The error bars shown are the standard deviation of 36 measurements made for adhesive force (on an area of 20x20 μm²) for both bare and modified Koch membrane surface at each respective dwell time.

CHAPTER 7

CONCLUSIONS AND RECOMMENDATIONS

7.1   Conclusions

Commercial RO membranes are prone to biofouling the −Achilles heel of the seawater desalination process. The objectives of this study were to: (i) develop (ii) optimize (iii) successfully apply the developed zwitterionic antifouling coatings onto the surface of commercial RO membranes to combat their biofouling (iv) evaluate and compare the performance of the modified and unmodified (commercial) RO membranes. These objectives were achieved by a systematic scheme of synthesis route to fabricate antifouling coatings, through surface and compositional characterization of the deposited coatings and performance evaluation of the modified RO membranes.

Firstly, various chemistries of copolymer coatings poly(4-vinylpyridine-co-ethylene glycol diacrylate) (p(4-VP-co-EGDA) were synthesized via iCVD. By systematically varying the flow rate of monomers, thicker copolymer films (up to 250 nm) with the 4-VP content (the precursor of zwitterionic moieties) ranging from 25% to 85% were deposited on Si wafers. The deposited chemistries were then converted to surface zwitterionic moieties by reacting with vapors of the 3-bromopropionic acid (3-BPA).

The next step was to unearth the optimum chemistry of the synthesized coatings. This was accomplished by knowing the chemical composition, hydrophilicity and biopolymer adsorption. The composition of the copolymer coatings were determined by FTIR and high-resolution N1s XPS spectra. The copolymer chemistry with 85% 4-VP contents (p(85% 4-VP-co-EGDA) yielded the highest surface hydrophilicity (indicative of the lowest contact angle) and the lowest protein (BSA) adsorption (as evidenced by QCM-D

analysis). Both CA and QCM-D results suggest that copolymer chemistry with 85% 4-VP is the optimal chemistry, improving the hydrophilicity of commercial ROs and yielding sufficient zwitterionic content to provide ultra-low fouling properties in BSA. Much improved antifouling characteristics of optimized zwitterionic copolymer coatings were also found by QCM-D analysis with regard to two other model foulants (HA and SA).

Ultrathin films (~35 nm) of the optimized chemistry were then successfully deposited onto the surface of commercial RO membranes (Koch) via iCVD to modify/improve the active layers on these membranes. These copolymer coatings were converted to zwitterionic structures containing polycarboxybetaine acrylic acetate (pCBAA) units via a gas phase post-deposition quaternizing reaction with 3-BPA. Biofouling propensity of the modified and commercial (unmodified) membranes was investigated by testing their inertness to irreversible bacterial adhesion under static conditions in three different bacterial strains. Static bacterial adhesion tests showed significant reduction (~98%, ~96.5% and ~96.1%) in bacterial cells (E-coli, pseudomonas aeruginosa and bacillus cells, respectively) attachment on membranes modified with optimized zwitterionic chemistry compared to unmodified bare Koch membranes.

Finally, Koch membranes modified with the optimized chemistry were further tested for their performance (permeate flux, salt rejection and alginate fouling) evaluation and compared to commercial Koch membranes. Modified membranes showed ~18% flux decline when compared to unmodified Koch membranes. The slightly higher permeated flux reduction of the modified Koch membranes was compensated for their relatively better (~2% more) salt rejection when compared to unmodified RO membranes. Another attribute of the modified Koch membranes was their reduced surface-foulant interaction under flow conditions. The foulant layer deposited on the surface of the modified

membranes was found to be discontinuous/ sporadic as opposed to a continuous/denser foulant deposition on commercial RO membranes. Discontinuous deposition of foulant (SA) on the modified Koch membranes resulted in modest permeate flux decline indicating reduced foulant-membrane interactions as opposed to much higher flux decline for the case of bare Koch membranes under cross flow testing.

As a final conclusion, it can be carefully said that the newly developed zwitterionic antifouling coatings have great potential for the surface modification of commercial RO membranes to considerably enhance their biofouling resistance. Nevertheless, further studies are needed to uncover their full utilization as a surface modification strategy for the seawater RO membranes.

7.2   Recommendations

Preliminary studies have shown the development of antifouling zwitterionic coatings and their successful application to Koch membranes. Short term permeation tests on modified membranes revealed the satisfactory permeate flux and better salt rejection, and reduced alginate fouling under cross flow conditions revealed the enhanced antifouling properties of the modified membranes as compared to commercial (bare) Koch membranes. However, long term fouling (200+ hours) under flow conditions in the presence of model foulants HA and SA is essential to know the fouling behavior of the coatings under prolonged exposure to these foulants. And even more complex fouling situation (in the presence of Ca^{++} ions or Na^{+} ions) along with these foulants would be an important study to test the antifouling potential of the synthesized zwitterionic coatings under aggravated conditions of these foulants.

Furthermore, another good study would be to examine the anti-biofouling propensity of the zwitterionic coatings under flow conditions. In this pursuit, bacterial adhesion under cross flow conditions can be tested in the presence of a particular bacterial strain by running a number of permeation tests at different permeation variables such as trans-membrane pressure, temperature, pressure and pH.

Finally, performance evaluation of the developed zwitterionic coatings under real conditions, e.g. with seawater/brackish water, testing with higher salt concentrations (35000 ppm: average value for seawater and 45000-55000 ppm: typical values for the Arabian Gulf) and higher temperature (up to 40 °C; which is quite common in Gulf region) are must to perform in order to investigate their full utilization as antifouling coatings to seawater desalination RO membranes.

References

[1]   M. Al-Ahmad, F. Abdul Aleem, A. Mutiri, and A. Ubaisy, "Biofuoling in RO membrane systems Part 1: Fundamentals and control," *Desalination,* vol. 132, pp. 173-179, 2000.

[2]   M. A. Shannon, P. W. Bohn, M. Elimelech, J. G. Georgiadis, B. J. Marinas, and A. M. Mayes, "Science and technology for water purification in the coming decades," *Nature,* vol. 452, pp. 301-310, 2008.

[3]   R. W. Baker, *Membrane technology*: Wiley Online Library, 2000.

[4]   J. Mallevialle, P. E. Odendaal, and M. R. Wiesner, *Water treatment membrane processes*: American Water Works Association, (1996).

[5]   M. I. Dova, K. B. Petrotos, and H. N. Lazarides, "On the direct osmotic concentration of liquid foods: Part II. Development of a generalized model," *Journal of food engineering,* vol. 78, pp. 431-437, 2007.

[6]   K.-i. Yamamoto, M. Matsuda, M. Hayama, J. Asutagawa, S. Tanaka, F. Kohori*, et al.*, "Evaluation of the activity of endotoxin trapped by a hollow-fiber dialysis membrane," *Journal of membrane science,* vol. 272, pp. 211-216, (2006).

[7]   A. Prakash Rao, N. Desai, and R. Rangarajan, "Interfacially synthesized thin film composite RO membranes for seawater desalination," *Journal of membrane science,* vol. 124, pp. 263-272, 1997.

[8]   J. Vrouwenvelder, J. Van Paassen, L. Wessels, A. Van Dam, and S. Bakker, "The membrane fouling simulator: a practical tool for fouling prediction and control," *Journal of Membrane Science,* vol. 281, pp. 316-324, 2006.

[9]   H.-C. Flemming, "Reverse osmosis membrane biofouling," *Experimental thermal and fluid science,* vol. 14, pp. 382-391, 1997.

[10]   J. Baker and L. Dudley, "Biofouling in membrane systems—a review," *Desalination,* vol. 118, pp. 81-89, 1998.

[11]   D. McDougald, S. A. Rice, N. Barraud, P. D. Steinberg, and S. Kjelleberg, "Should we stay or should we go: mechanisms and ecological consequences for biofilm dispersal," *Nature Reviews Microbiology,* vol. 10, pp. 39-50, 2011.

[12]   B. Rosche, X. Z. Li, B. Hauer, A. Schmid, and K. Buehler, "Microbial biofilms: a concept for industrial catalysis?," *Trends in biotechnology,* vol. 27, pp. 636-643, 2009.

[13]   S. Sadr Ghayeni, P. Beatson, R. Schneider, and A. Fane, "Adhesion of waste water bacteria to reverse osmosis membranes," *Journal of Membrane Science,* vol. 138, pp. 29-42, 1998.

[14]   R. Neihof and G. Loeb, "Dissolved organic-matter in seawater and electric charge of immersed surfaces," *Journal of marine research,* vol. 32, pp. 5-12, 1974.

[15]   R. P. Schneider, "Conditioning film-induced modification of substratum physicochemistry—analysis by contact angles," *Journal of colloid and interface science,* vol. 182, pp. 204-213, 1996.

[16]   A.-C. Olofsson, M. Hermansson, and H. Elwing, "N-acetyl-L-cysteine affects growth, extracellular polysaccharide production, and bacterial biofilm formation on solid surfaces," *Applied and environmental microbiology,* vol. 69, pp. 4814-4822, 2003.

[17] A. Matin, Z. Khan, S. Zaidi, and M. Boyce, "Biofouling in reverse osmosis membranes for seawater desalination: phenomena and prevention," *Desalination,* vol. 281, pp. 1-16, 2011.

[18] H. Flemming, "Biofouling in water treatment," in *Biofouling and Biocorrosion in Industrial Water Systems*, ed: Springer, 1991, pp. 47-80.

[19] T. Griebe and H.-C. Flemming, "Biocide-free antifouling strategy to protect RO membranes from biofouling," *Desalination,* vol. 118, pp. 153-IN9, 1998.

[20] J.-J. Qin, B. Liberman, and K. A. Kekre, "Direct osmosis for reverse osmosis fouling control: principles, applications and recent developments," *The Open Chemical Engineering Journal,* vol. 3, pp. 8-16, 2009.

[21] N. H. Lin, M.-m. Kim, G. T. Lewis, and Y. Cohen, "Polymer surface nano-structuring of reverse osmosis membranes for fouling resistance and improved flux performance," *Journal of Materials Chemistry,* vol. 20, pp. 4642-4652, 2010.

[22] X. Wei, Z. Wang, Z. Zhang, J. Wang, and S. Wang, "Surface modification of commercial aromatic polyamide reverse osmosis membranes by graft polymerization of 3-allyl-5, 5-dimethylhydantoin," *Journal of Membrane Science,* vol. 351, pp. 222-233, 2010.

[23] V. Freger, J. Gilron, and S. Belfer, "TFC polyamide membranes modified by grafting of hydrophilic polymers: an FT-IR/AFM/TEM study," *Journal of Membrane Science,* vol. 209, pp. 283-292, 2002.

[24] A. Adout, S. Kang, A. Asatekin, A. M. Mayes, and M. Elimelech, "Ultrafiltration membranes incorporating amphiphilic comb copolymer additives prevent irreversible adhesion of bacteria," *Environmental science & technology,* vol. 44, pp. 2406-2411, 2010.

[25] Q. Sun, Y. Su, X. Ma, Y. Wang, and Z. Jiang, "Improved antifouling property of zwitterionic ultrafiltration membrane composed of acrylonitrile and sulfobetaine copolymer," *Journal of membrane science,* vol. 285, pp. 299-305, 2006.

[26] G. Kang, M. Liu, B. Lin, Y. Cao, and Q. Yuan, "A novel method of surface modification on thin-film composite reverse osmosis membrane by grafting poly (ethylene glycol)," *Polymer,* vol. 48, pp. 1165-1170, 2007.

[27] L. D. Chambers, K. R. Stokes, F. C. Walsh, and R. J. Wood, "Modern approaches to marine antifouling coatings," *Surface and Coatings Technology,* vol. 201, pp. 3642-3652, 2006.

[28] C. Werner, M. F. Maitz, and C. Sperling, "Current strategies towards hemocompatible coatings," *Journal of materials chemistry,* vol. 17, pp. 3376-3384, 2007.

[29] N. Wisniewski and M. Reichert, "Methods for reducing biosensor membrane biofouling," *Colloids and Surfaces B: Biointerfaces,* vol. 18, pp. 197-219, 2000.

[30] G.-d. Kang and Y.-m. Cao, "Development of antifouling reverse osmosis membranes for water treatment: a review," *Water research,* vol. 46, pp. 584-600, 2012.

[31] S. Krishnan, C. J. Weinman, and C. K. Ober, "Advances in polymers for anti-biofouling surfaces," *Journal of Materials Chemistry,* vol. 18, pp. 3405-3413, 2008.

[32] M. Chapman Wilbert, J. Pellegrino, and A. Zydney, "Bench-scale testing of surfactant-modified reverse osmosis/nanofiltration membranes," *Desalination,* vol. 115, pp. 15-32, 1998.

[33] Y. Zhou, S. Yu, C. Gao, and X. Feng, "Surface modification of thin film composite polyamide membranes by electrostatic self deposition of polycations for improved fouling resistance," *Separation and Purification Technology,* vol. 66, pp. 287-294, 2009.

[34] C. Ba and J. Economy, "Preparation and characterization of a neutrally charged antifouling nanofiltration membrane by coating a layer of sulfonated poly (ether ether ketone) on a positively charged nanofiltration membrane," *Journal of Membrane Science,* vol. 362, pp. 192-201, 2010.

[35] C. Y. Tang, Y.-N. Kwon, and J. O. Leckie, "Probing the nano-and micro-scales of reverse osmosis membranes—a comprehensive characterization of physiochemical properties of uncoated and coated membranes by XPS, TEM, ATR-FTIR, and streaming potential measurements," *Journal of Membrane Science,* vol. 287, pp. 146-156, 2007.

[36] A. Kulkarni, D. Mukherjee, and W. N. Gill, "Flux enhancement by hydrophilization of thin film composite reverse osmosis membranes," *Journal of membrane science,* vol. 114, pp. 39-50, 1996.

[37] W. E. Mickols, "Composite membrane with polyalkylene oxide modified polyamide surface," ed: Google Patents, 2001.

[38] S. P. Hong, J.-y. Koo, J. H. Lee, and K. Y. Ryu, "Selective membrane having a high fouling resistance," ed: Google Patents, 2009.

[39] R. Yang, J. Xu, G. Ozaydin-Ince, S. Y. Wong, and K. K. Gleason, "Surface-tethered zwitterionic ultrathin antifouling coatings on reverse osmosis membranes by initiated chemical vapor deposition," *Chemistry of Materials,* vol. 23, pp. 1263-1272, 2011.

[40] J. M. Harris, *Introduction to biotechnical and biomedical applications of poly (ethylene glycol)*: Springer, 1992.

[41] S. C. Tu, V. Ravindran, W. Den, and M. Pirbazari, "Predictive membrane transport model for nanofiltration processes in water treatment," *AIChE Journal,* vol. 47, pp. 1346-1362, 2001.

[42] S. Chen, J. Zheng, L. Li, and S. Jiang, "Strong resistance of phosphorylcholine self-assembled monolayers to protein adsorption: insights into nonfouling properties of zwitterionic materials," *Journal of the American Chemical Society,* vol. 127, pp. 14473-14478, 2005.

[43] H. Kitano, T. Mori, Y. Takeuchi, S. Tada, M. Gemmei-Ide, Y. Yokoyama*, et al.*, "Structure of Water Incorporated in Sulfobetaine Polymer Films as Studied by ATR-FTIR," *Macromolecular bioscience,* vol. 5, pp. 314-321, 2005.

[44] S. Jiang and Z. Cao, "Ultralow-Fouling, Functionalizable, and Hydrolyzable Zwitterionic Materials and Their Derivatives for Biological Applications," *Advanced Materials,* vol. 22, pp. 920-932, 2010.

[45] G. Li, G. Cheng, H. Xue, S. Chen, F. Zhang, and S. Jiang, "Ultra low fouling zwitterionic polymers with a biomimetic adhesive group," *Biomaterials,* vol. 29, pp. 4592-4597, 2008.

[46] S. Chen, L. Li, C. Zhao, and J. Zheng, "Surface hydration: principles and applications toward low-fouling/nonfouling biomaterials," *Polymer,* vol. 51, pp. 5283-5293, 2010.

[47] R. Yang, A. Asatekin, and K. K. Gleason, "Design of conformal, substrate-independent surface modification for controlled protein adsorption by chemical vapor deposition (CVD)," *Soft Matter,* vol. 8, pp. 31-43, 2012.

[48] M. T. Bernards, G. Cheng, Z. Zhang, S. Chen, and S. Jiang, "Nonfouling polymer brushes via surface-initiated, two-component atom transfer radical polymerization," *Macromolecules,* vol. 41, pp. 4216-4219, 2008.

[49] J. Yuan, J. Zhang, J. Zhu, J. Shen, S. Lin, W. Zhu*, et al.*, "Reduced platelet adhesion on the surface of polyurethane bearing structure of sulfobetaine," *Journal of biomaterials applications,* vol. 18, pp. 123-135, 2003.

[50] P.-S. Liu, Q. Chen, X. Liu, B. Yuan, S.-S. Wu, J. Shen*, et al.*, "Grafting of zwitterion from cellulose membranes via ATRP for improving blood compatibility," *Biomacromolecules,* vol. 10, pp. 2809-2816, 2009.

[51] J. Xu, Y. Yuan, B. Shan, J. Shen, and S. Lin, "Ozone-induced grafting phosphorylcholine polymer onto silicone film grafting 2-methacryloyloxyethyl phosphorylcholine onto silicone film to improve hemocompatibility," *Colloids and Surfaces B: Biointerfaces,* vol. 30, pp. 215-223, 2003.

[52] L. R. Carr, Y. Zhou, J. E. Krause, H. Xue, and S. Jiang, "Uniform zwitterionic polymer hydrogels with a nonfouling and functionalizable crosslinker using photopolymerization," *Biomaterials,* vol. 32, pp. 6893-6899, 2011.

[53] Y. Chang, W. Yandi, W.-Y. Chen, Y.-J. Shih, C.-C. Yang, Y. Chang*, et al.*, "Tunable bioadhesive copolymer hydrogels of thermoresponsive poly (N-isopropyl acrylamide) containing zwitterionic polysulfobetaine," *Biomacromolecules,* vol. 11, pp. 1101-1110, 2010.

[54] B. Yameen, M. Ali, R. Neumann, W. Ensinger, W. Knoll, and O. Azzaroni, "Single conical nanopores displaying pH-tunable rectifying characteristics. Manipulating ionic transport with zwitterionic polymer brushes," *Journal of the American Chemical Society,* vol. 131, pp. 2070-2071, 2009.

[55] H. Liu, C. Li, H. Liu, and S. Liu, "pH-responsive supramolecular self-assembly of well-defined zwitterionic ABC miktoarm star terpolymers," *Langmuir,* vol. 25, pp. 4724-4734, 2009.

[56] N. Karanikolopoulos, M. Pitsikalis, N. Hadjichristidis, K. Georgikopoulou, T. Calogeropoulou, and J. R. Dunlap, "pH-responsive aggregates from double hydrophilic block copolymers carrying zwitterionic groups. Encapsulation of antiparasitic compounds for the treatment of leishmaniasis," *Langmuir,* vol. 23, pp. 4214-4224, 2007.

[57] D.-S. Han and M.-S. Gong, "Zwitterionic sulfobetaine-containing polyelectrolyte for controlling humidity-sensitivity," *Sensors and Actuators B: Chemical,* vol. 145, pp. 254-258, 2010.

[58] Z. Zhang, T. Chao, S. Chen, and S. Jiang, "Superlow fouling sulfobetaine and carboxybetaine polymers on glass slides," *Langmuir,* vol. 22, pp. 10072-10077, 2006.

[59] Z. Zhang, S. Chen, Y. Chang, and S. Jiang, "Surface grafted sulfobetaine polymers via atom transfer radical polymerization as superlow fouling coatings," *The Journal of Physical Chemistry B,* vol. 110, pp. 10799-10804, 2006.

[60] Z. Yi, L.-P. Zhu, Y.-Y. Xu, X.-N. Gong, and B.-K. Zhu, "Surface zwitterionicalization of poly(vinylidene fluoride) porous membranes by post-

reaction of the amphiphilic precursor," *Journal of Membrane Science,* vol. 385-386, pp. 57-66, 2011.

[61] N. Chomsky, "What is Special About Language?," in *SBS Lecture Series: Noam Chomsky*, ed: University of Arizona, 2012.

[62] S. Zhang, P. Rolfe, G. Wright, W. Lian, A. Milling, S. Tanaka*, et al.*, "Physical and biological properties of compound membranes incorporating a copolymer with a phosphorylcholine head group," *Biomaterials,* vol. 19, pp. 691-700, 1998.

[63] J. Ladd, Z. Zhang, S. Chen, J. C. Hower, and S. Jiang, "Zwitterionic polymers exhibiting high resistance to nonspecific protein adsorption from human serum and plasma," *Biomacromolecules,* vol. 9, pp. 1357-1361, 2008.

[64] Y. Chang, S. Chen, Z. Zhang, and S. Jiang, "Highly protein-resistant coatings from well-defined diblock copolymers containing sulfobetaines," *Langmuir,* vol. 22, pp. 2222-2226, 2006.

[65] C. Rodriguez Emmenegger, E. Brynda, T. Riedel, Z. Sedlakova, M. Houska, and A. B. Alles, "Interaction of blood plasma with antifouling surfaces," *Langmuir,* vol. 25, pp. 6328-6333, 2009.

[66] A. M. Coclite, R. M. Howden, D. C. Borrelli, C. D. Petruczok, R. Yang, J. L. Yagüe*, et al.*, "25th Anniversary Article: CVD Polymers: A New Paradigm for Surface Modifi cation and Device Fabrication," *Advanced Materials,* vol. 25, pp. 5392-5423, 2013.

[67] R. Yang, H. Jang, R. Stocker, and K. K. Gleason, "Synergistic Prevention of Biofouling in Seawater Desalination by Zwitterionic Surfaces and Low-Level Chlorination," *Advanced Materials,* 2013.

[68] T. Kondo, K. Nomura, M. Murou, M. Gemmei-Ide, H. Kitano, H. Noguchi*, et al.*, "Structure of water in the vicinity of a zwitterionic polymer brush as examined by sum frequency generation method," *Colloids and Surfaces B: Biointerfaces,* vol. 100, pp. 126-132, 2012.

[69] R. W. Baker, "Membrane transport theory," *Membrane Technology and Applications, Second Edition,* pp. 15-87, 2004.

[70] C. Y. Tang, Y.-N. Kwon, and J. O. Leckie, "Effect of membrane chemistry and coating layer on physiochemical properties of thin film composite polyamide RO and NF membranes: I. FTIR and XPS characterization of polyamide and coating layer chemistry," *Desalination,* vol. 242, pp. 149-167, 2009.

[71] D. Braun, H. Cherdron, H. Ritter, D. Braun, and H. Cherdron, *Polymer synthesis: theory and practice*: Springer, 2005.

[72] R. D. Deegan, O. Bakajin, T. F. Dupont, G. Huber, S. R. Nagel, and T. A. Witten, "Capillary flow as the cause of ring stains from dried liquid drops," *Nature,* vol. 389, pp. 827-829, 1997.

[73] M. Ma, Y. Mao, M. Gupta, K. K. Gleason, and G. C. Rutledge, "Superhydrophobic fabrics produced by electrospinning and chemical vapor deposition," *Macromolecules,* vol. 38, pp. 9742-9748, 2005.

[74] Z. Yang, X. Lei, J. Wang, R. Luo, T. He, H. Sun*, et al.*, "A novel technique toward bipolar films containing alternating nano–layers of allylamine and acrylic acid plasma polymers for biomedical application," *Plasma Processes and Polymers,* vol. 8, pp. 208-214, 2011.

93

[75]   K. K. Lau, Y. Mao, H. G. Pryce Lewis, S. K. Murthy, B. D. Olsen, L. S. Loo, *et al.*, "Polymeric nanocoatings by hot-wire chemical vapor deposition (HWCVD)," *Thin Solid Films,* vol. 501, pp. 211-215, 2006.

[76]   J. L. Yagüe, A. M. Coclite, C. Petruczok, and K. K. Gleason, "Chemical Vapor Deposition for Solvent-Free Polymerization at Surfaces," *Macromolecular Chemistry and Physics,* vol. 214, pp. 302-312, 2013.

[77]   W. E. Tenhaeff and K. K. Gleason, "Initiated and oxidative chemical vapor deposition of polymeric thin films: iCVD and oCVD," *Advanced Functional Materials,* vol. 18, pp. 979-992, 2008.

[78]   R. J. Petersen, "Composite reverse osmosis and nanofiltration membranes," *Journal of membrane science,* vol. 83, pp. 81-150, 1993.

[79]   S. Hong and M. Elimelech, "Chemical and physical aspects of natural organic matter (NOM) fouling of nanofiltration membranes," *Journal of membrane science,* vol. 132, pp. 159-181, 1997.

[80]   T. Martin, S. Kooi, S. Chang, K. Sedransk, and K. Gleason, "Initiated chemical vapor deposition of antimicrobial polymer coatings," *Biomaterials,* vol. 28, pp. 909-915, 2007.

[81]   G. Ozaydin-Ince and K. K. Gleason, "Transition between kinetic and mass transfer regimes in the initiated chemical vapor deposition from ethylene glycol diacrylate," *Journal of Vacuum Science & Technology A,* vol. 27, pp. 1135-1143, 2009.

[82]   S. H. Baxamusa, S. G. Im, and K. K. Gleason, "Initiated and oxidative chemical vapor deposition: a scalable method for conformal and functional polymer films on real substrates," *Physical Chemistry Chemical Physics,* vol. 11, pp. 5227-5240, 2009.

[83]   X. Zhou, S. Goh, S. Lee, and K. Tan, "XPS and FTi. r. studies of interactions in poly (carboxylic acid)/poly (vinylpyridine) complexes," *Polymer,* vol. 39, pp. 3631-3640, 1998.

[84]   K. Sakurai, E. P. Douglas, and W. J. MacKnight, "Spectroscopic study of an ionic blend made from the acid form of sulfonated polystyrene and poly [ethyl acrylate-co-(4-vinylpyridine)]," *Macromolecules,* vol. 25, pp. 4506-4510, 1992.

[85]   Z. Zhang, S. Chen, and S. Jiang, "Dual-functional biomimetic materials: nonfouling poly (carboxybetaine) with active functional groups for protein immobilization," *Biomacromolecules,* vol. 7, pp. 3311-3315, 2006.

[86]   G. Zhai, L. Ying, E. Kang, and K. Neoh, "Poly (vinylidene fluoride) with grafted 4-vinylpyridine polymer side chains for pH-sensitive microfiltration membranes," *Journal of Materials Chemistry,* vol. 12, pp. 3508-3515, 2002.

[87]   C.-J. Huang and Y.-C. Chang, "In Situ Surface Tailoring with Zwitterionic Carboxybetaine Moieties on Self-Assembled Thin Film for Antifouling Biointerfaces," *Materials,* vol. 7, pp. 130-142, 2013.

[88]   S. Yang, S. P. Zhang, F. M. Winnik, F. Mwale, and Y. K. Gong, "Group reorientation and migration of amphiphilic polymer bearing phosphorylcholine functionalities on surface of cellular membrane mimicking coating," *Journal of Biomedical Materials Research Part A,* vol. 84, pp. 837-841, 2008.

[89]   K. Futamura, R. Matsuno, T. Konno, M. Takai, and K. Ishihara, "Rapid development of hydrophilicity and protein adsorption resistance by polymer

surfaces bearing phosphorylcholine and naphthalene groups," *Langmuir,* vol. 24, pp. 10340-10344, 2008.

[90]	L. Ruiz, J. Hilborn, D. Leonard, and H. Mathieu, "Synthesis, structure and surface dynamics of phosphorylcholine functional biomimicking polymers," *Biomaterials,* vol. 19, pp. 987-998, 1998.

[91]	A. Yamasaki, Y. Imamura, K. Kurita, Y. Iwasaki, N. Nakabayashi, and K. Ishihara, "Surface mobility of polymers having phosphorylcholine groups connected with various bridging units and their protein adsorption-resistance properties," *Colloids and Surfaces B: Biointerfaces,* vol. 28, pp. 53-62, 2003.

[92]	J. Zheng, L. Li, H.-K. Tsao, Y.-J. Sheng, S. Chen, and S. Jiang, "Strong repulsive forces between protein and oligo (ethylene glycol) self-assembled monolayers: A molecular simulation study," *Biophysical journal,* vol. 89, pp. 158-166, 2005.

[93]	S. Herrwerth, W. Eck, S. Reinhardt, and M. Grunze, "Factors that determine the protein resistance of oligoether self-assembled monolayers-Internal hydrophilicity, terminal hydrophilicity, and lateral packing density," *Journal of the American Chemical Society,* vol. 125, pp. 9359-9366, 2003.

[94]	F. Höök, M. Rodahl, B. Kasemo, and P. Brzezinski, "Structural changes in hemoglobin during adsorption to solid surfaces: effects of pH, ionic strength, and ligand binding," *Proceedings of the National Academy of Sciences,* vol. 95, pp. 12271-12276, 1998.

[95]	A. Matin, Z. Khan, K. Gleason, M. Khaled, S. Zaidi, A. Khalil*, et al.*, "Surface-Modified Reverse Osmosis Membranes applying a Copolymer Film to Reduce Adhesion of Bacteria as a Strategy for Biofouling Control," *Separation and Purification Technology,* 2014.

[96]	R. Yang and K. K. Gleason, "Ultrathin antifouling coatings with stable surface zwitterionic functionality by initiated chemical vapor deposition (iCVD)," *Langmuir,* vol. 28, pp. 12266-12274, 2012.

[97]	A. Asatekin, A. Menniti, S. Kang, M. Elimelech, E. Morgenroth, and A. M. Mayes, "Antifouling nanofiltration membranes for membrane bioreactors from self-assembling graft copolymers," *Journal of membrane science,* vol. 285, pp. 81-89, 2006.

[98]	A. Widjaya, T. Hoang, G. W. Stevens, and S. E. Kentish, "A comparison of commercial reverse osmosis membrane characteristics and performance under alginate fouling conditions," *Separation and Purification Technology,* vol. 89, pp. 270-281, 2012.

[99]	S. Y. Kwak, S. G. Jung, Y. S. Yoon, and D. W. Ihm, "Details of surface features in aromatic polyamide reverse osmosis membranes characterized by scanning electron and atomic force microscopy," *Journal of Polymer Science Part B Polymer Physics,* vol. 37, pp. 1429-1440, 1999.

[100]	G. Ozaydin-Ince, A. Matin, Z. Khan, S. Zaidi, and K. K. Gleason, "Surface modification of reverse osmosis desalination membranes by thin-film coatings deposited by initiated chemical vapor deposition," *Thin Solid Films,* vol. 539, pp. 181-187, 2013.

[101]	A. Matin, H. Shafi, Z. Khan, M. Khaled, R. Yang, K. Gleason*, et al.*, "Surface modification of seawater desalination reverse osmosis membranes: Characterization studies & performance evaluation," *Desalination,* 2013.

[102] S. G. Im and K. K. Gleason, "Solvent-free modification of surfaces with polymers: The case for initiated and oxidative chemical vapor deposition (CVD)," *AIChE journal,* vol. 57, pp. 276-285, 2011.

[103] V. Dupres, C. Verbelen, and Y. F. Dufrêne, "Probing molecular recognition sites on biosurfaces using AFM," *Biomaterials,* vol. 28, pp. 2393-2402, 2007.

[104] C. J. Weinman, N. Gunari, S. Krishnan, R. Dong, M. Y. Paik, K. E. Sohn*, et al.*, "Protein adsorption resistance of anti-biofouling block copolymers containing amphiphilic side chains," *Soft Matter,* vol. 6, pp. 3237-3243, 2010.

[105] J. S. Louie, I. Pinnau, I. Ciobanu, K. P. Ishida, A. Ng, and M. Reinhard, "Effects of polyether–polyamide block copolymer coating on performance and fouling of reverse osmosis membranes," *Journal of Membrane Science,* vol. 280, pp. 762-770, 2006.

[106] R. E. Holmlin, X. Chen, R. G. Chapman, S. Takayama, and G. M. Whitesides, "Zwitterionic SAMs that resist nonspecific adsorption of protein from aqueous buffer," *Langmuir,* vol. 17, pp. 2841-2850, 2001.

[107] V. A. Tegoulia, W. Rao, A. T. Kalambur, J. F. Rabolt, and S. L. Cooper, "Surface properties, fibrinogen adsorption, and cellular interactions of a novel phosphorylcholine-containing self-assembled monolayer on gold," *Langmuir,* vol. 17, pp. 4396-4404, 2001.

Vitae

HAFIZ ZAHID SHAFI

Department of Mechanical Engineering,

King Fahd University of Petroleum and Minerals,

Dhahran 31261, Saudi Arabia.   hafizahdi@kfupm.edu.sa

EDUCATION

PhD, Mechanical Engineering	*2015*
King Fahd University of Petroleum & Minerals	Dhahran, Saudi Arabia
MS, Materials Science and Engineering	*2007*
Pakistan Institute of Engineering and Applied Sciences	Islamabad, Pakistan
B.S. Engineering: Metallurgical Engineering & Materials Science	*2005*
University of Engineering & Technology (UET)	Lahore, Pakistan

RESEARCH AND TEACHING EXPERIENCE

Visiting PhD Scholar at MIT, Cambridge, USA   *January-December, 2013*

- Spent two academic semesters at Massachusetts Institute of Technology (MIT), MA, USA as a visiting PhD scholar working on KFUPM-MIT project entitled, "*Multi-Scale Design of Next Generation Reverse Osmosis (RO) Membranes for Seawater Desalination*".
- Developed, optimized and successfully applied new zwitterionic copolymer coatings onto the surface of RO membranes via state-of-the-art initiated chemical vapor deposition (iCVD) technique.
- Thoroughly characterized the synthesized coatings by sophisticated equipments such as quartz crystal monitoring by dissipation (QCM-D), molecular force mapping (MFP), AFM, contact angle (CA), FTIR & XPS/AR-XPS for foulant adsorption, surface topology and morphology, hydrophilicity and compositional analysis.
- Achieved ultralow fouling (both organic and biofouling) of the surface-modified ROs and better performance under cross flow permeation testing conditions compared to virgin ROs.
- Accomplished the assigned task and produced one patent and three publications in reputable journals.

PhD Scholar/Lecturer-B   *2011-2015*
King Fahd University of Petroleum & Minerals (KFUPM)   Dhahran, Saudi Arabia

- Extensively characterized bare and the modified RO membranes for their antifouling, rejection and separation performances.
- Developed and performed bacterial adhesion testing protocols to characterize the anti-adhesion properties of the modified RO membranes.
- Evaluated the long term organic fouling (with alginate and humic acid exposure) under cross-flow filtration conditions.
- Achieved ultralow fouling (organic and biofouling) of surface modified commercial ROs and satisfactory performance under cross flow permeation testing compared to bare ROs.
- Improved and advanced data acquisition, analysis and research results publication skills.
- Taught two undergraduate Materials Science & Engineering courses: ME 205 and ME 217 every semester during the course of lectureship (two sections: 36 students), which comprised of lectures as well as laboratories.
- Prepared exams, graded reports, conducted review sessions and tutored students during office hours.
- Got departmental Graduate Ranking of 9.0/10 and undergraduate Instructor score of 8.5/10.

Junior Engineer   *2007-2010*
Senior Engineer   *01/2010-2011*
National Institute of Lasers & Optronics INILOP)   Islamabad, Pakistan

- Person in-charge of Spectroscopic Ellipsometery, Photo-spectrometry & AFM laboratories in Quantum devices group at NILOP.
- Synthesized III-V & IV-IV semiconducting optical thin films by various PVD methods such as: Pulsed Laser Deposition (PLD), Magnetron sputtering and e-beam sources.
- Characterized the deposited thin films by photo-spectrometer, photoluminescence, spectroscopic ellipsometer, atomic force microscope (AFM), SEM and FTIR for their optical, structural, morphological and compositional analysis.
- Acquired and analyzed the data obtained from aforementioned equipments and published it in local/international conferences and journals.
- Delivered strong technical support to users for thin film deposition and characterization (optical, compositional & structural).
- Trained users (students and junior staff) in effective use of PVD systems, and thermal annealing related equipment.
- Developed new techniques/methodologies/protocols to meet NILOP research needs.

PATENT AND PUBLICATIONS

[1]. <u>Hafiz Zahid Shafi,</u> Zafarullah Khan, Rong Yang and Karen K. Gleason, *"Development of Zwitterionic Coatings for Ultralow Fouling of Reverse Osmosis (RO) Membranes"*. [USPTO No.: 14/324,656; patent filed July 7, 2014].

[2]. Asif Matin, H. Z. Shafi and Zafar Khan Rong Yang and Karen K. Gleason, *"Surface Modification of Seawater Desalination Reverse Osmosis Membranes: Characterization Studies & Performance Evaluation"*, Desalination Vol. 343, (2104), pp 128-139. **(IF =3.96)**

[3]. Hafiz Zahid Shafi, Zafrullah Khan, Rong Yang and Karen K. Gleason*, "Surface Modification of RO Membranes with Zwitterionic Coatings for Improved Resistance to Fouling",* Desalination (2015) pp. 93-103, [article in press, DOI:10.1016/j.desal.2015.02.009]. **(IF =3.96)**

[4]. Zafarullah Khan, F.M. Kafiah, Hafiz Zahid Shafi, F. M. Nufaiei and S. Furqan, *"Morphology, Mechanical Properties and Surface Characteristics of Electrospun Polyacrylonitrile (PAN) Nanofiber Mats"*, International Journal of Advanced Engineering and Nano Technology (IJAENT) ISSN: 2347-6389, Volume-2 Issue-3, pp. 15-22, (2015). **(IF =1.41)**

[5]. H.Z. Shafi**,** A. Mahmood, Z. Ali and M. Mahmood, *"Optical and Structural Analysis of GeC Thin Films Deposited by Reactive Pulsed Laser Ablation Technique"*. Key Engineering Materials Vol. 442 (2010) pp 178-186 (2010) Trans Tech Publications, Switzerland. **(IF =0.36)**

[6]. A. Mahmood, M. Iqbal, Zahid Ali, H. Z. Shafi, A. Shah, D. Batani, **"***Optical Analysis of Germanium Carbide Thin Films Deposited by Reactive Pulsed Laser Ablation*"*,* JLMN-Journal of Laser Micro/Nanoengineering Vol. 5, No. 3, 2010. **(IF =0.73)**

[7]. Hafiz Zahid Shafi**,** Asif Matin, Zafarullah Khan and Karen K. Gleason, *"Surface Modification of Reverse Osmosis Membranes Using an Initiated CVD Technique: Performance under Organic Fouling Conditions"*, [article submitted to the Journal of Separation Science and Technology, Ref.: LSST-2015-8566].

[8]. Asif Matin, H. Zahid Shafi, Zafarullah Khan Minghui Wang, Karen K. Gleason and Faizur Rahman, *"Enhancement of Alginate Fouling Resistance in Surface-Modified Reverse Osmosis Membranes",* [article submitted to the Journal of Membranes Science, Ref.: JMS-15-743].

[9]. Hafiz Zahid Shafi, Asif Matin, Zafarullah Khan, Amjad Khalil and Karen K. Gleason, "*Surface Modification of Reverse Osmosis Membranes with Zwitterionic Coatings: A Potential Strategy for the Control of Biofouling*", [submitted to the journal of Surface & Coatings Technology, Ref.: SURFCOAT-D-15-00900].